Development and Evaluation of a Composite Hydrogel for Growth Plate Repair

by

Jingming Chen

B.S. Biochemistry and Molecular Biology/Biotechnology, Michigan State University, 2011

Submitted to the Graduate Faculty of

Swanson School of Engineering in partial fulfillment

of the requirements for the degree of

Doctor of Philosophy

University of Pittsburgh

2019

UNIVERSITY OF PITTSBURGH

SWANSON SCHOOL OF ENGINEERING

This dissertation was presented

by

Jingming Chen

It was defended on

July 12, 2019

and approved by

Lance Davidson, Ph.D., Professor, Departments of Bioengineering and Developmental Biology

Charles Sfeir, D.D.S., Ph.D., Associate Professor, Departments of Periodontics and Preventive Dentistry, Oral Biology, and Bioengineering

William Wagner, Ph.D., Professor, Departments of Surgery, Bioengineering, and Chemical Engineering

Dissertation Director: Juan Taboas, Ph.D., Assistant Professor, Departments of Bioengineering and Oral Biology

Development and Evaluation of a Composite Hydrogel for Growth Plate Repair

Jingming Chen, Ph.D.

University of Pittsburgh, 2019

The growth plate is the area of cartilaginous tissue located at ends of long bones that drives skeletal growth in children. Damage to the growth plate can cause formation of bony tethers bridging the epiphysis and metaphysis, ultimately leading to growth disturbances. Surgical procedures are required to correct these deformities, particularly when lower limbs are involved. However, they are costly and often ineffective, driving a clear need for a regenerative approach for growth plate repair.

The growth plate consists of populations of chondrocytes at distinct stages of differentiation. The coordinated proliferation and differentiation of the chondrocytes drive bone growth. Prior studies have attempted to restore the growth plate using tissue engineering methods. Nevertheless, no approach has succeeded in preventing bony tethers and restoring growth plate structure.

In this dissertation, a composite hydrogel (PGH) was developed and evaluated for growth plate repair. It consists of **P**oly (ethylene glycol) diacrylate, methacrylated **G**elatin (GEL-MA), and methacrylated **H**eparin. The PGH hydrogel was fabricated in-house and characterized for physiochemical properties including mechanical stiffness, swelling properties, and cytocompatibility. To evaluate the potential of the hydrogel to regenerate the growth plate cartilage, its effects on chondrocyte phenotype progression were analyzed and compared to a GEL-MA only hydrogel. To evaluate its ability to drive differentiation of stem cells to growth plate

chondrocytes, its effects on stem cell chondrogenic and osteogenic differentiation were evaluated. Finally, the efficacy of the stem cell-laden PGH hydrogel in regenerating cartilage and preventing bony tethers was accessed in a growth plate defect model in goats. The results showed that compared to the GEL-MA hydrogel, the PGH hydrogel maintained glycosaminoglycan production by hypertrophic chondrocytes, arrested terminal differentiation, and inhibited mineralization. While supporting chondrogenesis, it did not permit osteogenesis or mineral deposition by stem cells. When implanted into a growth plate defect, the PGH hydrogel was biodegradable and supported chondrogenesis. Although unable to completely prevent bony tether formation, implantation of the PGH hydrogel reduced bone and increased fat content at the defect site. This work advanced understanding of the regenerative approach for growth plate repair. The PGH hydrogel also showed great potential in regenerating stable cartilage.

Table of Contents

List of Figures

Acknowledgments

To my parents and husband:

Shiheng Chen & Jing Luo, and Da-Tren Chou

Who have always been there to give me love and support.

First, I would like to express my most sincere appreciation to my dissertation adviser, Dr. Juan Taboas, for seven years of invaluable mentorship and support. He has always been patient, open-minded, and encouraging, willing to hear my ideas, ask challenging questions, and provide constructive suggestions. His guidance and trust allowed me to pursue my passion and become the person I am today.

I would also like to state my special thanks to the rest of my committee – Dr. Lance Davidson, Dr. Charles Sfeir, and Dr. William Wagner. Their insights, feedback, and advice have motivated me to deepen my understanding of this research topic and strengthen my skills of distilling story from obscure data. They have made me a better student and scientist.

The Center for Craniofacial Regeneration (CCR) has been my home during my time at the University of Pittsburgh. I want to thank all the CCR faculty: Dr. Alejandro Almarza, Dr. Heather Szabo-Rodgers, Dr. Dobrawa Napierala, Dr. Elia Beniash, Dr. Konstantinos Verdelis, Dr. Fatima Syed-Picard, Dr. Alexandre Vieira, and Dr. Giuseppe Intini for their support and assistance. I also thank my friends, CCR lab mates, staff, and alumni: Dr. Jingyao Wu, Dr. Wendy Zhang, Dr. Ellie Liu, Dr. Jiaqi Zhao, Tyler Swenson, Adam Chin, Mariana Bezamat, Vicente Telles, Xinyun Liu, Wuyang Li, Emanuelle Cunha, Dr. Patrick Donnelly, George Hung, Rong Chong, Dr. Amalie Donius, Dr. Jesse Lowe, Sindhu Gopal, Mauro Tudares, Daisy Monier, Dr. Sana Khalid, Dr. Mairobys Socorro, Kristi Rothermund, Dr. Yong Wan, Michele Leahy, Elaine Dizak, Jill Smith,

and Diane Turner for all the help and fun times. In addition, I want to thank our collaborator Dr. Kurt Weiss for performing the animal surgeries.

Finally, I would like to extend my thanks to Dr. Lynne Porter, Dr. Alan Hirschman, and the Innovation Institute for their mentorship and support during my pursuit of entrepreneurship.

1.0 Introduction

1.1 Bone and Growth Plate Formation

The 206 bones in our bodies allow us to sit, walk, and conduct everyday life. Despite coming in different sizes and shapes, all bones are formed using one of the two methods, intramembranous or endochondral ossification, and both begin with mesenchymal condensations [1, 2].

The scapula, craniofacial bones, clavicles, and parts of the pelvis form via intramembranous ossification, where the mesenchymal condensation directly differentiate into osteoblasts, produce matrix rich in type I collagen, and later mineralize and mature. Intramembranous ossification also takes place at the periosteum of all bones [1-3].

The appendicular skeleton, vertebrae, and the base of the skull form by endochondral ossification, a sophisticated and highly coordinated process, where the mesenchymal stem cells undergo chondrogenesis and form anlagen, a cartilaginous model, abundant in type II collagen and glycosaminoglycans. The chondrocytes proliferate and secrete cartilage matrix, resulting in enlargement of the anlagen. Maturation of the chondrocytes first appears in the central region of the anlagen, characterized by exiting the cell cycle, hypertrophy, and production of type X collagen. The hypertrophic chondrocytes secrete molecular signals to attract blood vessels, chondroclasts, and osteoclasts from the perichondrium, forming the primary ossification centers. These chondrocytes also facilitated the formation of bone collars by inducing the neighboring perichondrial cells to become osteoblasts. At the last stage of life, hypertrophic chondrocytes undergo apoptosis. Osteoblasts use the cartilage matrix as a scaffold to lay down trabecular bone,

followed by the formation of bone marrow. During the establishment of the primary ossification centers, the anlagen continue to grow, driven by chondrocyte proliferation. In long bones, a subset of chondrocytes assume a flat shape and exhibit anisotropic arrangement; they stack into parallel columns, along the direction of longitudinal growth [1-3].

While the primary ossification centers establish in the late fetal period, the secondary ossification centers emerge soon after birth, at one or both epiphyses, through a similar mechanism as the former. The discoid cartilaginous region between the primary and secondary ossification centers is called the primary growth plate, or physis, responsible for uniaxial elongation of the long bones. Like the primary growth plate, the secondary growth plate, also known as the acrophysis, is located at the ends of the long bones. It drives the growth of the secondary ossification center [1-5]. The growth plate discussed henceforth refers to the primary growth plate.

1.2 Growth Plate Physiology and Bone Growth

The growth plate is relatively flat during infanthood, and gradually become undulated as children grow. The formation of new cartilage on one side and clearance of calcified cartilage on the other is intricately balanced. Therefore, the height of the growth plate remains reasonably constant until late adolescence when the growth plate narrows and eventually fuses [2, 5].

The growth plate is highly cellular, with chondrocytes organized into anisotropic, columnar structures [5, 6]. Growth plate chondrocytes can be categorized into five distinct zones, namely the reserve zone (RZ), the proliferative zone (PZ), the prehypertrophic zone (PHZ), the hypertrophic zone (HZ), and the calcified zone (Figure 1-1). The reserve zone, also known as the

resting zone, is located at the leading edge of the growth plate, adjoining the epiphyseal trabecular bone. The reserve zone cells (Figure 1-2 A) are round and dispersed, residing in a matrix primarily made of horizontally aligned type II collagen fibers. They are believed to give rise to chondrocytes in the adjacent proliferative zone. Chondrocytes in the proliferative zone (Figure 1-2 B) have high mitotic activity, as the name suggests. After mitosis, the daughter cells do not move throughout their life. Proliferative chondrocytes are flat and discoid, lie one on top of another, forming chondrocyte columns along the direction of bone growth. Cartilage matrix rich in glycosaminoglycans and vertically aligned type II collagen is produced in this zone. In young children, the average cell cycle time for proliferative chondrocytes is approximately 20 days. Under the orchestration of several signaling pathways, proliferative chondrocytes, starting with ones at the bottom of the column, exit the cell cycle and enter the prehypertrophic phase. The prehypertrophic zone is sometimes deemed as part of the hypertrophic zone. Cells in the prehypertrophic zone (Figure 1-2 C) then undergo massive cell volume enlargement, namely hypertrophy, hallmarked by the production of type X collagen. Hypertrophic chondrocytes (Figure 1-2 D) exhibit high metabolic activity, evident by a significant increase in the mean cellular mitochondrial volume, the mean cellular surface area of Golgi membranes, and the rough endoplasmic reticulum. Hypertrophic chondrocytes deposit hydroxyapatite into the surrounding matrix, through matrix vesicles, resulting in cartilage mineralization. Hypertrophic chondrocytes are also responsible for attracting blood vessels from the metaphyseal bone, by secreting vascular endothelial growth factor (VEGF). These cells then undergo apoptosis or transdifferentiate into osteoblast and osteocytes. Roughly, 70% of the calcified cartilage is resorbed by chondroblasts and the remaining 30% functions as a template for new bone formation. This sequential differentiation process, beginning with chondrocyte proliferation at the top of the columns and

ending with terminal cell removal at the bottom of the columns, repeats and drives growth until late adolescence [2, 6-12].

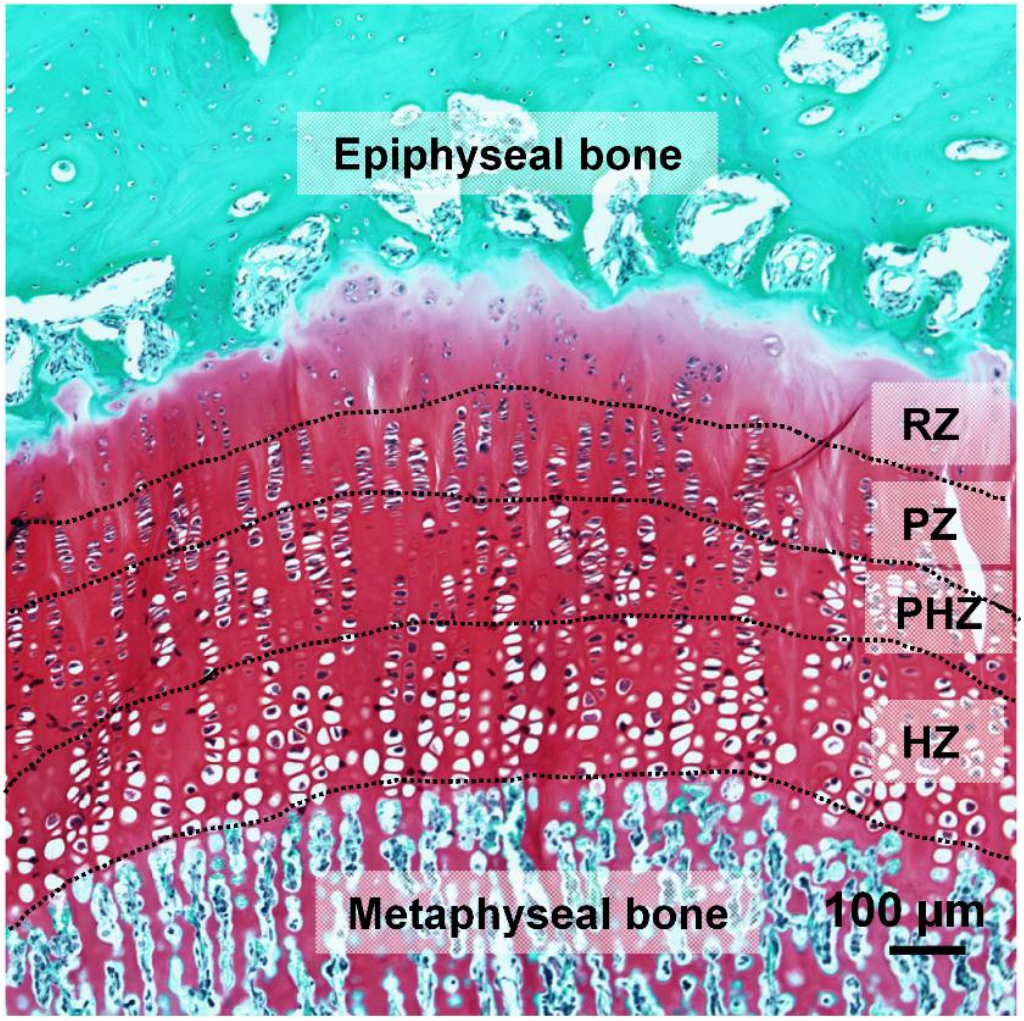

Figure 1-1 Growth plate cellular architecture (goat). Safranin O, Fast Green, and hematoxylin stain. Pink and red = cartilage; green = bone; dark purple = nuclei.

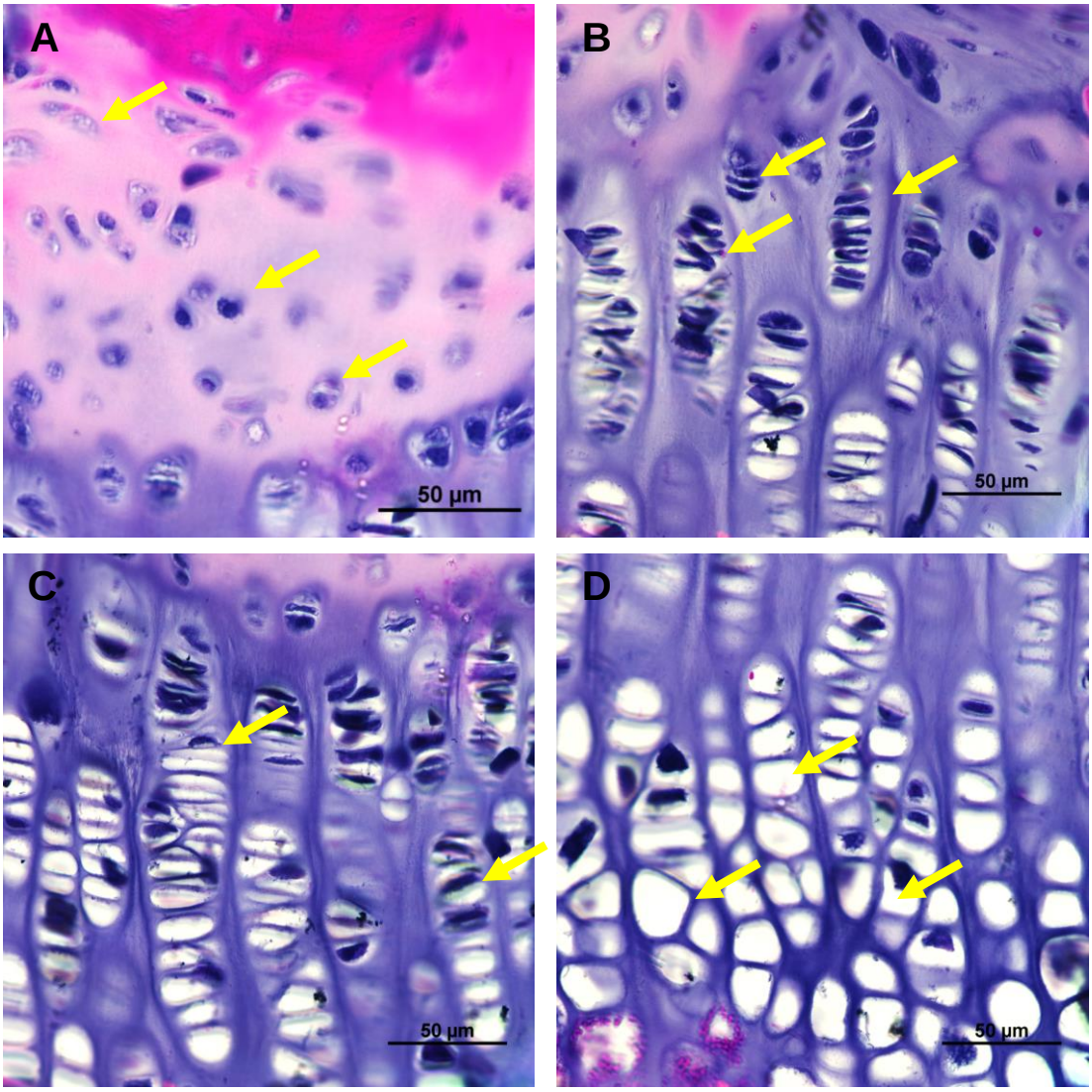

Figure 1-2 Growth plate chondrocytes (goat): A) resting ; B) proliferative; C) prehypertrophic; D) hypertrophic. Hematoxylin and eosin. Scale bar = 50 µm.

Parathyroid hormone-related protein (PTHrP) and Indian hedgehog (IHH) are two essential paracrine factors that collaboratively regulate proliferation and differentiation of chondrocytes in the growth plate (Figure 1-3). Proliferative chondrocytes and perichondrial cells are the primary sources of PTHrP. Binding of PTHrP and PTH/PTHrP receptors (PPRs) on

proliferative chondrocytes signal the cells to continue dividing. As chondrocyte columns elongate, the PTHrP source moves away from the cells at the bottom. When the distance is far enough, these cells become prehypertrophic and begin to produce IHH. IHH secreted by prehypertrophic and early hypertrophic chondrocytes then diffuses towards the epiphysis. It binds to its receptor Patched-1 (Ptc-1) on proliferative chondrocytes to promote cell division and PTHrp production. Besides the PTHrP/IHH feedback loop, other pivotal pathways in endochondral bone formation include fibroblast growth factor (FGF), bone morphogenetic proteins (BMPs), insulin-like growth factors (IGFs), retinoids, and Wnt/B-catenin [2, 9].

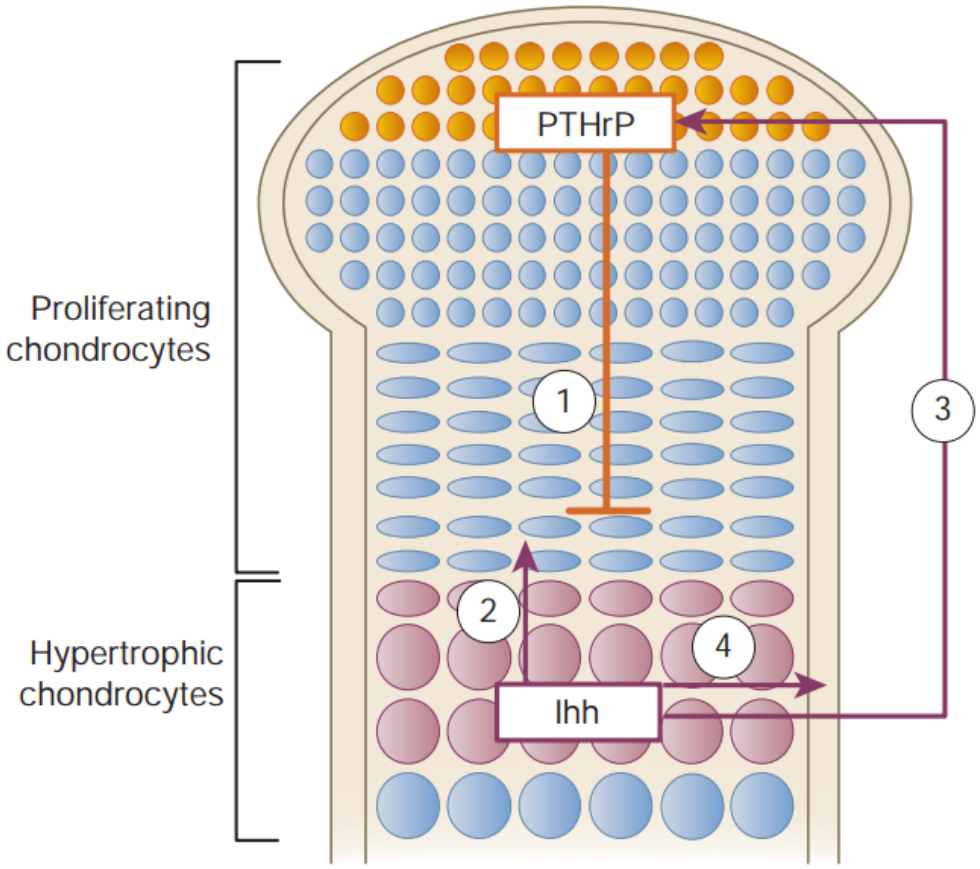

Figure 1-3 PTHrP and IHH signaling in the growth plate. Adapted from source, used with permission of [2].

On average, children between 5 and 8 years old grow 1-4 cm each year. The proliferative zone and the hypertrophic zone are critical to growth (Figure 1-4). The daily growth rate can be calculated by multiplying the number of proliferative chondrocytes, their division rate, and the average height of mature hypertrophic chondrocytes [10, 13, 14].

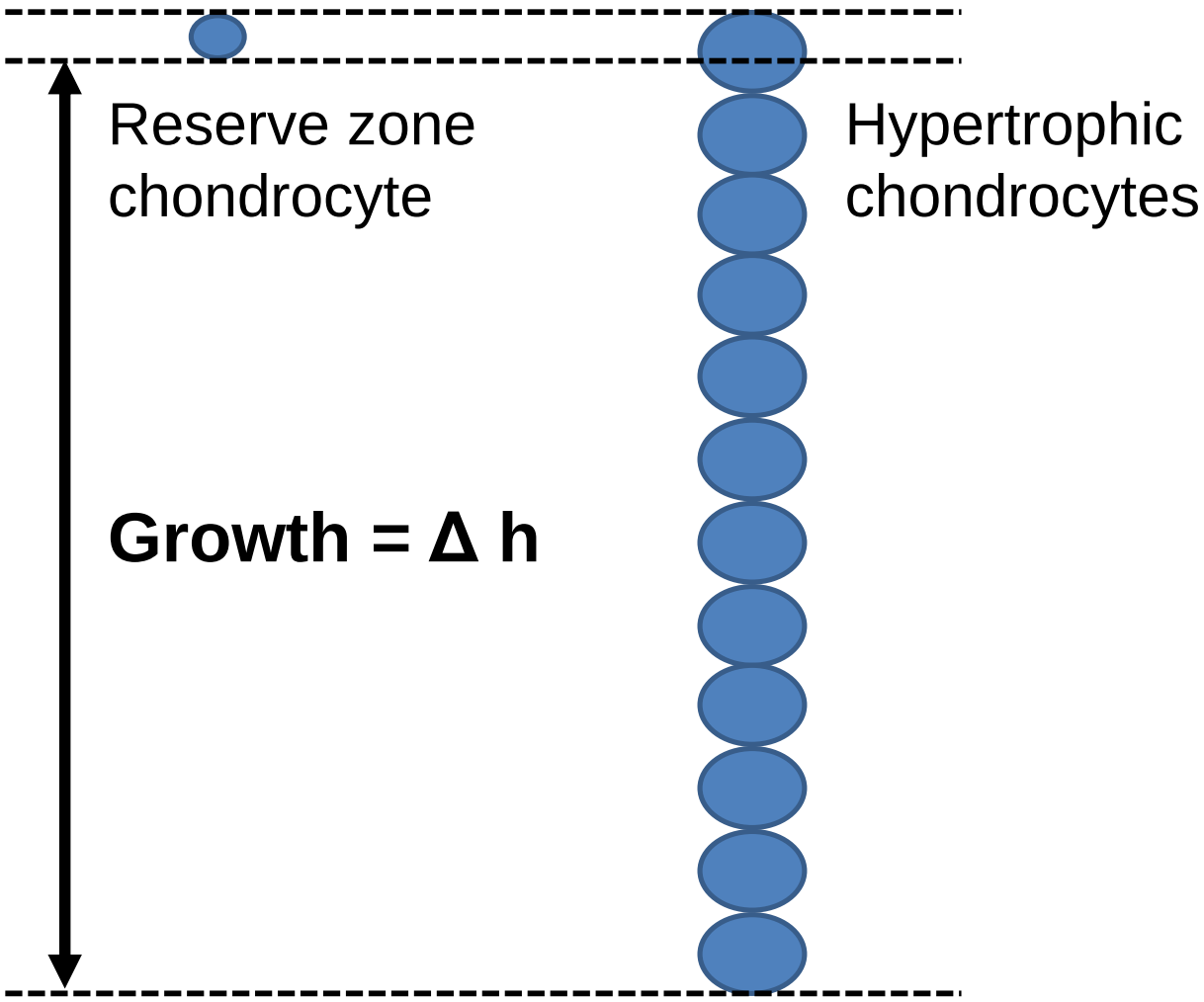

Figure 1-4 The height difference between the hypertrophic chondrocyte column and the original reserve zone cell is the amount of growth contributed by that progenitor cell.

1.3 Growth Plate Injury and Bony Tether Formation

Due to its soft cartilaginous nature, the growth plate is highly susceptible to fractures. Growth plate related bone fractures account for 15% to 30% of all pediatric skeletal injuries. Less common etiologies of growth plate injury include infection, cancer, radiation, ischemia, and iatrogenic damage [12, 15-17].

The Salter-Harris classification system (Figure 1-5) is the standard system used to evaluate growth plate fractures. It was established in 1963 by Robert B. Salter and W. Robert Harris. It categorizes all growth plate fractures into five types based on their pattern and severity. 80% of growth plate fractures are type I and type II, which are not transphyseal and able to heal on their own, unlikely to cause growth disturbances. Types III-V injuries involve damaged epiphyseal blood supply and sometimes allow transphyeal blood vessel invasion, likely to result in bony tethers and subsequent premature growth arrest [9, 12, 18]. Clinically, bony tethers are often detected months after injury. They are first identified or suggested by radiographs, then confirmed by magnetic resonance imaging [17].

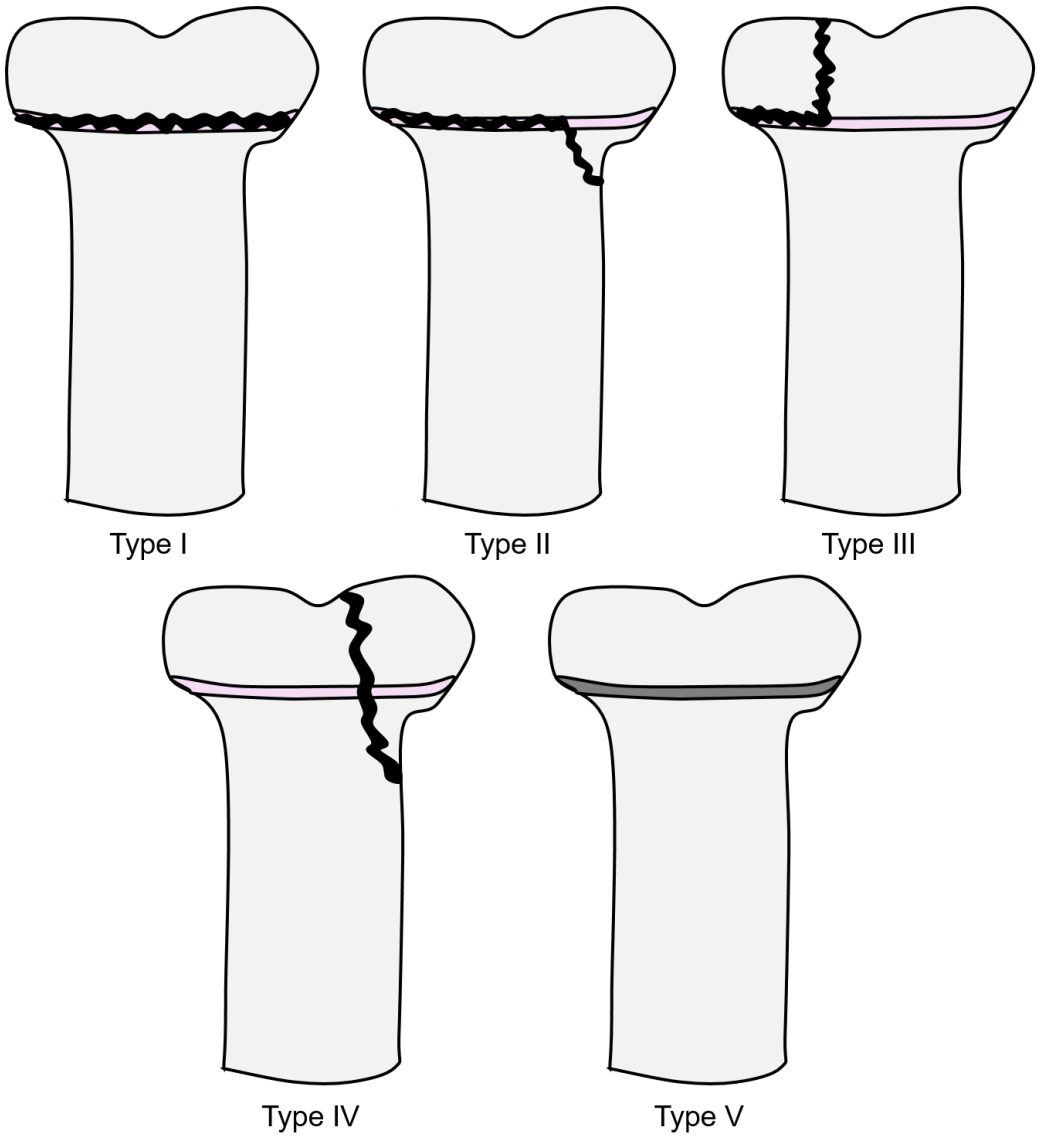

Figure 1-5 Salter-Harris classification system [12].

Bony tether formation begins with infiltration of inflammatory cells (Figure 1-6 A), including neutrophils, macrophages, and lymphocytes, into the fracture site. Expression of transforming growth factor β-1 (TGFβ-1) and bone morphogenetic proteins (BMPs) increase during this phase. In rats, neutrophil chemokine Cinc1 (equivalent to interleukin 8 in human) is

present in the damaged growth plate shortly following the injury, then decreases over time. The neutrophil-mediated inflammatory response is believed to regulate gene expressions during downstream repair processes. Pro-inflammatory cytokines interleukin 1 beta (Il1b) and tumor necrosis factor alpha (TNFα) are up-regulated at the injured site. TNFα has been shown to play an essential role in stem cell recruitment, proliferation, and differentiation during bone fracture repair. Arasapam et al. have demonstrated that the inhibition of cyclooxygenase 2 enzyme and inducible nitric oxide synthase activity decreased chondrogenesis of the recruited mesenchymal cells. Likewise, Chung et al. showed that blocking neutrophil activity favored expression of osteogenic genes such as Runx2 and osteocalcin, and decreased expression of chondrogenic genes such as Sox9 and type II collagen. [9, 19, 20]. Modulating inflammatory responses during growth plate fracture repair may have beneficial effects on bony tether prevention. Infiltration of a mixed population of mesenchymal cells (Figure 1-6 B) occurs following the inflammatory responses, with stem cell-like cells, osteoprogenitor cells, pre-osteoblasts, and pre-chondroblasts. Production of platelet-derived growth factor (PDGF) and fibroblast growth factor 2 (FGF2) increases during this phase; they are responsible for promoting cell proliferation, migration, and angiogenesis. These cells then undergo chondrogenic and osteogenic differentiation, produce bone matrix proteins such as type I collagen and osteocalcin, and eventually lay down bony trabeculae. Ultimately, bone matrix matures and become bony tethers (Figure 1-6 C, D) [9].

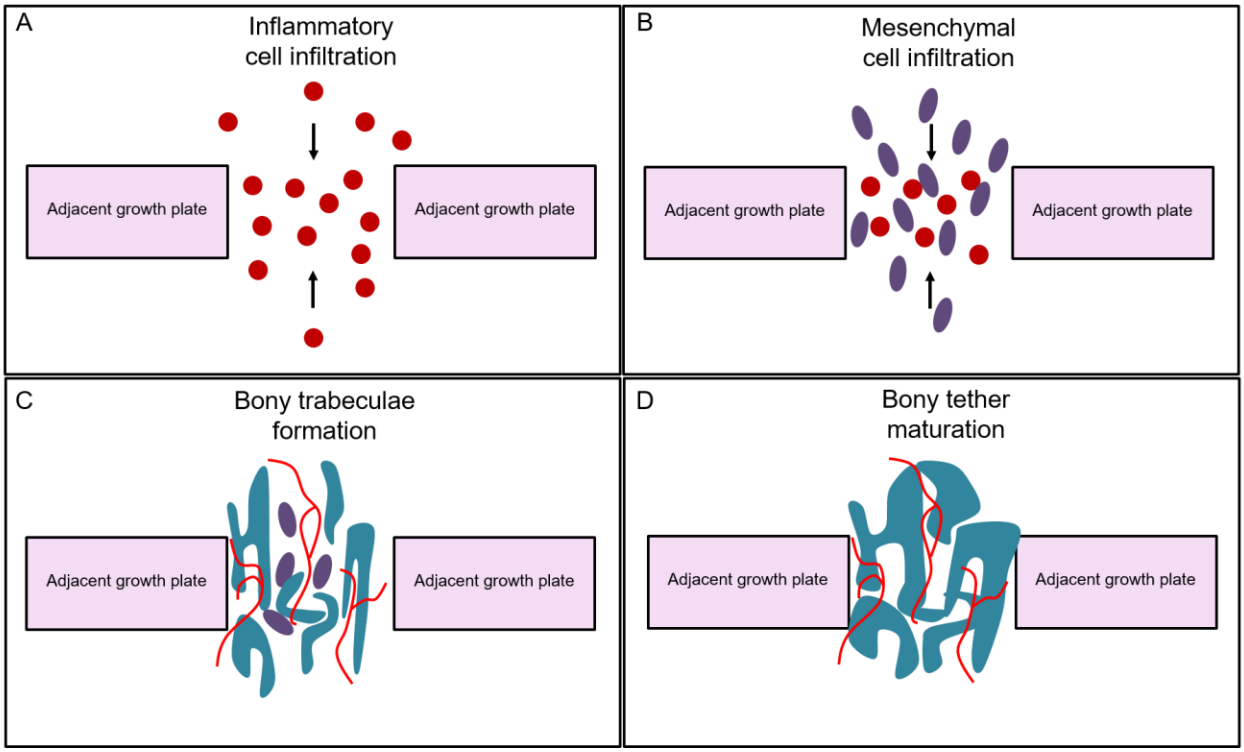

Figure 1-6 Bony tether formation. A) Infiltration of inflammatory cells; B) infiltration of mesenchymal cells; C) bone formation; D) bone maturation.

1.4 Treatments for Growth Plate Injuries

Bony tethers formed following growth plate injuries can cause lifelong disabilities such as limb length discrepancy and angulation deformities. These patients may suffer from cosmetic deformity, early-onset arthritis, lower back pain, and gait disturbances. Growth disturbances are not well tolerated, especially in the lower limbs. The distal femur, distal tibia, and proximal tibia are the most common sites affected by bony tethers post trauma, accounting for 81% of the cases. Injury to the growth plate in the distal femur is particularly worrisome, as 71% of the uniaxial

growth of the femur and 40% of the lower extremity elongation is driven by the distal femur growth plate [12, 14, 17, 21].

Surgical interventions are often required to prevent or correct severe growth disturbances. When bony tethers affect over 50% of the growth plate, epiphysiodesis is recommended. Young children with bony tethers comprise less than 50% of the growth plate area are typically treated with tether excision [17]. To prevent reformation of bony tethers, surgeons fill the resection sites with interpositional materials. This procedure was first proposed by Langenskiöld et al. in 1949 [22], and confirmed by Österman et al. in 1972 [23]. In the past 60 years, various materials have been tested for this procedure, including polymeric silicone, autologous fat, muscle, bone wax, and bone cement. Although this procedure is reported effective in rabbits, it only has 18%-35% success rate in human patients [22, 24, 25]. These non-regenerative interpositional materials either break down over time, being replaced by new bony tethers or fail to integrate with host tissues. Other treatments to reconstruct growth plate function include distal limb transfer, rotationplasty, wedge osteotomy, and distraction osteogenesis [9, 12]. These surgical treatments are costly, both monetarily and psychologically. They may restrict children's activity during their formative years and subjects them to painful procedures, repeated clinic visits, multiple surgeries, and rehabilitation.

1.5 Regenerative Approaches for Growth Plate Repair

In search of a more effective solution for growth plate repair, biological treatments have been explored in the past three decades. An ideal regenerative approach should not only prevent

bony tether formation but also restore the growth plate cartilage and facilitate normal growth for children with significant defect size [9, 12, 26].

Prior studies have attempted to regenerate growth plate cartilage using tissue engineering methods translated from articular cartilage engineering, including combinations of cells, growth factors, and biomaterials. Bruce Foster and colleagues are pioneers of studying cell-based therapy for growth plate application. In 1990, they demonstrated that the use of a chondrocyte-laden collagen gel successfully prevented bony tether formation in sheep [27]. In 1998, Lee et al., implanted chondrocyte-laden agarose gel in rabbits and showed alleviation of leg length discrepancy and angulation deformity [28]. Despite the promising results, chondrocyte based therapies suffer from shortcomings such as source limitations, donor site morbidity, and lengthy harvesting and culturing processes, making them unsuitable to be used clinically [9, 12, 24].

Bone marrow-derived mesenchymal stem cells (BMSCs) have gained popularity as an alternative cell source, owing to their abundance and superior chondrogenic capability under proper conditions. Several studies have reported some degree of success in the rabbit model; nevertheless, such therapy has not succeeded in large animals [9, 29, 30].

Currently, there is no biological therapy available to regenerate the growth plate cartilage and prevent bony tether formation. Recapitulating the unique cellular architecture in the growth plate may be the key to regenerate functional growth plate cartilage [12]. The field is open to new tools and means to regenerate the growth plate and restore healthy growth. In order to successfully generate the growth plate cartilage, the interpositional material has to meet five criteria: 1) support cartilage formation; 2) prevent bony tether; 3) restore the zonal cell organization; 4) reestablish the appropriate signaling; 5) restore normal growth. Recreating the appropriate cellular architecture and signaling of the natural growth plate is exceptionally challenging, as it is a highly

stratified and dynamic tissue and the signaling mechanisms that orchestrate the proper chondrocyte maturation are not fully understood. Therefore, this work focused on developing an interpositional material that meets the first two criteria. Four specific aims have been crafted as discussed henceforward.

1.6 Specific Aims

The goal of this work is to develop a stem cell-laden composite hydrogel as the interpositional material for growth plate repair. This hydrogel should support cartilage development while preventing bone formation. We choose to develop a photocrosslinkable composite hydrogel consisting of poly (ethylene glycol) (PEG) diacrylate (PEGDA), methacrylated gelatin (GEL-MA), and methacrylated heparin (HEP-MA). The rationale of polymer selection is elucidated in section 2.1.

The specific hypothesis to be tested by the specific aims below is that the PEGDA-(GEL-MA)-(HEP-MA) composite hydrogel (PGH) will:

1) Support cartilaginous matrix deposition by proliferative chondrocytes but inhibit terminal differentiation and mineralization by chondrocytes,
2) Support stem cell chondrogenesis while inhibiting osteogenesis, and
3) Regenerate growth plate cartilage while preventing bony tether formation.

A summary of the specific aims of this dissertation to achieve the work described above are given below:

Specific Aim 1: Fabricate and characterize the PGH hydrogel.

In this specific aim, the PGH hydrogel was fabricated using PEGDA, GEL-MA, and HEP-MA synthesized in-house. Modification of the polymers was confirmed and calculated by proton nuclear magnetic resonance (^{1}H NMR). Material properties of the hydrogel were evaluated by mechanical testing and swelling assay. Cytocompatibility was assessed by Live/Dead assay.

Specific Aim 2: Evaluate the effects of the PGH hydrogel on chondrocyte phenotypes in a murine subcutaneous implant model.

This experiment modeled response of growth plate chondrocytes to the PGH hydrogel. Tri-layered PGH hydrogels encapsulating growth plate-like chondrocytes obtained from embryonic chick sternum were implanted into mouse dorsal subcutaneous pockets for 1, 3, and 8 weeks. Production of GAGs, types I, II, and X collagen, alkaline phosphatase activity, mineral deposition, and apoptosis were analyzed.

Specific Aim 3: Evaluate the effects of the PGH hydrogel on stem cell chondrogenesis and osteogenesis in *vitro* and in *vivo*.

In this specific aim, stem cell-laden PGH hydrogels were subject to chondrogenic and osteogenic medium *in vitro*. Production of GAGs and minerals were analyzed. Also, the stem cell-laden PGH hydrogels were implanted into mouse dorsal subcutaneous pockets for 8 weeks. Production of GAGs and minerals, as well as gene expression of cartilage and bone markers were analyzed.

Specific Aim 4: Assess the efficacy of the stem cell-laden PGH hydrogel in cartilage regeneration and bony tether prevention in a growth plate injury model in goats.

Ultimately, stem cell-laden PGH hydrogels were implanted into growth plate defects in 3-month-old goats. Bony tether formation, tissue composition within the injured site, and the fate of the hydrogels and encapsulated stem cells were analyzed and discussed.

2.0 Specific Aim 1: Fabricate and Characterize the PGH Hydrogel

2.1 Introduction

Hydrogels have been widely used for cartilage regeneration since the 1990s. The three-dimensional (3D) hydrophilic characteristic of hydrogels provide a microenvironment resembling the native cartilage extracellular matrix (ECM), supporting encapsulated cells to adhere, proliferate, and differentiate. Also, their porous framework enables cell migration as well as diffusion of growth factors, nutrients, and metabolites [31].

Among a variety of biomaterials, we chose to develop a photocrosslinkable composite hydrogel consisting of poly (ethylene glycol) (PEG) diacrylate (PEGDA), methacrylated gelatin (GEL-MA), and methacrylated heparin (HEP-MA).

We have focused on photopolymerizable hydrogels because they can be used to encapsulate different cell types and to incorporate numerous growth factors to guide the regeneration of cartilaginous interfacial tissues [32-34]. Also, the photocrosslinkable nature allows the hydrogels to be used as a potential injectable material to match irregular defects in the growth plate [31].

The PEG component was incorporated as a bioinert base to maintain spherical cell shape and resist cell-mediated contraction [35, 36]. Gelatin is a highly biocompatible and biodegradable natural polymer obtained by partially hydrolyzing collagen [31]. It offers integrin-mediated adhesion sites crucial for chondrocyte survival, proliferation, column formation, and hypertrophy [37-40]. The addition of heparin, the most negatively charged glycosaminoglycan (GAG), further mimics the matrix composition of cartilage and prolongs retention of growth factors produced by

encapsulated chondrocytes [41-47]. Heparin is selected as an analog to heparan sulfate (HS) proteoglycans, which are critical for normal intercellular signaling in the growth plate. Severe deficiency of HS in the growth plate leads to multiple osteochondromas [48, 49]. Also, heparin and other sulfated GAG-containing proteins have been shown to inhibit the formation of amorphous calcium phosphate, aggregation, and growth of crystalline apatite [50-53], and mineralization by osteoblasts *in vitro* [54-56].

In this aim, the PGH hydrogel was fabricated in-house and characterized for physiochemical properties including mechanical stiffness, swelling properties, and cytocompatibility. These properties were compared to the commonly employed GEL-MA only hydrogel (GEL). Chondrocytes are mechanosensitive, and their phenotype can be altered by substrate stiffness and mechanical stress [57, 58]. Swelling property of the hydrogels affects the mechanical properties, growth factor and metabolite diffusion, and surface properties [59].

2.2 Materials and Methods

2.2.1 Materials

Poly (ethylene glycol) (PEG) (MW ~4000), type B gelatin from bovine skin (MW~45000), dichloromethane, triethylamine, diethyl ether, methacrylic anhydride, molecular sieves (4Å), and dialysis tubing were obtained from Sigma-Aldrich (St. Louis, MO). Heparin sodium salt (MW = 15000) and other chemicals for material synthesis were obtained from Thermo Fisher Scientific (Hampton, NH). Cell culture supplies were purchased from Atlanta Biologicals

(Flowery Branch, GA) and Thermo Fisher Scientific (Waltham, MA). Live/Dead® Viability/Cytotoxicity kit was purchased from Invitrogen (Carlsbad, CA). Human BMSCs (hBMSC) and expansion medium were purchased from RoosterBio, Inc (Frederick, MD). Deuterium oxide was purchased from Sigma-Aldrich.

2.2.2 Synthesis of PEGDA, GEL-MA, HEP-MA, and Photoinitiator

PEGDA was synthesized as described previously [60]. Briefly, 33% (w/v) PEG solution in dichloromethane was prepared and reacted with methacrylated anhydride and triethylamine for four days in the dark at room temperature. The reaction mixture was then precipitated in diethyl ether, dialyzed against five changes of distilled water over 12 hours, frozen and lyophilized. GEL-MA was synthesized as described previously [59, 61]. Briefly, a 10% (w/v) gelatin solution in phosphate buffered saline (PBS, pH 7.2) was prepared and reacted with methacrylated anhydride under stirring at 50°C on a hot plate for 1 hour. The reaction mixture was then neutralized to pH 7.4, dialyzed against five changes of PBS over 48 hours, and lyophilized. HEP-MA was synthesized as described previously [62]. Briefly, a 10% (w/v) heparin solution in distilled water was prepared and reacted overnight with methacrylic anhydride at pH 8.5, 4°C. The reaction mixture was then precipitated in ethanol, dialyzed against five changes of distilled water over 48 hours, and lyophilized. The photoinitiator lithium phenyl-2,4,6-trimethylbenzoyl phosphinate (LAP) was synthesized in-house via the method of Majima et al. 1991 [63]. Briefly, 4,6-trimethylbenzoyl chloride was added dropwise to dimethyl phenylphosphonite and stirred over 18 hours. An excess of lithium bromide in 2-butanone was added and heated to 50°C for 10 minutes. The product was filtered, washed with 2-butanone, and dried.

2.2.3 NMR Analysis

Degrees of modification of the polymers were determined using ^{1}H NMR. Briefly, 30 mg of modified or unmodified polymers were dissolved in 0.6 mL deuterium oxide (D_2O). ^{1}H spectra were measured at 300 MHz (Advance III, Bruker, Germany), phase corrected and integrated. Three characteristic signals corresponding to the vinyl double bond were observed at 1.8, 5.7, and 6.2 ppm. The degree of modification (DOM) of PEGDA was calculated as described previously [64]. Briefly, the integration of vinyl protons at 5.8-6.2 ppm was compared to the integration of the two methylene bridge protons (-CH2-) at the terminal ends at 4.3 ppm. DOM=average integral of allylic proton/average integral of terminal methylene bridge proton. The degree of modification of GEL-MA was calculated as described previously [65]. Briefly, the integral ratio of lysine residues at 2.9 ppm (2.8 – 2.95) after modification to pre-modification was calculated (signal is lost with modification). DOM = 1- (integral of lysine signal of GEL-MA/ integral of lysine signal of unmodified gelatin). The degree of modification of HEP-MA was calculated as described previously [66]. Briefly, integration of the two methacrylate vinyl protons at 5.7 and 6.1 ppm were compared to the integration of the protons on the disaccharide unit of heparin at 3.0-4.6 ppm. DOME=average integral of the vinyl protons/average integral of the protons on the disaccharide unit.

2.2.4 Hydrogel fabrication

The hydrogel solutions were prepared by dissolving the modified polymers at 10% (w/v) in PBS. The PEG-DA solution was degassed before use. The photoinitiator LAP was added to hydrogel solutions at a final concentration of 0.01% (w/v). The PGH hydrogel was composed of

PEGDA, GEL-MA, and HEP-MA at a 63:21:16 mass ratio. The GEL hydrogel was 10% (w/v) GEL-MA only. For the cytocompatibility assay, cells were added to the hydrogel solutions at 1 million/mL. The hydrogel solutions were poured to a height of 2.0 mm into a polydimethylsiloxane mold with a glass bottom and polymerized with 2.5 J/cm2/mm UV-A (365 nm filter) from an Omnicure S1000 light source (InPro Technologies, Frederick, MD) for 3.5 minutes. Cylindrical hydrogel constructs were cut using biopsy punches.

2.2.5 Mechanical Testing

Cylindrical hydrogels were made using an 8.0 mm biopsy punch. The unconfined compression properties of the hydrogels were determined using an Insight 1 electromechanical testing system with a 10 N load cell (MTS Systems, Eden Prairie, MN) and PBS bath at room temperature (n=3 per hydrogel type). Samples were equilibrated for 1 hour in PBS before testing. Immediately before testing, cylinder diameter and height were measured with calipers, and then cylinders placed between aluminum platens and preloaded to 0.02 N at 0.008 mm/s. After 30 minutes of relaxation, cylinder height was recorded, and then cylinders were pre-conditioned with 10 cycles of 10% strain at 0.0015 strain/s. Force versus displacement data was then recorded for a 10% strain ramp (0.0015 strain/s) followed by 30 minutes stress relaxation using TestWorks (v4.11C, MTS Systems.) Engineering stress and strain were used to determine dynamic modulus (using the tangent to the linear region of the force/displacement curve at the last 1% of applied strain) and relaxation modulus for isotropic viscoelastic solids.

2.2.6 Swelling analysis

Cylindrical hydrogels were made using a 5.0 mm biopsy punch. Each cylinder was immersed in 2 ml of PBS and incubated at 37°C with PBS exchanged every week. Samples were retrieved at the indicated time-points (Figure 2-3, n=3 per time-point), blotted, weighed (Ws = wet weight), dried, and weighed (Wd = dry weight). The swelling ratio (Q) was calculated as follows: $Q= (Ws-Wd)/Wd$.

2.2.7 Cytocompatibility

Human BMSCs were expanded for three passages (1 week each) for experimental use. Cells were cultured until 80% confluence, trypsinized, and plated at 7.5×10^5 cells per 175 cm^2 cell culture flasks. 5 mm diameter cell-laden cylinders were fabricated as described in section 2.2.4. They were incubated in culture medium (alpha minimum essential medium (α-MEM), 1% penicillin/streptomycin (P/S), 10% fetal bovine serum (FBS)) for one day post-crosslinking and stained with the Live/Dead® Viability/Cytotoxicity Kit following the manufacturer's protocol. The percentage of live cells was calculated based on the number of green stained cells divided by the total number of cells (green and red stained cells, dual stained counted once as dead).

2.3 Results

2.3.1 NMR Analysis

The NMR spectra (Figure 2-1) showed that PEGDA was 92.5% modified; GEL-MA was 100% methacrylated due to the absence of the amine signals at 2.8–2.95 ppm; the degree of modification for HEP-MA was 10.4% (10.4 methacrylate groups/100 disaccharide units). There was no evidence of residual organic solvents or metharylic anhydride.

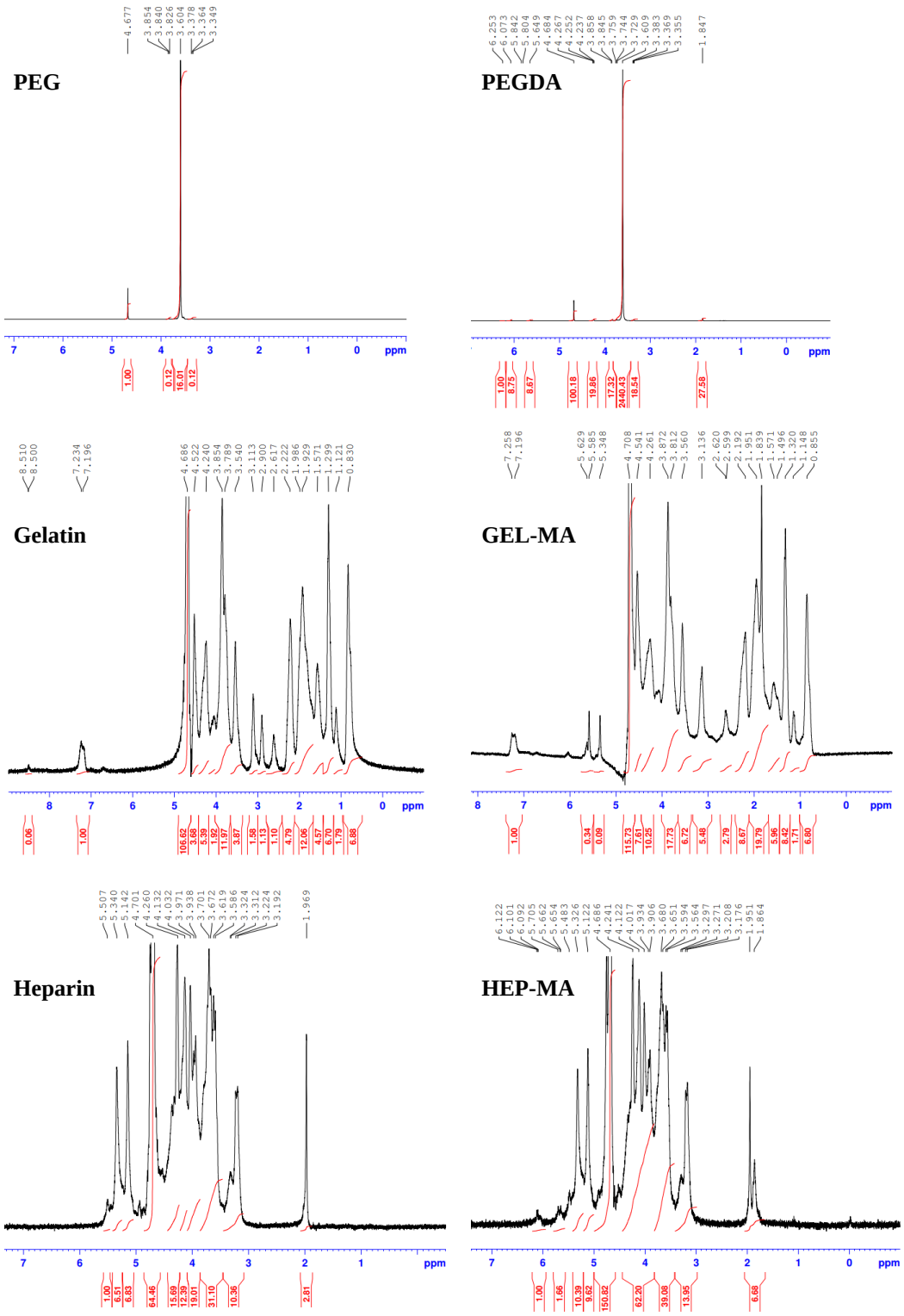

Figure 2-1 ^{1}H NMR spectra of unmodified and modified polymers.

2.3.2 Physical Properties and Cytocompatibility

The PGH hydrogel showed a significantly lower relaxation modulus (9.5 kPa, p=0.01) and peak stress (1.9 kPa, p=0.038) at 10% strain in unconfined compression compared to GEL (17.2 kPa and 2.4 kPa respectively, Figure 2-2). The dynamic modulus was not significantly different between hydrogels.

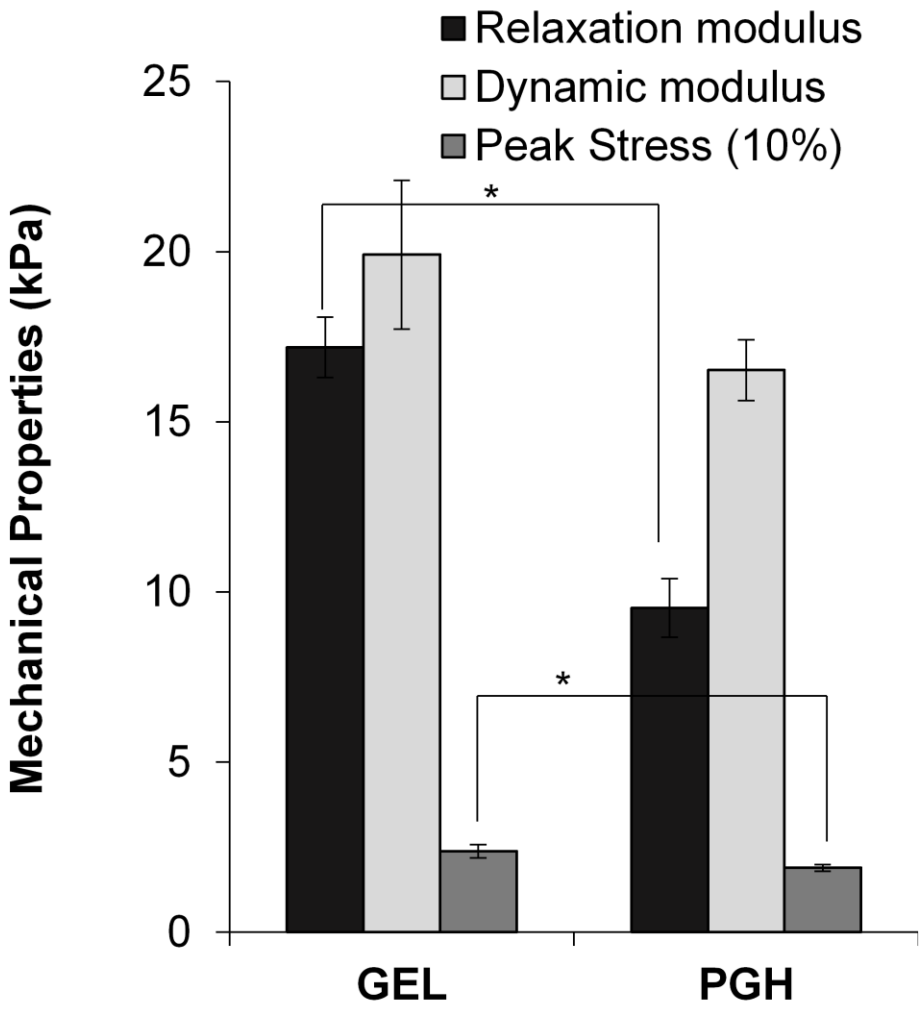

Figure 2-2 Unconfined compression moduli and peak stress at 10% strain for GEL and PGH (both 10% w/v) at room temperature in PBS bath (* = p < 0.05).

The PGH hydrogel likewise showed significantly greater swelling than the GEL hydrogel immediately after immersion in PBS (within 2 hours, Figure 2-3). Both hydrogel types swelled immediately after two hours and appeared stable over the six-week assay. The GEL hydrogel seemed to shrink somewhat in the first weeks. We attribute this possible shrinkage to the syneresis of the scaffold. Both hydrogels were slightly off the designed 10% (w/v) density. Both hydrogels displayed similar cytocompatibility after one day post-fabrication, approximately 86% (Figure 2-4).

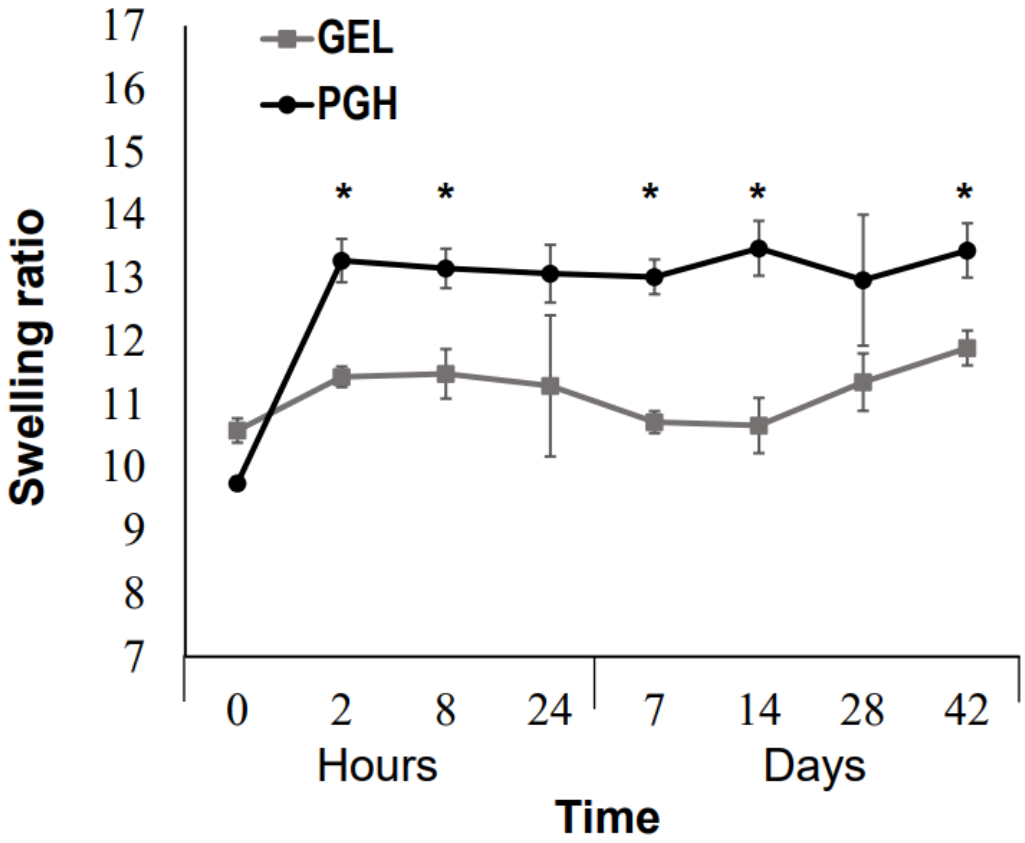

Figure 2-3 Swelling behavior of PGH and GEL hydrogels (* p<0.01).

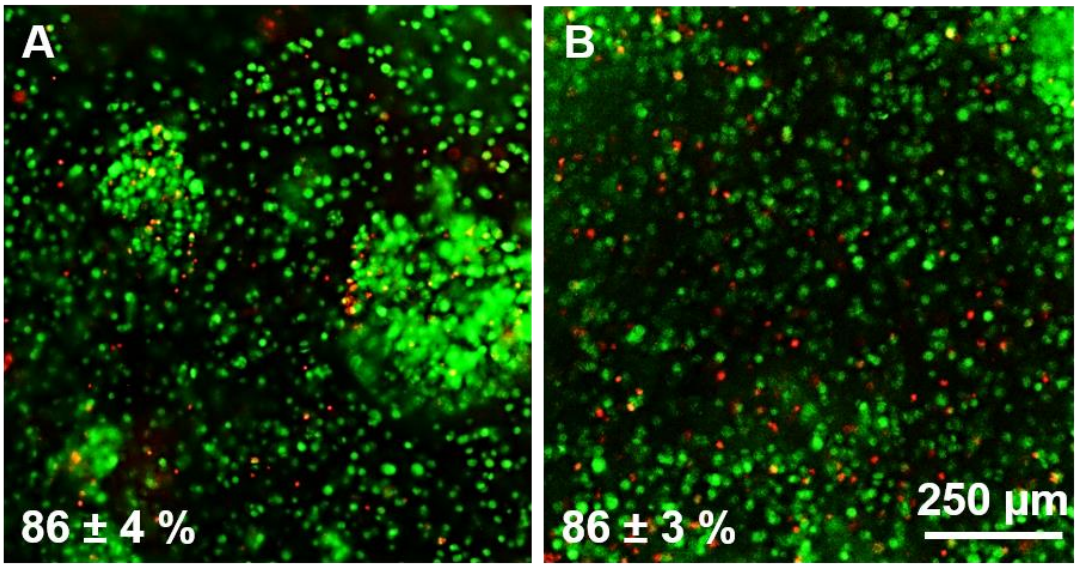

Figure 2-4 Live/Dead staining of BMSCs embedded in the PGH and GEL hydrogels one day post-crosslinking in expansion medium. (A) The fraction of viable cells in GEL hydrogels. (B) The fraction in PGH hydrogels.

2.4 Discussion

Regarding the physical and cytocompatibility properties of the hydrogels, the significantly weaker in relaxation modulus of PGH hydrogels compared to GEL hydrogels suggests a lower crosslink density in PGH. The comparable dynamic modulus suggests similar permeability between the hydrogels. The low density of the fixed-charge sulfate groups in PGH likely does not add significant electrostatic repulsion to the relaxation modulus or streaming potential in the flow-dependent viscoelastic behavior. Thus, these contributing factors would result in a lower relaxation modulus. The significantly greater swelling of the PGH hydrogel immediately on immersion likely arises from the lower crosslink density and increased Donnan osmotic pressure

due to the heparin sulfate groups. The variation in the starting density of both hydrogels arose from the error in weighing the low masses of polymer precursors for small-batch manufacturing. In the future, the degradation property of the PGH hydrogel should also be investigated. The gelatin and heparin components of the PGH hydrogel are expected to degrade first through enzymatic mechanisms, while the PEG component is expected to degrade slowly via oxidation of the ether backbone and hydrolysis of the esters. As components of the hydrogel degrade, the polymer network weakens and eventually falls apart. The PGH hydrogels studied in this dissertation were composed of PEG, gelatin, and heparin at 63:21:16 mass ratio. This design enabled the hydrogel constructs to remain for a longer time so that we could retrieve the samples for analysis at the end of the experiments. The cytocompatibility assays were performed after one day post-crosslinking to capture potential necrosis which may occur over time due to the hydrogel components and irradiation, as opposed to that from merely handling the cells for encapsulation (e.g., trypsinization, pipetting, mixing). The 86% viability is similar to other hydrogels [67, 68]. LAP and GEL-MA have been used by Allevi, a 3D bioprinting company, for tissue engineering. Allevi has demonstrated that when combining with photocrosslinkable polymers, the activated photoinitiator did not affect cell viability, whereas unreacted photoinitiators could pose harm on cells. It is important to note that in our experiment, no methods were used to augment viability under radical initiated crosslinking (e.g., ascorbate pretreatment of cells).

2.5 Conclusion

The PGH hydrogel was successfully fabricated with comparable cytocompatibility as other hydrogels for tissue engineering. Characterization of the physical properties of the hydrogel

allows us to optimize the PGH hydrogel for cartilage regeneration and bony tether prevention in the future.

3.0 Specific Aim 2: Evaluate the Effects of the PGH hydrogel on Chondrocyte Phenotypes in a Murine Subcutaneous Implant Model

3.1 Introduction

The growth plate (physis), consists of spatially discrete but proximate populations of chondrocytes at distinct states of differentiation. The populations can be grouped into five zones in the growth plate: 1) reserve zone (RZ), a reservoir of round dispersed progenitor cells; 2) proliferative zone (PZ), stacks of disk-like proliferating chondrocytes originated from progenitor mitosis and "gliding" reorganization; 3) prehypertrophic zone (PHZ), an interface where stacking cells leave the proliferative state and commit to terminal differentiation; 4) hypertrophic zone (HZ), where chondrocytes undergo terminal differentiation accompanied by massive cell enlargement; and 5) calcified zone (CZ), an interface of trabecular bone and the growth plate cartilage, where chondrocytes deposit minerals and eventually undergo apoptosis [8, 69-72]. Bioactive factors released by growth plate chondrocytes and the surrounding perichondrium interact with cells in both neighboring and distant zones and orchestrate chondrocyte maturation [2]. The coordinated progression of chondrocytes through all states of differentiation drives endochondral ossification and limb growth. Growth begins with immature resting RZ cells exiting from a metabolically quiescent state and entering a column forming phase as PZ cells. Next, they leave the cell cycle and increase secretion of cartilage matrix molecules such as type II collagen (Col2) and proteoglycans containing glycosaminoglycans (GAGs) as PHZ. Then they undergo hypertrophy hallmarked by type X collagen (Col10) production and a 10-fold increase in cell volume as HZ cells. HZ chondrocytes facilitate mineralization of the cartilage matrix by

depositing hydroxyapatite via matrix vesicles, and are eventually are removed by apoptosis or transdifferentiate into osteoblast and osteocytes [8, 11, 73-76].

To fully repair the growth plate cartilage and restore growth, it may be necessary to re-establish the zonal organization [12]. However, no study has been able to regenerate the natural cellular architecture of the growth plate. Transplantation of the intact physis has been pioneered for severe pathology but is extremely invasive and high risk rendering it unsuitable for most needs [77, 78]. Thus, the field is open to new tools and means to regenerate the growth plate and restore normal growth.

Control over chondrogenesis and chondrocyte phenotype progression is needed to inhibit boney tether formation in injured growth plates, and to ultimately regenerate the cellular architecture of growth plate.

To better understand the potential of the hydrogel to recreate the growth plate structure, we evaluated the effect of GEL (GEL-MA only) and PGH on the progression of growth plate-like chondrocytes through their states of differentiation. We hypothesized that the PGH would support enhanced matrix deposition by proliferative chondrocytes but inhibit terminal differentiation and mineralization by chondrocytes, whereas the GEL would support normal chondrocyte maturation and mineral deposition. We utilized a layered-photocrosslinking technique to fabricate tri-layered hydrogel constructs that mimicked the growth plate zonal architecture. Namely, we isolated PZ, PHZ, and HZ chondrocytes from discrete regions of day 17 chick sterna and encapsulated them in discrete layers within a monolithic hydrogel construct. The chick sternum is composed of chondrocytes of similar phenotype to growth plate chondrocytes. The caudal region of the sternum contains immature PZ-like chondrocytes, producing collagen type II, IX, XI, and PTHrp. The middle region contains PHZ-like

chondrocytes, producing Indian hedgehog (IHH). The cephalic (cranial) region contains HZ-like chondrocytes, producing Col10, alkaline phosphatase (ALP) and driving mineralization [74, 79-81]. The chick sterna were harvested and repeatedly dissected into consistent regions from which a large number of cells required for this study were pooled. The hydrogels were implanted in subcutaneous pockets of immunocompromised mice and allowed to mature over eight weeks of growth. Subsequently, the constructs were harvested, and chondrocyte phenotype and matrix composition analyzed via histochemical and immunohistochemical analysis.

3.2 Materials and Methods

3.2.1 Materials

PEGDA, GEL-MA, HEP-MA, and LAP were synthesized in-house as described in section 2.2.2. Collagenase (#C1764 from Clostridium histolyticum), dimethyl sulfoxide (DMSO), sucrose, ALP activity stain (BCIP®/NBT Liquid Substrate System), and Alizarin red were purchased from Sigma-Aldrich (St. Louis, MO). O.C.T. Compound was purchased from Thermo Fisher Scientific (Hampton, NH). Cell culture supplies including alpha minimum essential medium (α-MEM), penicillin/streptomycin, phosphate buffered saline (PBS, pH 7.2), and plastic ware were purchased from Thermo Fisher Scientific. Fetal bovine serum was purchased from Atlantic biologicals (Frederick, MD). The Von Kossa Stain Kit was purchased from American MasterTech (Lodi, CA). Antibodies were purchased from Abcam (Cambridge, United Kingdom). The TUNEL stain kit (ApopTag®) was purchased from Millipore (Burlington, MA).

3.2.2 Chondrocyte Isolation and Culture

White Leghorn chicken eggs were purchased from Eichner's Farm (Wexford, PA) and incubated at 39°C. At embryonic day 17, sterna were removed from hundreds of embryos and freed of connective tissues and perichondrial membrane using careful dissection. Separate regions of the sterna containing immature proliferative (PZ), prehypertrophic (PHZ), and hypertrophic (HZ) chondrocytes were cut as depicted in Figure 3-1, based on our immunohistochemical characterization of cell phenotype and the published sternum anatomy [74, 80], and pooled by region. The separate pools were incubated in tissue digestion medium (α-MEM, 10% fetal bovine serum, 1% penicillin-streptomycin, 20% collagenase) overnight at 37 °C. The chondrocytes were isolated by centrifugation and plated in fresh tissue culture medium (α-MEM, 10% fetal bovine serum, 1% penicillin-streptomycin) overnight to recover. Subsequently, all chondrocytes were released with trypsin treatment and frozen in freeze back medium (10% DMSO and 90% FBS) for future use. Before embedding within hydrogels, the chondrocytes were thawed, plated in the tissue culture medium, and cultured overnight.

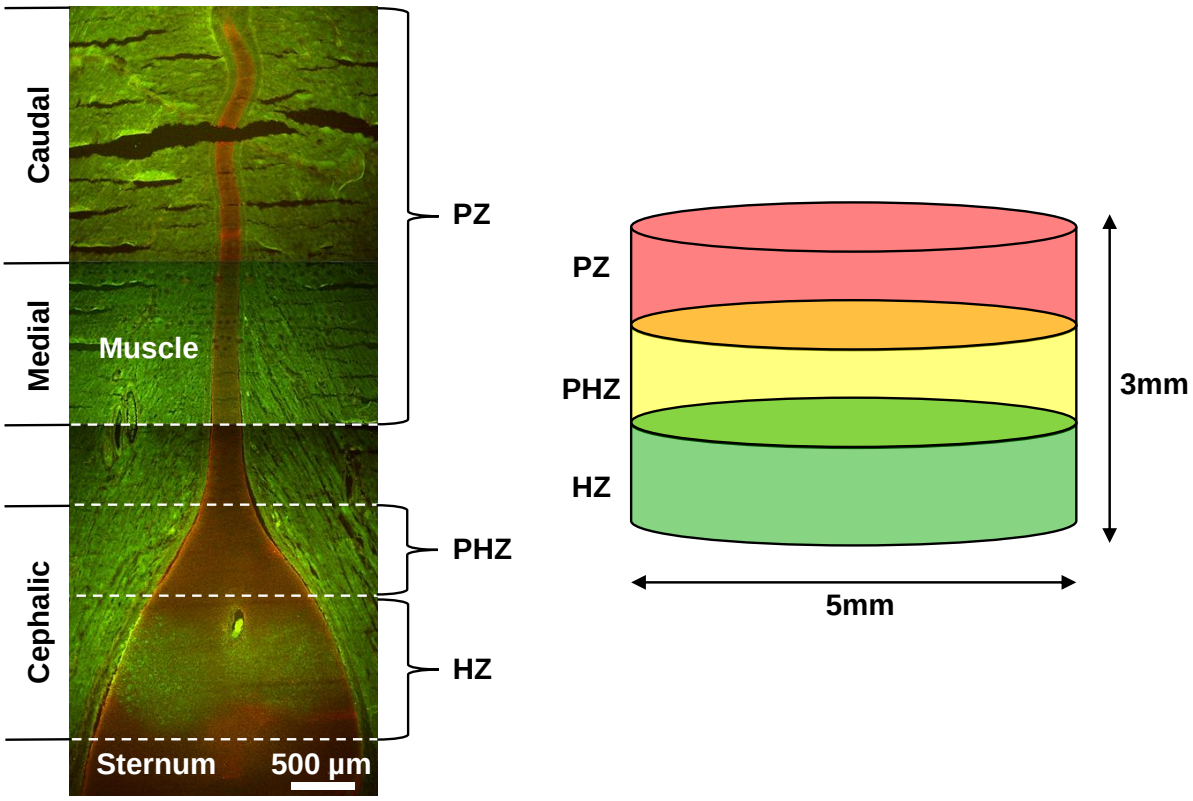

Figure 3-1 (Left) Cell cource for chondrocyte PZ, PHZ, and HZ populations from sternum after egg incubation for 17 days. Immunostain with red = Col2; green = Col10; surrounding muscle autofluoresces green. (Right) Design of cylindrical constructs for subcutaneous growth experiments in mice.

3.2.3 Hydrogel Construct Fabrication

The tri-layered hydrogel constructs that mimicked the growth plate zonal architecture were fabricated by sequentially casting 1.0 mm thick hydrogel layers containing the HZ, PHZ, and PZ chondrocytes in that order (Figure 3-1). Constructs were made of entirely PGH or GEL using a similar casting procedure as described in Aim 1. Separate solutions of the hydrogel precursor were mixed with cells of each population type at 30 million/mL. The first layer was

cast and irradiated, and the next layer immediately cast and irradiated. Bonding between layers was assured by casting in ambient air, which inhibits polymerization at the near surface, thus ensuring crosslinking between layers. Molecular oxygen quenches the radicals involved in crosslinking. The final layer was polymerized under nitrogen gas to crosslink the top surface entirely. Cylindrical constructs of 3 mm height x 5 mm diameter were cut out using a biopsy punch. The constructs were made the day of surgical implantation and placed in tissue culture medium before implantation in the mice.

3.2.4 Murine Subcutaneous Model

The hydrogel constructs (n=3 minimum per hydrogel) were implanted into separate dorsal subcutaneous pockets of immunodeficient mice (5-week old males) under an IACUC approved protocol (#15025263) at the University of Pittsburgh. The hydrogel constructs were implanted face up or down, randomly. The mice, NOD.CB17-Prkdcscid/SzJ, were purchased from Jackson Laboratory (Bar Harbor, ME). The animals were euthanized at 1, 3, and 8 weeks, and constructs were collected for analysis. The constructs were immersed in 30% (w/v) sucrose in PBS overnight, and then in 40% (v/v) O.C.T. Compound in PBS for two days. They were then snap frozen, embedded in O.C.T., and cryosectioned at 10 μm. The implants were analyzed with histochemical and immunohistochemical staining for GAGs (Safranin O / Fast Green/ Hematoxylin), collagen types I (Col1, Sigma-Aldrich AB752P), II (Col2, abcam ab34712), and X (Col10, Thermo Fisher Scientific MA5-14268), mineral (Von Kossa and Alizarin Red), ALP activity, and apoptosis (TUNEL method). Images were captured using a Nikon Eclipse TiE epifluorescent microscope (Nikon Instruments Inc., Melville NY) fitted with an ORCA-Flash4.0

camera (high sensitivity CMOS, Hamamatsu, Middlesex NJ) and NIS-Elements AR v4 software (Laboratory Imaging s.r.o., Praha, Czech Republic). The area and intensity of the positive signal for each histochemical and antibody stain were quantified using NIS-Element AR. The area of matrix deposition per layer was calculated as $\frac{Stained\ area}{Total\ Scaffold\ layer\ area}$. The average content of the matrix deposited was calculated as $\frac{Sum\ of\ the\ stain\ intensity\ over\ the\ layer}{Total\ scaffold\ layer\ area}$. The concentration of matrix deposition was calculated as $\frac{Sum\ of\ the\ stain\ intensity}{Stained\ area}$. These measures of average content and concentration were normalized to the group HZ in GEL at one week. The total number of cells per layer and those positive for GAG, Col1, Col2, and Col10 were counted, and the fraction calculated.

3.2.5 Statistical Methods

Statistical analysis was performed on histology measures using two-way ANOVA (hydrogel type and time within a chondrocyte population type) with Tukey's HSD post-hoc tests. Data are presented as mean ± standard deviation.

3.3 Results

3.3.1 Model Characterization

At the time of cell harvest (17 days of egg incubation), the long narrow caudal and medial regions of the chick sternum from which PZ were isolated stained lower for GAG than the

cephalic region from which PHZ and HZ cells were isolated (Figure 3-2 A). The PZ region showed no mineral staining, while the PHZ and HZ regions showed ALP activity but only a few sparse nodules of focal mineralization (Figure 3-2 B and 3-1 C). Only the HZ region expressed Col10; the PHZ did not (Figure 3-2 D). The upper cephalic region did stain stronger for GAGs but was excluded from the HZ due to lack of Col10 expression and interfacing with fibrous tissue. Col1 and Col2 were expressed in all three zones (Figure 3-2 D and Figure 3-2 E), with Col1 staining faint compared to Col2.

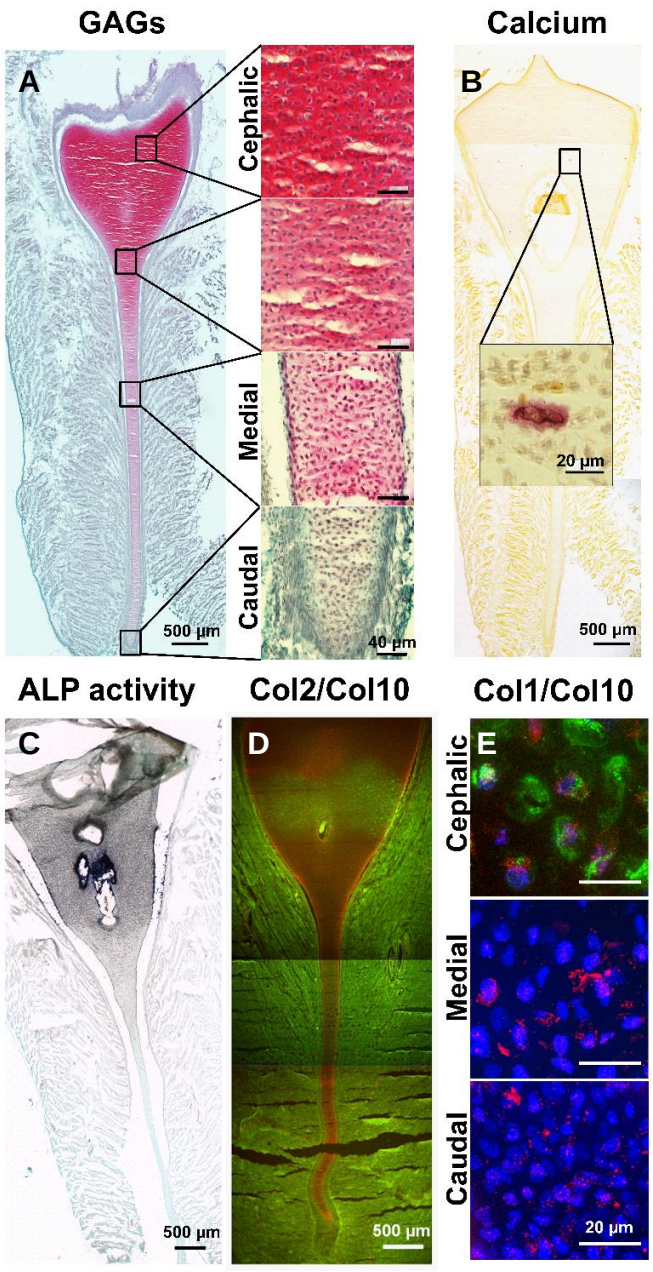

Figure 3-2 Day 17 chick sternum. A) Safranin O (red and pink) = GAG, Fast Green (green) = fibrous tissue, hematoxylin stain (purple) = cell nuclei. B) Alizarin Red stain (red) = calcium deposition. C) BCIP stain (dark purple) = ALP activity, counterstained with Fast Green. D) Immunostain with red = Col2; green = Col10; DAPI (blue) = nuclei, surrounding muscle autofluoresces green. E) Immunostain with red = Col1; green = Col10; blue = nuclei.

3.3.2 Chondrogenesis

GAGs and Col2 are among the most abundant ECM components of growth plate cartilage [76, 82]. The heparin component of PGH also stained positive for GAGs with Safranin O; this background was taken into account during image analysis. Overall, PGH showed greater GAG accumulation by all three chondrocyte populations compared to GEL (Figure 3-3 A-F). The area of GAG deposition for all three chondrocyte populations significantly increased over time ($p<0.0001$, **Error! Reference source not found.** A), with the HZ layer showing the lowest increase of 68%. However in GEL, only the PZ layer showed a significant increase in GAG deposition over the 8 weeks of growth (7.0-fold, $p<0.0001$). The PHZ layer in GEL showed a 1.2-fold increase at week 3 ($p=0.0057$), but then a 42% decrease from week 3 to week 8 ($p=0.0304$). The HZ layer in GEL showed no significant accumulation of GAGs over time. Comparing between hydrogel types, all chondrocyte populations showed a significantly greater area of GAG deposition in PGH than in GEL at week 8 ($p<0.0001$), with 11% for PZ, 2.2-fold for PHZ, and 7.4-fold for HZ. At earlier time-points, PHZ cells did not show differences between hydrogel types. The area of GAG deposition for PZ and HZ layers were significantly greater in PGH than GEL at week 1 by 2.2- and 12-fold respectively ($p<0.0001$). At week 3, only the HZ layer showed a greater area of GAG deposition in PGH than GEL by 4.3-fold ($p<0.0001$). The fraction of HZ cells that were positive for GAG deposition was at least twofold greater in PGH than in GEL at all time-points ($p<0.0001$, **Error! Reference source not found.** B). However in PGH, the fraction of HZ cells positive for GAG did show a 20% decrease over time ($p=0.0225$); no significant change occurred in GEL.

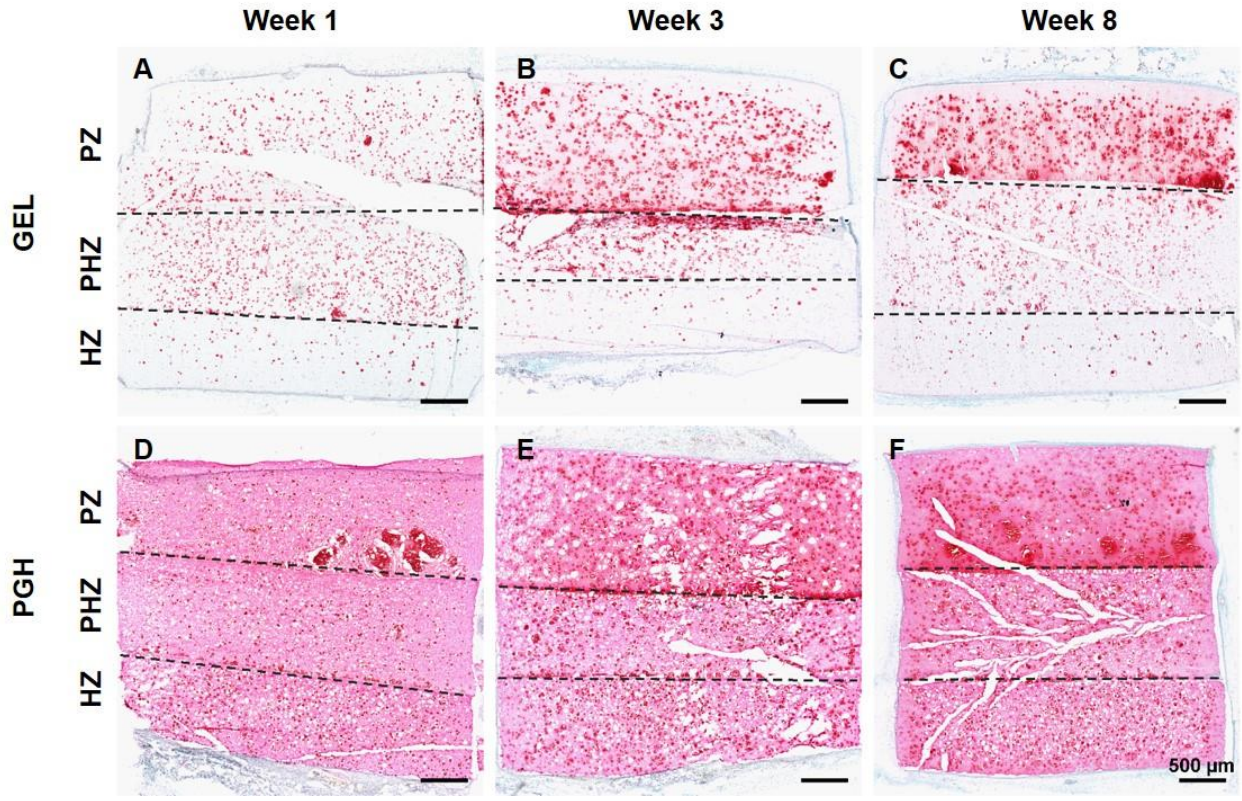

Figure 3-3 GAG deposition in GEL (A-C) and PGH (D-F) hydrogels by the different chondrocyte populations at 1, 3, and 8 weeks of growth in vivo within dorsal subcutaneous pockets in immunocompromised mice. Safranin O (red and pink) = GAG, Fast Green (green) = fibrous tissue, hematoxylin (purple) = nuclei.

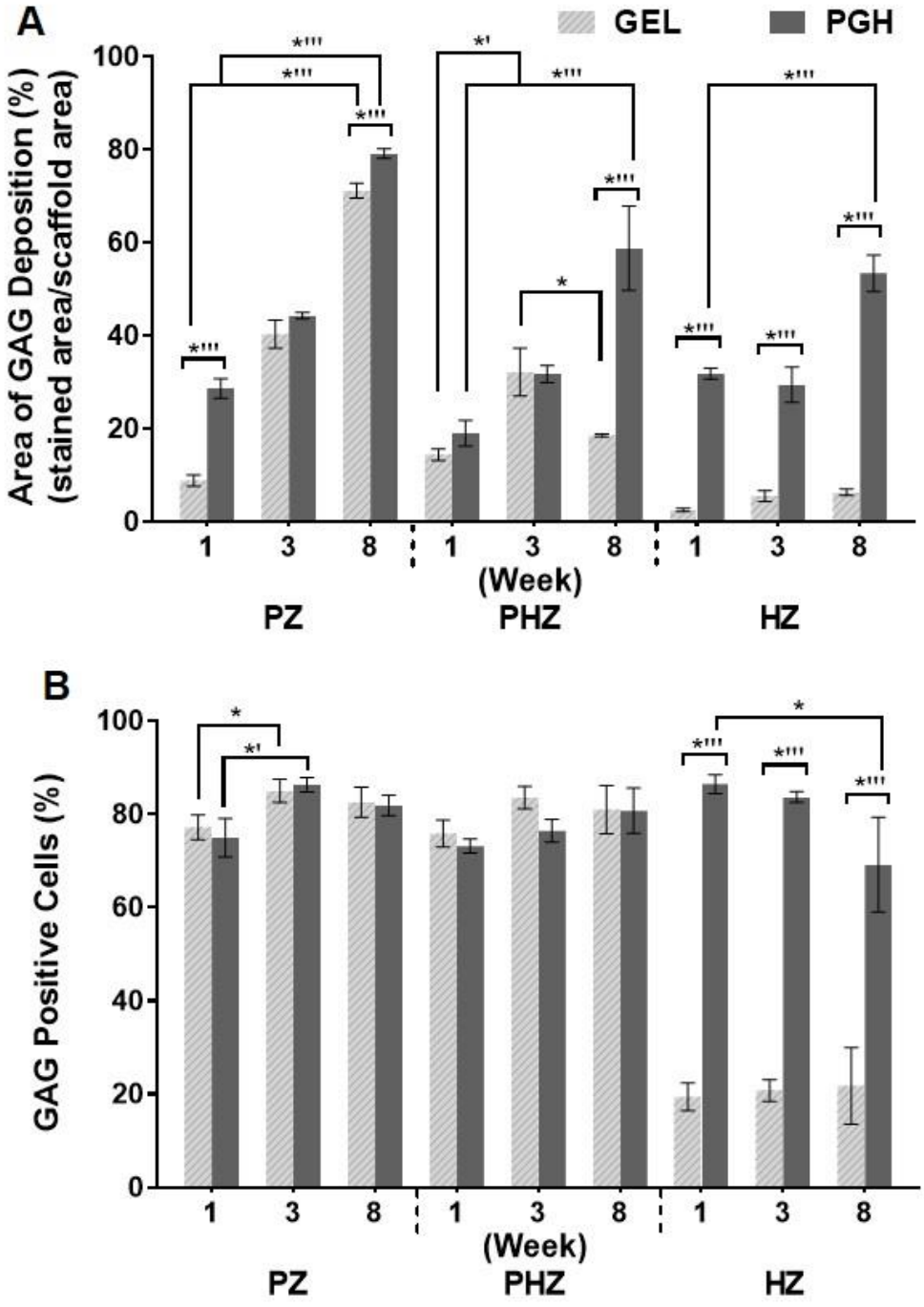

Figure 3-4 Area of GAG deposition (A) and fraction of GAG positive cells (B) were quantified by image analysis. *’’’ = p < 0.0001; *’’ = p ⩽ 0.001; *’ = p ⩽ 0.01; * = p < 0.05. Error bars = standard deviation of the mean.

In contrast, GEL showed greater Col2 accumulation by all cell populations compared to PGH (Figure 3-5). The average Col2 content in the PZ layer significantly increased over time in GEL by 2.2-fold ($p<0.0001$, Figure 3-6Figure 3-6 A), while the PHZ layer showed no significant change over time. In the HZ layer in GEL, Col2 content first decreased at week 3 by 48% ($p=0.0113$), and then increased by 1.0-fold at week 8 ($p=0.0173$). In the PGH hydrogel, the PZ layer showed a significant increase in Col2 content at week 3 (1.2-fold, $p=0.0133$). The PHZ and HZ populations in PGH did not show significant changes in Col2 content over time. Compared between hydrogel types, the average Col2 content was significantly greater in GEL than in PGH at week 8 for all chondrocyte populations, with threefold for PZ, 2.4-fold for PHZ, and 1.7-fold for HZ layers ($p\leq0.0023$). The PHZ and HZ layers in GEL were significantly greater in Col2 content at week 1 by 1.5-fold and 1.0-fold respectively ($p\leq0.0076$). No significant differences were detected between PGH and GEL at week 3.

The Col2 deposition became distributed throughout the GEL constructs over time, beginning in the PZ layer at week 3 and then evident in the PHZ and HZ layers at week 8 (Figure 3-5). Deposition remained more pericellular in PGH than in GEL (Figure 3-7). The concentration of Col2 deposition was significantly greater in PGH than GEL for all cell populations at week 1 and 3 ($p\leq0.002$, Figure 3-6 B), consistent with a greater diffusion of Col2 away from cells in GEL. By week 8, the concentration of Col2 was impacted by the hydrogel type. The PZ layer in GEL showed a greater concentration of Col2 than in PGH (13%, $p=0.0186$), consistent with the observed increase in average Col2 content. The PHZ layer in PGH maintained a greater concentration of Col2 than GEL (27%, $p<0.0001$). No significant difference was found between hydrogel types for HZ layer at week 8. Changes over time in the concentration of Col2 were smaller than changes in the average content of Col2. All layers in PGH showed a significant

decrease in the concentration of Col2 over time ($p<0.0001$ for PZ and PHZ, $p=0.0002$ for HZ from week 1 to week 8). Though the average Col2 content of the PZ layer in PGH increased at week 3 ($p=0.013$), the Col2 concentration decreased ($p<0.0001$), likely due to farther diffusion of the molecule. From week 3 to week 8, there was no significant change in Col2 concentration for the PZ and PHZ layers in PGH, while the HZ layer decreased by 22% ($p=0.0215$). In GEL hydrogels, only the PZ layer showed a significant increase in the concentration of Col2 deposition by week 8 (34%, $p<0.0001$). No significant changes over time were observed in GEL for the PHZ and HZ layers. The fraction of cells positive for Col2 significantly decreased in PGH across all populations from week 3 to week 8 of growth, by 45% for the PZ, 30% for PHZ, and 25% for HZ layers ($p\leq0.0006$, Figure 3-6 C). At week 8, the fraction was significantly greater in GEL than PGH by 86% for PZ, 49% for PHZ, and 40% for HZ layers ($p<0.0001$). No significant differences between hydrogels were detected at earlier time-points. In GEL, only the HZ layer showed a significant increase in the fraction of Col2 positive cells over time ($p<0.0001$). No alignment of cells into growth plate-like columns was observed at any time.

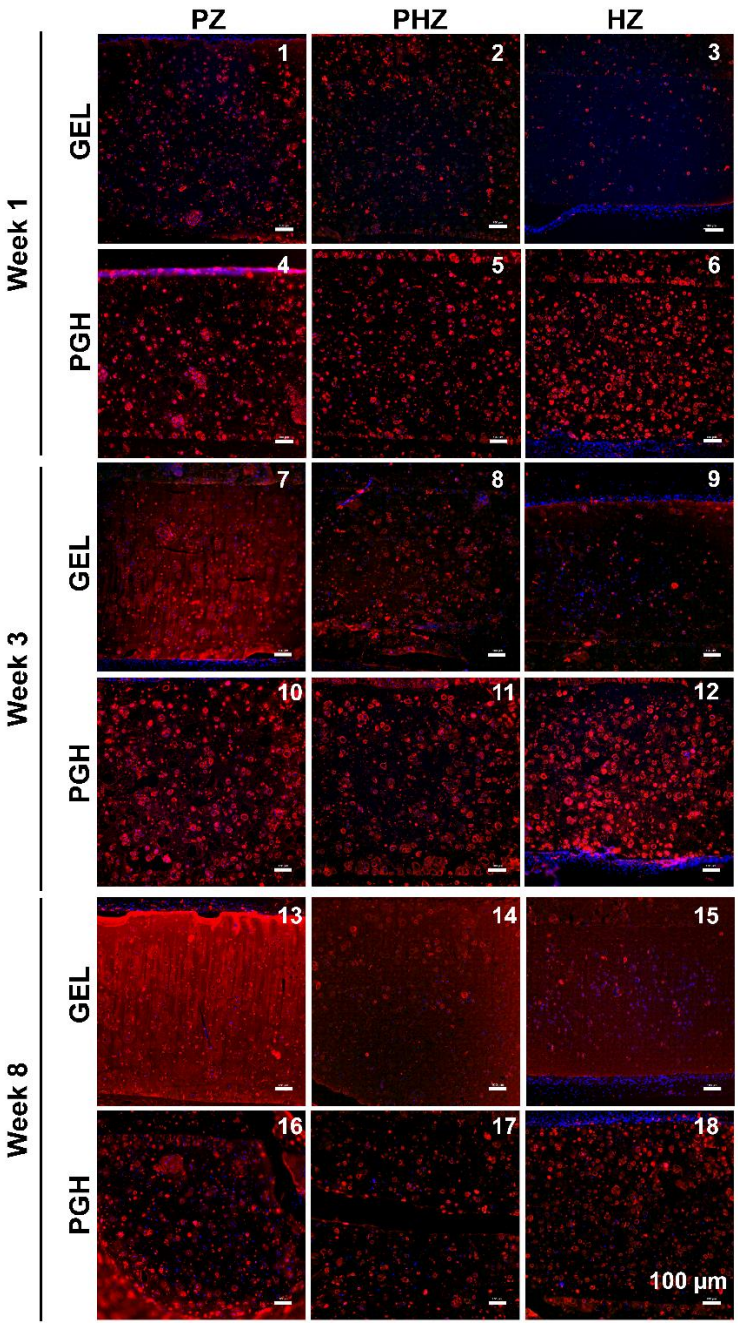

Figure 3-5 Col2 deposition by the different chondrocyte populations over 1, 3, and 8 weeks of growth in vivo in GEL (1-3, 7-9, 13-15) and PGH (4-6, 10-12, 16-18) hydrogel constructs. Immunostain red = Col2, blue = nuclei.

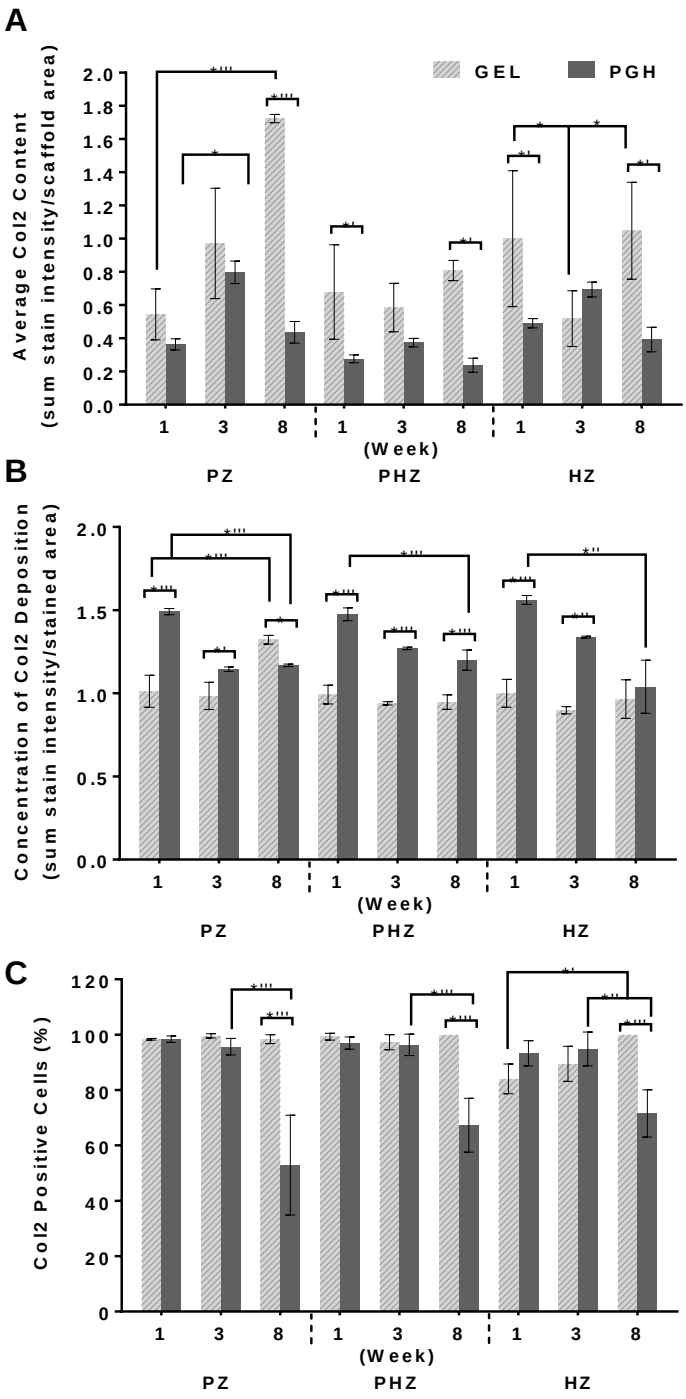

Figure 3-6 Analysis of Col2 deposition in GEL and PGH hydrogel constructs by the different chondrocyte populations over 1, 3, and 8 weeks of growth in vivo. Average Col2 content (A), concentration of Col2 deposition (B), and fraction of Col2 positive cells (C) were quantified by image analysis. *''' = $p < 0.0001$; *'' = $p \leq 0.001$; *' = $p \leq 0.01$; * = $p < 0.05$. Error bars = standard deviation of the mean.

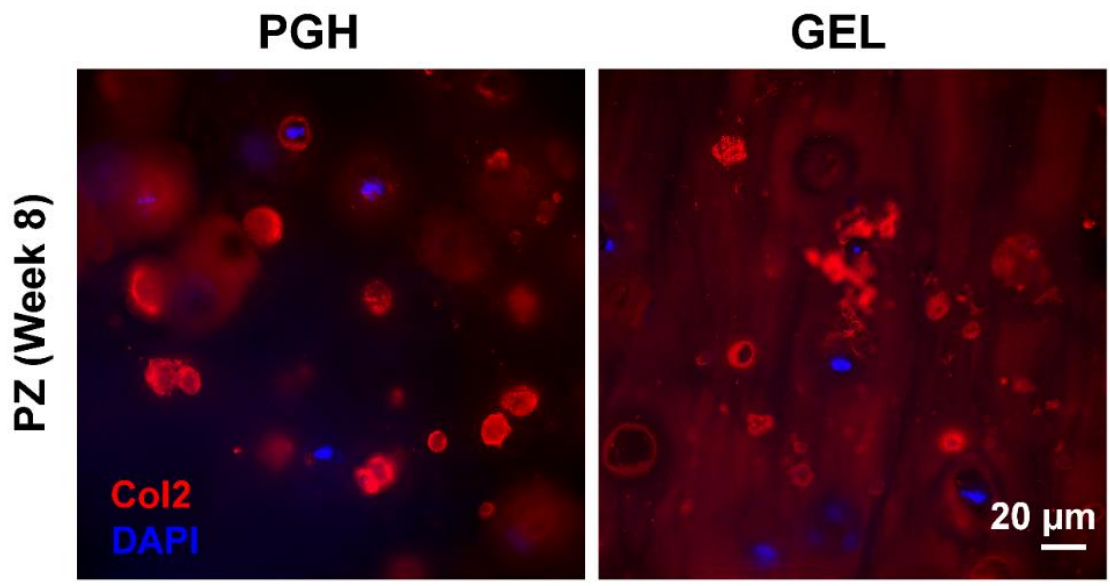

Figure 3-7 Distribution of Col 2 deposition by PZ chondrocytes at 8 weeks of growth. Col2 (red) appeared more localized to the pericellular matrix in PGH than in GEL hydrogels.

3.3.3 Hypertrophy

Chondrocyte hypertrophy can be characterized by cellular enlargement and expression of Col10 and ALP [83-85]. In the hypertrophic zone, Col10 makes up close to half of the total collagen [86]. Overall, PGH showed delayed and reduced accumulation of Col10 by PHZ chondrocytes. No significant Col10 production by PZ cells occurred at any time-points regardless of hydrogel type (Figure 3-8). In GEL, the average Col10 content in PHZ and HZ layers increased significantly at week 3, by 5.4- and 7.2-fold respectively ($p<0.0001$, Figure 3-9 A). Col10 content then decreased at week 8 by 72% and 92% ($p<0.0001$). However in PGH, only PHZ showed a significant increase in Col10 content at week 3 (15-fold, $p= 0.0003$); no significant change occurred at week 8 in both PHZ and HZ layers in PGH. Differences in the average Col10 content between hydrogel types became evident at the later time points. At week 3, the average Col10

content in the PHZ layer was 61% lower in PGH than in GEL at week 3 ($p<0.0001$. In contrast, the HZ layer in PGH showed significantly higher Col10 content at week 1 and week 8 compared to GEL (4.2-fold, $p=0.0069$, and 6.0-fold, $p= 0.0109$).

Similar to Col2, Col10 deposition appeared more pericellular in PGH while farther distributed in GEL by week 3 and onward (Figure 3-8 and Figure 3-10). The concentration of Col10 deposition was higher in PGH than GEL for the PHZ and HZ layers at all time-points ($p \leq 0.0112$, Figure 3-9 B). No differences in concentration of Col10 deposition was detected for the PZ layer between hydrogel types. Similar to changes in the concentration of Col2 over time, the Col10 concentration in the PHZ and HZ layers in PGH decreased at week three by 33% ($p=0.0002$) and 26% ($p=0.0003$), respectively, as the average Col10 content by these populations increased, indicating diffusion of Col10 in PGH. However, the Col10 concentration increased at week 3 in the PHZ layer in GEL by 90% ($p=0.0005$) and subsequently plateaued. The Col10 concentration for HZ remained stable in GEL.

PGH delayed the deposition of Col10 by PHZ chondrocytes by at least one week compared to PHZ cell in GEL (Figure 3-8, Figure 3-9 C). Namely, the fraction of cells positive for Col10 was 11% for PHZ cells in PGH and 91% in GEL at week 1 ($p<0.0001$), and 93% for PHZ in PGH and 98% in GEL at week 3 (no significant difference). Although the fraction of Col10 positive PHZ cells in PGH caught up by week 3, the average Col10 content in PGH was still significantly lower. By week 8, the fraction of Col10 positive cells did not appear to change for PHZ cells in GEL but did significantly decrease in PGH by 54% ($p<0.0001$). In contrast for HZ cells, PGH consistently showed more Col10 positive HZ cells at all time-points (84% at week 1, $p<0.0001$; 1.9-fold at week 3, $p<0.001$; and 1.6-fold at week 8, $p=0.0006$). The fraction of Col10 positive HZ cells decreased over time regardless of hydrogel type ($p\leq0.0010$).

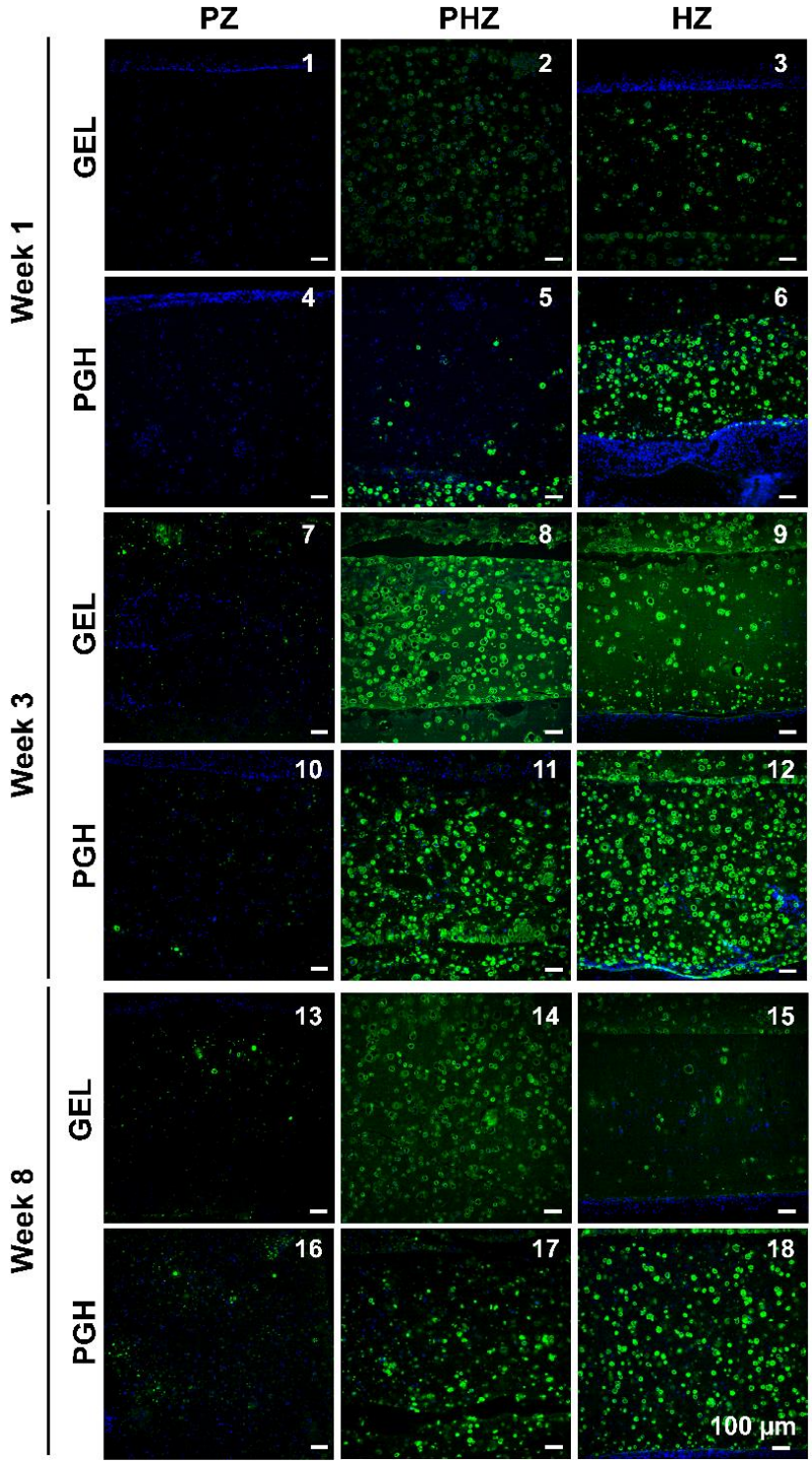

Figure 3-8 Col10 deposition by the different chondrocyte populations over 1, 3, and 8 weeks of growth in vivo in GEL (1-3, 7-9, 13-15) and PGH (4-6, 10-12, 16-18) hydrogel constructs. Immunostain green = Col10, blue = nuclei.

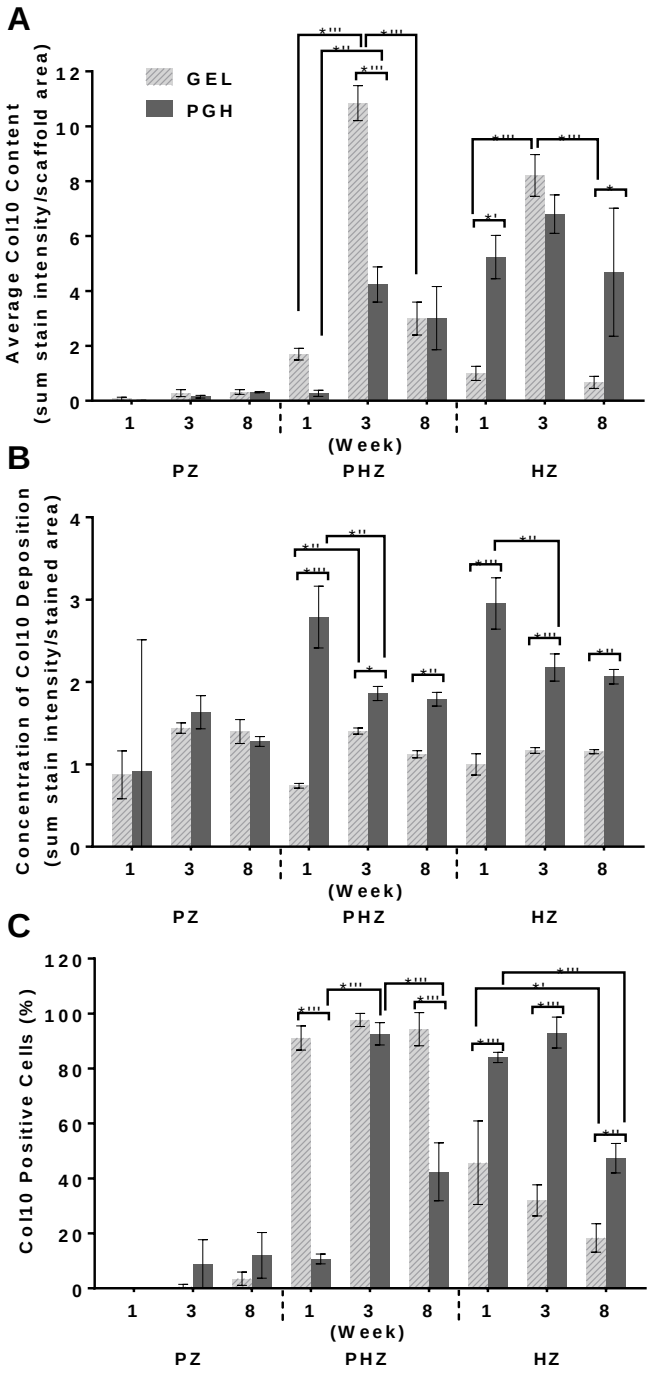

Figure 3-9 Analysis of Col10 deposition in GEL and PGH hydrogel constructs by the different chondrocyte populations over 1, 3, and 8 weeks of growth in vivo. Average Col10 content (A), concentration of Col10 deposition (B), and fraction of Col10 positive cells (C) were quantified by image analysis. *''' = $p < 0.0001$; *'' = $p \leq 0.001$; *' = $p \leq 0.01$; * = $p < 0.05$. Error bars = standard deviation of mean.

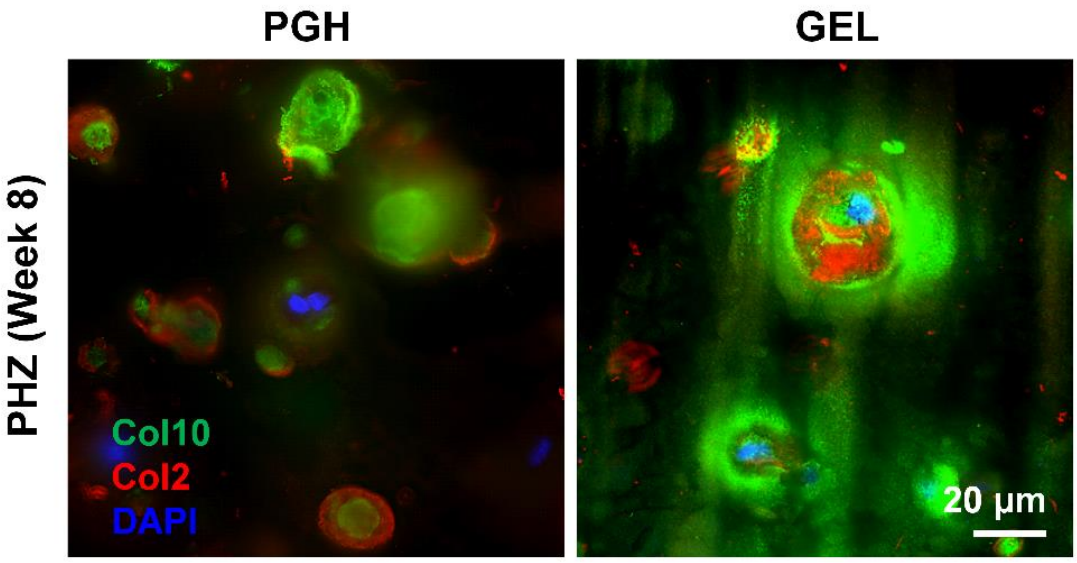

Figure 3-10 Distribution of Col 10 deposition by PHZ chondrocytes at 8 weeks of growth. Col10 (green) appeared more localized to the pericellular matrix in PGH than in GEL hydrogels.

Likewise, PGH showed a higher area of ALP activity in the HZ layer at week 1 and week 3 compared to GEL (13-and 14-fold, $p<0.0001$) (Figure 3-11). However, at week 8, the area of ALP activity decreased by 82% in PGH ($p<0.0001$), while more than quadrupled in GEL ($p=0.0174$), reaching similar levels between hydrogels with no significant difference. For the PZ and PHZ layers, there was no significant difference between hydrogel types at all time-points. The area fraction of ALP activity by PHZ significantly reduced between week 3 to week 8 by at 62% ($p=0.0019$) in PGH and 72% ($p<0.0001$) in GEL ($p\leq0.0019$). ALP staining was confined to the cellular and immediate pericellular area.

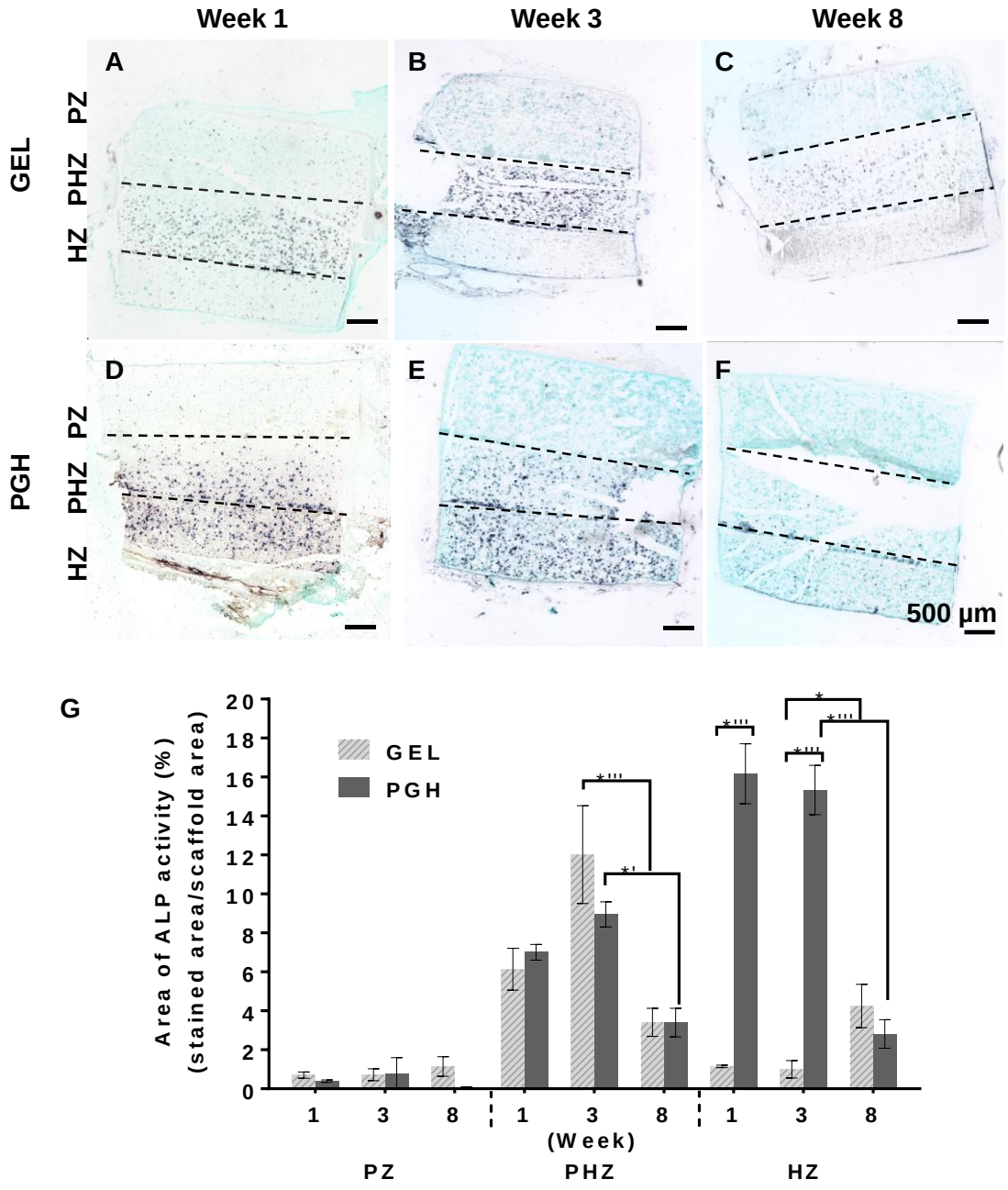

Figure 3-11 Activity of ALP (BCIP stain) secreted by the different chondrocyte populations in GEL (A-C) and PGH (D-F) hydrogel constructs over 1, 3, and 8 weeks of growth in vivo (ALP activity = dark purple, counterstained with Fast Green). Area of ALP activity was quantified by image analysis (G). *''' = $p < 0.0001$; *'' = $p \leq 0.001$; *' = $p \leq 0.01$; * = $p < 0.05$. Error bars = standard deviation of the mean.

3.3.4 Terminal Differentiation

During endochondral ossification, terminally differentiated chondrocytes mineralize the extracellular matrix, with many undergoing apoptosis, to create calcified cartilage that is later remodeled into bone [87]. PGH inhibited mineralization by both PHZ and HZ cells, while GEL permitted mineralization by both as shown by Alizarin red (Figure 3-12A-F) and Von Kossa staining (Figure 3-12 G-L). In GEL, the PHZ and HZ layers showed increasing mineral deposition over time, by 36-fold ($p= 0.0120$) and 6.1-fold ($p<0.0001$) from week 1 to week 8, respectively, as indicated by Alizarin Red stain (Figure 3-13 A), and 6.7-fold ($p=0.0111$) and 5.5-fold ($p<0.0001$) by Von Kossa stain (Figure 3-13 B). Mineralization by PHZ was delayed relative to HZ, evident at week 3 as opposed to week 1. By week 8, 29.44 ± 17.16% of the PHZ layer stained for Alizarin red and 14.769 ± 8.869% for Von Kossa, while 92.84 ± 7.77% of the HZ layer stained for Alizarin Red and 80.229 ± 4.933% for Von Kossa. PZ cells never mineralized regardless of the hydrogel type, consistent with their lack of hypertrophy as shown by low Col10 deposition and ALP activity. In addition, there were significantly more apoptotic HZ cells in GEL compared to PGH at week 8 (86.9% ± 3.6% standard deviation versus 28.1% ± 1.1% respectively, $p<0.0001$, Figure 3-14).

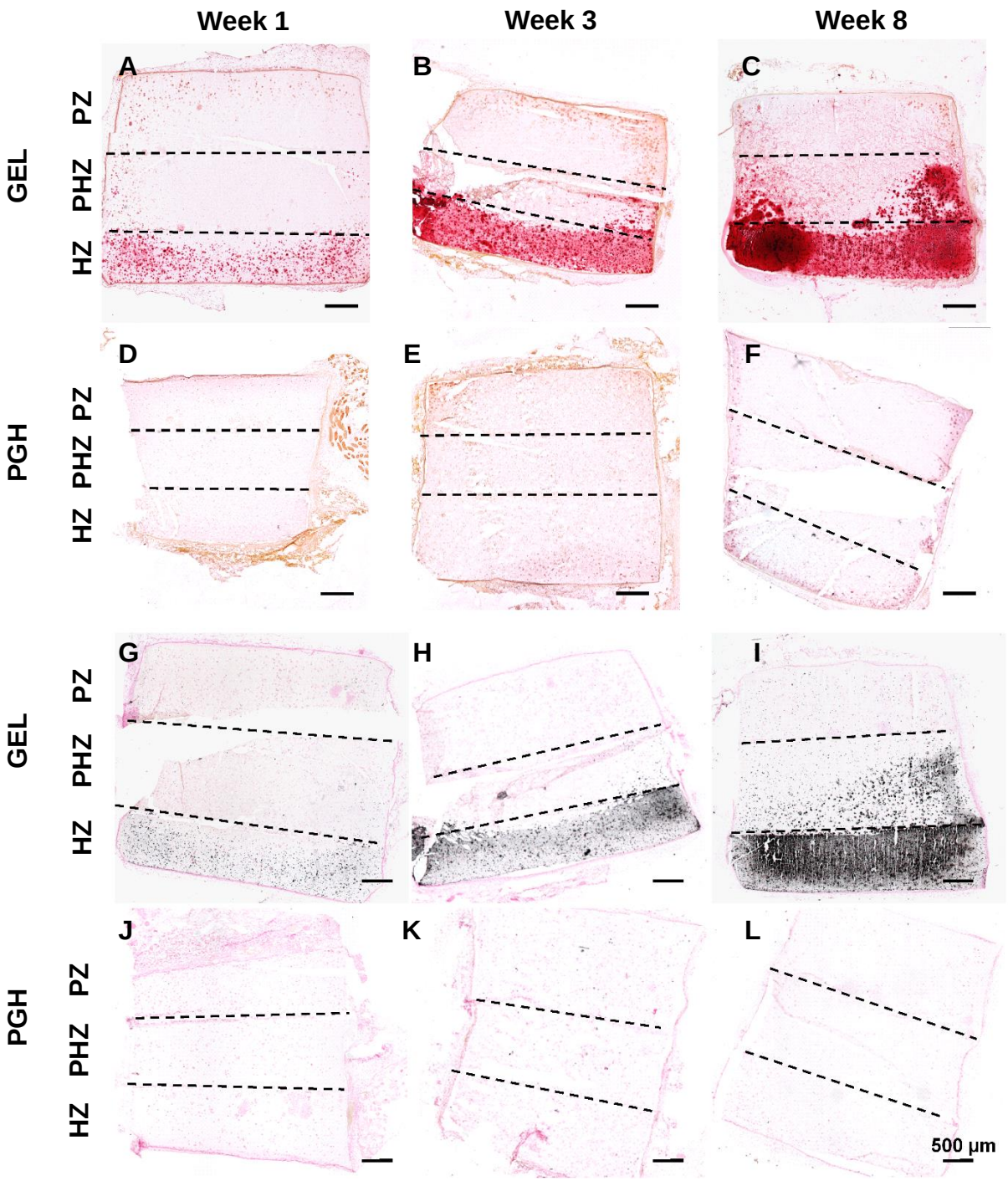

Figure 3-12 Mineral deposition in the different layers of chondrocyte populations in GEL and PGH hydrogel constructs over 1, 3, and 8 weeks of growth in vivo. GEL (A-C, G-I) and PGH hydrogels (D-F, J-L) by Alizarin Red (A-F, red) and Von Kossa stain (G-L, black, counterstained with Fast Red).

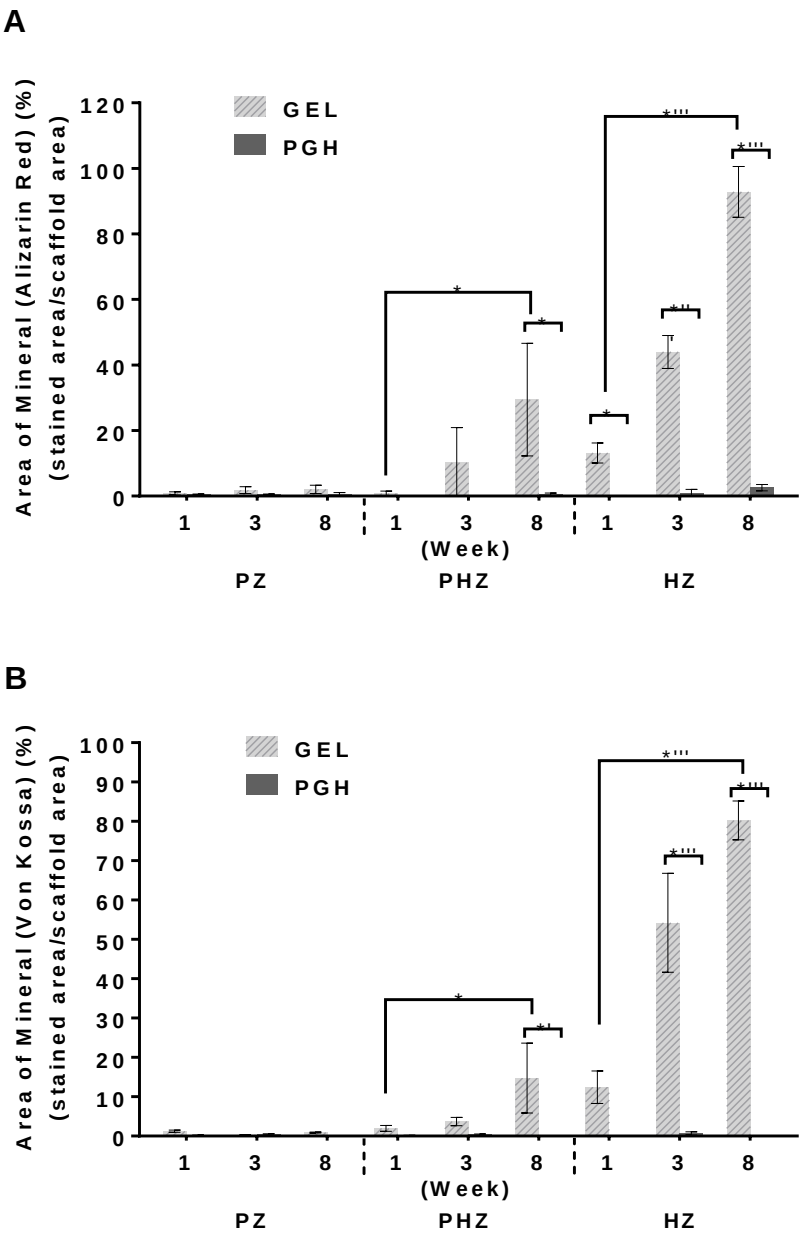

Figure 3-13 Area of mineral deposition was quantified by image analysis. A) Alizarin Red; B). Von Kossa. *''' = $p < 0.0001$; *'' = $p \leq 0.001$; *' = $p \leq 0.01$; * = $p < 0.05$. Error bars = standard deviation of the mean.

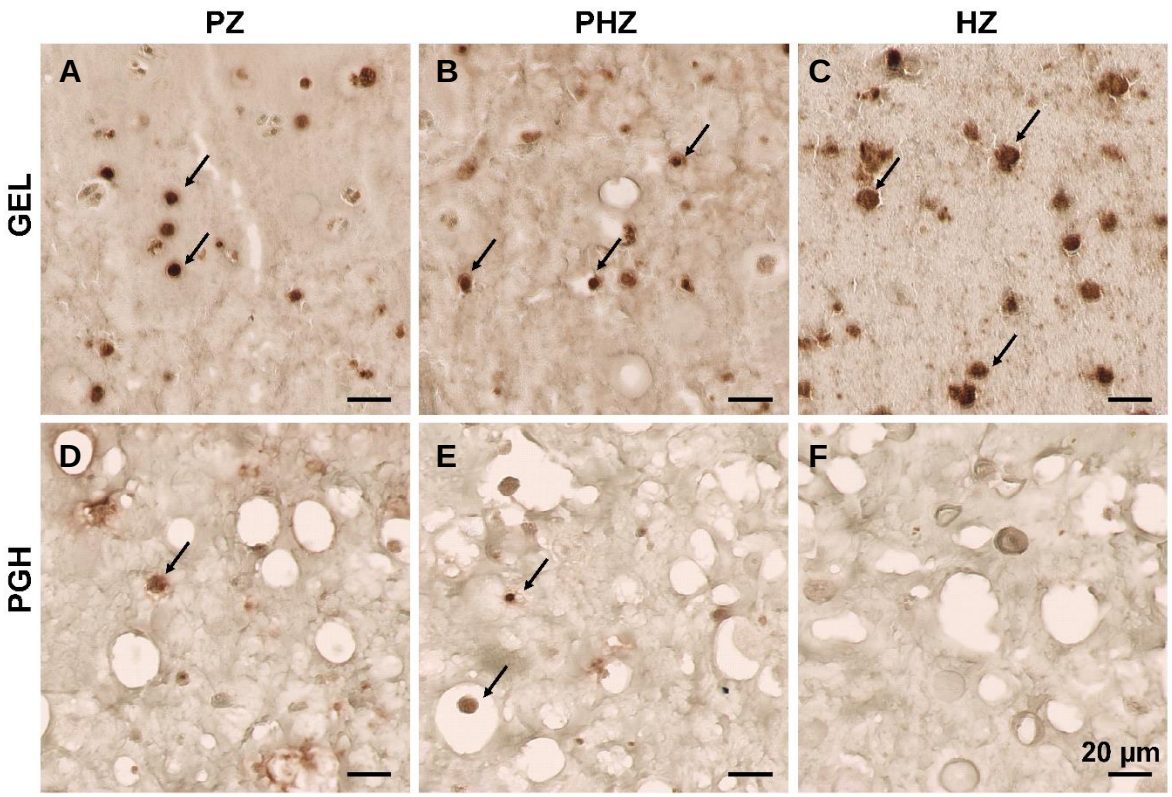

Figure 3-14 Apoptosis (DNA fragmentation) of the different chondrocyte populations in GEL (A-C) and PGH (D-F) hydrogels after 8 weeks growth in vivo. TUNEL stain (dark brown) = apoptotic cells. Arrows indicate examples of apoptotic cells.

3.3.5 Alternate Phenotype Effects

To further characterize the chondrocyte phenotype and investigate potential de-differentiation, we analyzed Col1 deposition over time *in vivo*. Col1 is a matrix molecule present in locations such as the territorial matrix of hypertrophic chondrocytes, bone matrix, and fibrocartilage [83, 84, 88]. Col1 was present, albeit weak, in the day 17 chick sterna from which the chondrocyte populations were harvested (Figure 3-2). In general, PGH delayed the accumulation of Col1 by all three populations by at least 3 weeks (Figure 3-15 and Figure 3-16

A). In PGH, no significant differences were found in average Col1 content over time until week 8, when a marked increase occurred, by 3.9-fold for the PZ ($p<0.0001$), 4.4-fold for PHZ ($p<0.0001$), and 3.5-fold for HZ layers ($p<0.0001$, Figure 3-16 A). However, all populations in GEL showed an earlier increase in Col1 content at week 3, by 3.0- ($p<0.0001$) for the PZ, 4.6- ($p<0.0001$) for PHZ, and 2.0-fold ($p=0.0451$) for HZ layers. Subsequently at week 8 in GEL, the PZ layered plateaued while PHZ and HZ layers decreased in Col1 content (52%, $p<0.0001$ and 71%, $p=0.0397$, respectively), consistent with mineralization of the latter. Comparing between hydrogel types, no significant differences in average Col1 content were apparent at week 1. By week 3, the PZ and PHZ layers in PGH showed 83% and 80% ($p<0.0001$) lower Col1 content compared to GEL. Yet by week 8, the PHZ and HZ layers showed greater Col1 content in PGH compared to GEL (1.2- and 9.2-fold, respectively, $p<0.0001$). Only PZ showed lower Col1 content in PGH than GEL at week 8 (15%, $p= 0.0034$). Overall, the concentration of Col1 deposition appeared higher in PGH than in GEL (Figure 3-16 B). Col1 concentration was significantly higher in PGH for the PZ and PHZ layers at week 1 (38%, $p<0.0001$, and 25%, $p=0.0006$). Only the PZ layer in PGH was significantly greater compared to GEL at week 3 (15%, $p=0.0024$), while both the PHZ and HZ layers in PGH at week 8 (23%, $p=0.0006$ and 21%, $p=0.0034$). The fraction of Col1 positive cells did not change for all three populations in PGH. However in GEL, the fraction of HZ cells positive for Col1 decreased 46% at week 8 ($p<0.0001$), consistent with greater apoptosis and high mineralization of the layer at this time; the fraction of Col1 positive PZ and PHZ cells did not change in GEL (Figure 3-16 C).

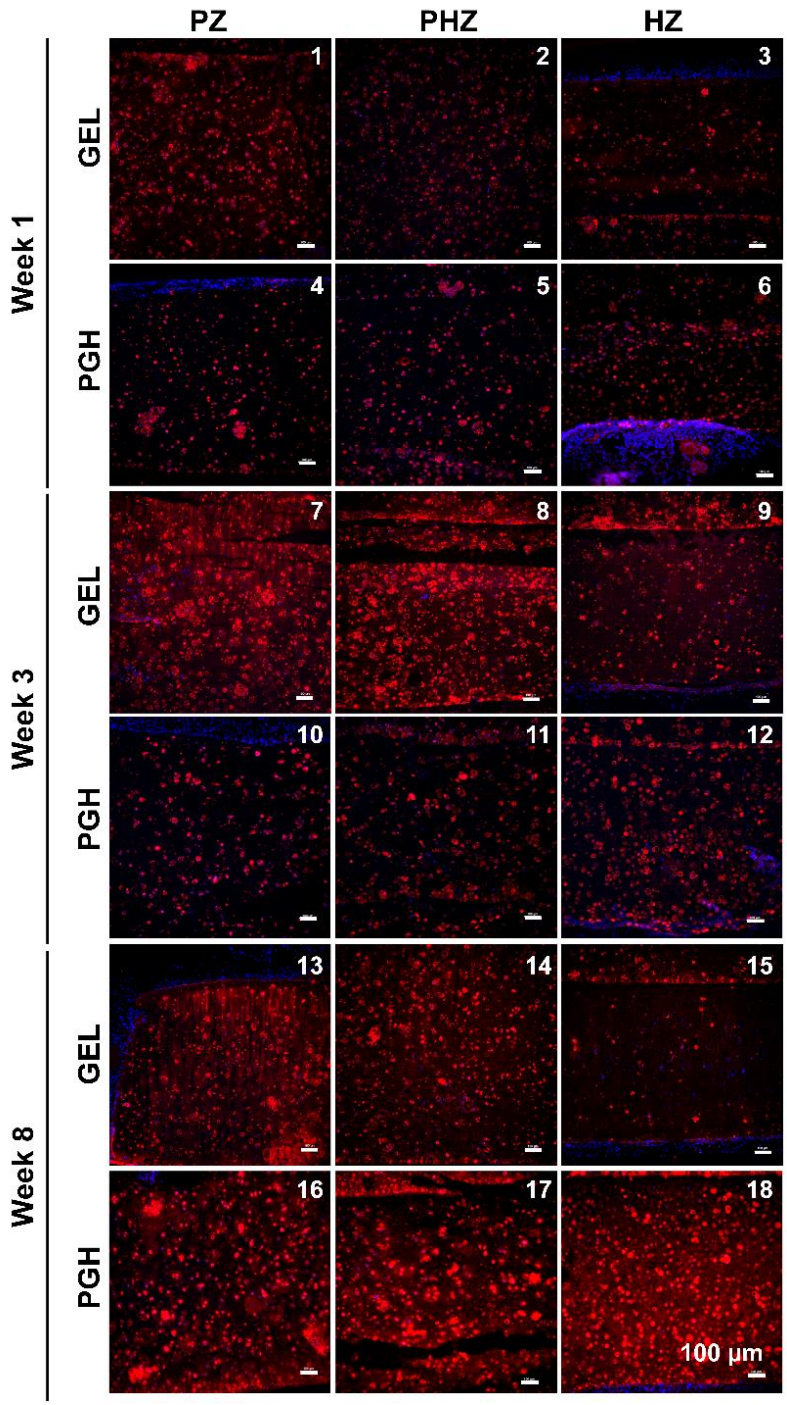

Figure 3-15 Col1 deposition by the different chondrocyte populations over 1, 3, and 8 weeks of growth in vivo in GEL (1-3, 7-9, 13-15) and PGH (4-6, 10-12, 16-18) hydrogel constructs. Immunostain red = Col1, blue = nuclei.

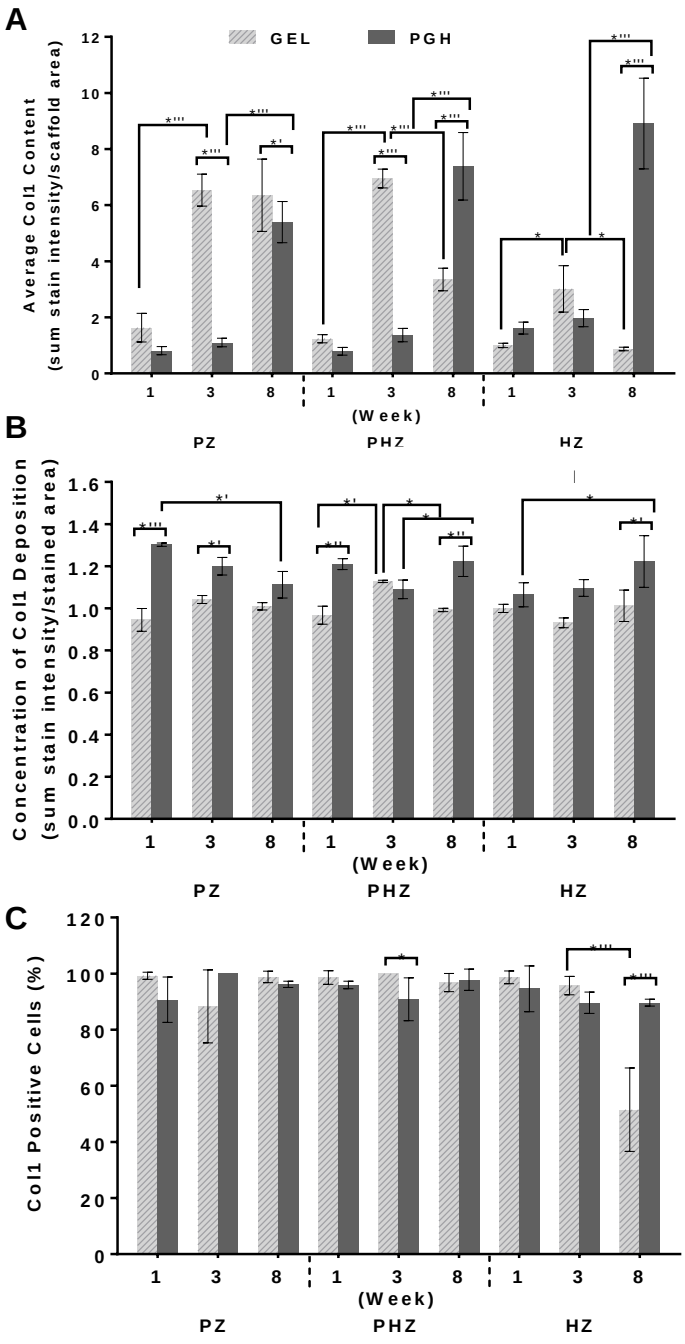

Figure 3-16 Analysis of Col1 deposition in GEL and PGH hydrogel constructs by the different chondrocyte populations over 1, 3, and 8 weeks of growth in vivo. Average Col1 content (B), concentration of Col1 deposition (C), and fraction of Col1 positive cells (D) were quantified by image analysis. *''' = $p < 0.0001$; *'' = $p \leq 0.001$; *' = $p \leq 0.01$; * = $p < 0.05$. Error bars = standard deviation of mean.

3.4 Discussion

This work shows that hydrogel composition alone can regulate the maturation of chondrocyte populations. We tested populations that are similar to those which compose cartilaginous interfacial tissues such as the growth plate. Compared to the host mouse cells, the encapsulated chicken chondrocytes were morphologically different (smaller size, round shape). Therefore, it was unnecessary to label implanted chicken cells to distinguish them from the host cells.

Contrary to the effects of GEL (gelatin only hydrogel) on HZ cells (hypertrophic chondrocytes), the PGH (hydrogel composed of PEG, gelatin, and heparin) maintained GAG accumulation, decreased ALP activity, and inhibited mineralization by HZ cells out to two months growth *in vivo,* while maintaining to a large degree the deposition of collagens (Col1, Col2, Col10). These results indicate that PGH arrested maturation and terminal differentiation of HZ cells, retaining them in a GAG producing state. Early HZ (aka "upper part" of the hypertrophic zone in the growth plate) are highly matrix synthetic, expressing Col2, Col10, and aggrecan proteoglycan (consisting of GAGs covalently linked to a protein core) [10, 89]. It is not until the late HZ or terminal differentiation region (aka "lower part" of the hypertrophic zone) that aggrecan synthesis declines, while Col2 continues and ALP synthesis increases. In native chick sternum (day 17 incubation at which time cells were isolated), we found the highest GAG content at the cephalic region, not the medial or caudal regions, consistent with an early HZ phenotype.

PGH promoted maintenance of HZ chondrocytes in an early hypertrophic state. After growth *in vivo* for 1 week, we found a significantly greater fraction of HZ cells in PGH were positive for GAG deposition compared to PHZ cells in PGH and HZ cells in GEL. We also observed a significantly greater area of GAG deposition by HZ cells in PGH compared to PHZ

cells in PGH and to all three populations in GEL (trend compared to PZ cells in PGH). However, the fraction of GAG positive HZ cells in PGH did significantly decline over time, approximately 19% by week 8, and the area of deposition in the HZ layer in PGH was ultimately exceeded by the PZ layer regardless of hydrogel type. Nevertheless, the fraction of GAG positive HZ cells at week 8 was not significantly different from that of PHZ cells at all time-points in PGH. Concomitantly, we did not observe any change over time in the average Col2 content, consistent with the literature; only the concentration slightly decreased, likely due to further diffusion away from cells. Thus, these results support the conclusion that PGH facilitated maintenance of HZ cells in an early hypertrophic state. It is worthwhile to note that the phenotype of HZ cells in PGH also resembles chondrocytes in the deep zone of healthy articular cartilage, which also express high GAG and low Col2 protein, and do not mineralize [90]. Indeed, Col10 protein and ALP are detectable in articular cartilage, particularly the deep zone [91-93].

This study demonstrates a new multi-cell type, tri-layered *in vivo* model to evaluate scaffold effects on chondrocyte populations and scaffold suitability for the repair of cartilaginous tissues that interface with bone such as the growth plate repair. Layered hydrogel fabrication has been used to recreate the zonal organization and matrix properties of articular cartilage [90, 94, 95]. However, these studies have not investigated the stability of the different articular chondrocyte phenotypes in engineered materials, specifically deep zone cells and their potential to undergo terminal hypertrophy and mineralization. In our work, we instead focused on growth plate-like chondrocyte populations, which do share some phenotype similarities with articular chondrocyte populations. We further employed a panel of matrix markers to characterize their phenotype in our hydrogel materials, including hypertrophy and matrix mineralization. Both PGH and GEL maintained the phenotype of PZ cells, evident by round cell morphology and production

of GAG and Col2. PGH and GEL also supported the maturation of PHZ and HZ cells, characterized by enlarged lacunae and pericellular Col10. However, PGH delayed maturation and inhibited terminal differentiation, while GEL was permissive for terminal differentiation and mineralization over a time-course that resembled the natural temporal profile in the chicken embryo [74, 96]. These results indicate that GEL is best suited for regenerating cartilages that mineralize or undergo endochondral ossification, such as the calcified zone of articular cartilage and the growth plate. This is of timely relevance to the field of cartilage regeneration, as GEL has been utilized for stem cell and chondrocyte based engineering of articular cartilage [97, 98], and is a popular bioink for bioprinting [65, 99]. Conversely, PGH is more suitable for scenarios where chondrocyte mineralization is undesirable, such as in the upper zones of articular cartilage and the resting zone of the growth plate.

Though unique, the composition of PGH is similar to other composite hydrogels developed for cartilage regeneration. As noted in section 1.6, we selected the PEG component to resist cell-mediated contraction, gelatin to promote chondrocyte survival, and heparin to mimic the GAG matrix composition of growth plate cartilage. Addition of hyaluronan (a non-sulfated but acidic GAG) and chondroitin sulfate (a sulfated GAG) to gelatin hydrogels has been shown to enhance re-differentiation of human articular chondrocytes and cartilage matrix secretion *in vitro* over 8 weeks [100]. Likewise, the addition of these GAG to collagen hydrogels creates an interpenetrating polymer network that supports articular chondrocyte matrix deposition [101]. Composite hydrogels of gelatin and hyaluronan are in development for stem cell-based cartilage regeneration [102].

Furthermore, incorporation of heparin into gelatin hydrogels has been shown to increase GAG accumulation by chondrocytes derived from articular cartilage [103]. Heparin modified

PEG hydrogels have been investigated, albeit for osteogenesis [62]. Gelatin modified PEG has been shown to improve chondrogenic differentiation by mesenchymal stem cells compared to PEG only hydrogels under chondrogenic conditions *in vitro* [40]. A three-part composite hydrogel composed of acrylated PEG, thiol-modified gelatin, and thiol-modified hyaluronan is commercially available (HyStem^{TM}, ESI BIO); however, it relies on different crosslink chemistry and little work has investigated its utility for cartilage regeneration [104]. Numerous other hydrogel formulations exist for cartilage engineering, including blends of several GAGs and polysaccharides, or single GAGs alone [105, 106]. We selected heparin over other GAGs because hyaluronan is not sulfated, and because chondroitin sulfate is less electronegative and has lower affinity for chondrogenic growth factors [107, 108]. Instead, heparin promotes signaling of numerous growth factors produced by chondrocytes, including transforming growth factor β-1 (TGFβ-1) [41-47]. As such, it can potentiate and interfere with autocrine cellular signaling. Affinity-based selection of alternate heparan sulfated GAGs with desired growth factor binding properties may provide a more targeted approach [109]. Nevertheless, no prior study with hydrogels has shown that they can inhibit terminal differentiation and mineralization by chondrocytes, as shown here.

Through control over chondrocyte phenotype, these photocrosslinkable hydrogels are of potential utility in engineering the complex cellular architectures of interfacial cartilages, particularly for regeneration *in situ*. For example, maintenance of chondrocyte phenotypes and protection from premature hypertrophy may facilitate the reestablishment of the interzonal signaling that orchestrates cell proliferation and maturation in the growth plate, and subsequently, restore normal endochondral ossification and bone growth. Hydrogels can be micropatterned to replicate the cellular architecture of the growth plate. Numerous techniques exist to create multi-

layered hydrogels with different biological functions in the layers (e.g., cell populations, drug-eluting microparticles, matrix molecules, stiffness gradients); for a review, see Liu et al. 2018 [110]. Cell sourcing and expansion issues limit the translation potential of patterning of different cell populations. More readily translatable approaches require delivery of spatial cues to guide the differentiation of progenitor cells *in situ*. However, the mechanoactive environment *in situ* engenders interstitial fluid flow that disrupts the spatial distribution of growth factors eluted from delivery vehicles embedded in hydrogels [41]. Therefore, we have focused on developing scaffold materials to guide cell differentiation and phenotype. The matrix molecules of the GEL and PGH hydrogels are insoluble by nature of their crosslinking and remain in place until degraded, presumably by which time the cellular architecture would be restored and self-sustained by endogenous matrix and intercellular signaling. Such an approach has not been adopted for growth plate regeneration.

It is important to note that these chick sternal chondrocyte populations, though similar in phenotype, are derived from a different developmental lineage than chondrocyte populations in the growth plate, and are subject to different epigenetic regulation. In our study, all cell populations expressed Col1 *in vivo*, with a strong cytoplasmic signal throughout the study, but with a faint extracellular signal detectable only at the later time points. Though the change over time in the Col1 content within the territorial matrix appeared large, it is important to note that the content measured was normalized to the HZ layer in GEL at week 1, which had very low signal. The absolute signal intensity increase was low, and staining remained faint throughout. It is unlikely that the source of extracellular Col1 was fibroblasts in the fibrous capsule and fascia which surrounded the implant, as the faint staining appeared stronger in the pericellular rather than territorial matrix. In the growth plate, Col1 has been detected intracellularly in hypertrophic

chondrocytes [111], and the territorial matrix of the "lower" hypertrophic zone (late hypertrophic chondrocytes) [84]. Col1 is also expressed in the perichondrium, osteoid, and new bone of [86, 112]. The strong cytoplasmic Col1 expression in HZ and PHZ cells is consistent with that of hypertrophic chondrocytes in the growth plate, including the prehypertrophic cells that become hypertrophic. However, Col1 expression by the PZ cells is not consistent with proliferative cells of the growth plate. In addition, Col1 expression in the chick sternum has not been reported [49]. However, in our study, we did observe weak Col1 expression in the native chick sternum by all three chondrocyte populations (Figure 3-2). Together with the continued GAG and Col2 expression, this likely excludes de-differentiation (from prolonged growth in an ectopic site) as a potential cause for Col1 expression by PZ [100, 113, 114]. It is possible that PZ were pushed to a more perichondrium-like phenotype, which includes expression of Col1, Col2, and GAG (namely aggrecan) [115], or that chick Col1 expression is another difference between avian and mammalian species [116].

The cellular mechanisms underlying the hydrogel effects on chondrocyte phenotypes have not been investigated in this study. Both hydrogels types had insignificant vascular invasion across all layers, precluding uncoupling of angiogenesis as the inhibitor of terminal hypertrophy and mineralization [70]. The unique composition of PGH may directly interfere with mineralization, provide matrix ligand and mechanical cues to directly alter phenotype, and/or bind endogenous growth factors to indirectly alter autocrine/paracrine signaling. Regarding physical inhibition of mineralization, the content of heparin in PGH is well above that shown to inhibit aggregation of hydroxyapatite crystals *in vitro* [50]. The incorporation of heparin into fixed tissues (bioprosthetic heart valves) can inhibit calcification [117]. The heparin component may affect the transport of anionic species required for mineralization (as opposed to binding of

calcium [118, 119]), namely phosphate. The continued GAG deposition by HZ and PHZ cells in PGH may also have physically inhibited hydrolysis of pyrophosphate by ALP [120] and thereby mineral nucleation and growth [119, 121]. Furthermore, PGH may have retained fewer matrix vesicles secreted by HZ and PHZ cells than GEL, due to differences in Col2 and Col10 content [11, 122, 123].

Regarding mechanical cues, the lower relaxation modulus of PGH compared to GEL is unlikely to drive the observed effects. Chondrocytes are mechanosensitive, and their phenotype can be altered by substrate stiffness and mechanical stress [57, 58].

No apparent differences in cell morphology were evident between the GEL and PGH hydrogels at week 1. Yet HZ cells in PGH showed greater RhoA gene expression than in GEL after culture for one week (not shown), though the PGH relaxation modulus (described in Aim 1) was lower. We speculate that the greater gelatin content and stiffness in GEL inhibited integrin receptor clustering and formation of focal adhesion complexes compared to PGH.

Regarding cell signaling, the effects of direct signaling by the hydrogel polymers are likely most evident at the early time point, as pericellular matrix deposition changes the ligand milieu. The gelatin polymer is a substrate for integrins αvβ3 and α5β1. Blocking of β1 integrin signaling decreases Col10 production and hypertrophic differentiation in organ explant cultures of chick sterna [79]. Targeted antagonism of α5β1 integrin decreases Col2 and Col10 expression decreases apoptosis and inhibits differentiation of prehypertrophic chondrocytes in embryonic mouse limbs (exo utero and in limb organ cultures) [124, 125]. This is consistent with the lower Col2 and Col10 deposition at week 1 by PZ and PHZ cell sin PGH, which contains about 5x less gelatin than GEL. However, this does not explain the higher Col10 deposition by HZ cells in PGH than in GEL at week 1, and the inhibition of terminal differentiation and mineralization by HZ cells

throughout. Instead, PGH may inhibit terminal differentiation by binding and promoting signaling of endogenous growth factors which hinder hypertrophy and terminal differentiation, such as Fibroblast growth factors (FGFs) [2, 126, 127], IHH [2], and TGFs [128-131]. Specifically, the heparin component of PGH interacts with these growth factors [46, 74, 132-136]. Inconsistent with our results, heparin has been found to decrease total collagen synthesis as well as type X collagen production by embryonic chicken chondrocytes[137]. Future work is needed to investigate the intracellular signaling mechanism underlying the inhibition of terminal differentiation and mineralization, particularly the Wnt/β-catenin pathway which is a key regulator of hypertrophy and endochondral ossification [138, 139].

In this present work, the three chondrocyte populations were encapsulated respectively in three neighboring hydrogel layers of the same construct rather than in three separate hydrogel constructs containing a homogenous cell population. This design mimicked the cellular organization of native growth plate and allowed us to analyze the phenotypes of chondrocytes when they were adjacent to cells at other differentiation stages. Image-based quantitative analysis of protein deposition was used because the individual layers could not be repeatably separated from the tri-layered constructs for reliable biochemical analysis. Such approach is a low-cost alternative and has been described by Kirkeby et al.in 2005 [140]. It is worth noting that the image-based analysis of histochemical stains (GAG, Alizarin Red, Von Kossa, and ALP activity) may not be as accurate as a biochemical method. Accuracy of the analyses is also sensitive to section thickness. We were careful to analyze sections of the same thickness (10 μm) and stained at the same time and for the same duration. We cannot fully characterize the precise phenotype of the chondrocyte populations using our limited but specific biochemical and antibody marker panel. This will require RNA sequencing and proteomics approaches. Future work is necessary

to elucidate the material and molecular mechanisms driving the hydrogel effects. This includes investigation of ratio of phosphate to pyrophosphate (a potent inhibitor of crystal growth), matrix vesicle secretion by chondrocytes [141], the composition and crystal structure of mineral deposited, the effect of substrate stiffness on cytoskeletal structure and focal adhesion complex (FAC), and potential changes in hydrogel stiffness during culture *in vivo* to understand mechanotransduction effects. It will also be interesting to determine if PGH will inhibit mineralization by osteoblasts or by HZ cells under thyroid hormone stimulation [142].

3.5 Conclusion

This work shows that hydrogel composition alone can regulate the maturation of growth plate-like chondrocyte populations. Compared to GEL (gelatin hydrogel), PGH (composite hydrogel) maintained GAG production by HZ cells (hypertrophic chondrocytes), arrested terminal differentiation, and inhibited mineralization. Through control over chondrocyte phenotype, the PGH hydrogel is of potentially critical utility in engineering the complex cellular architectures of the growth plate *in situ*.

4.0 Specific Aim 3: Evaluate the Effects of the PGH Hydrogel on Stem Cell Chondrogenesis and Osteogenesis *In Vitro* and *In Vivo*

4.1 Introduction

Hydrogels are very popular because they can mimic the hydrophilic matrix composition of cartilage, carry cells and drugs, and promote chondrogenesis, with novel studies seeking to develop biocompatible hydrogels that mimic cartilage compressive stiffness [143]. Yet the loss of chondrocyte phenotype remains a problem in the regeneration of hyaline cartilage, whether progression to hypertrophy or dedifferentiation into fibroblast-like cells [144, 145]. Bone marrow-derived mesenchymal stem cells (BMSCs) are a viable cell source for regeneration because they can be driven down multiple lineages, including cartilage. Indeed, commercial products exist that employ autologous BMSCs for cartilage regeneration [146]. However, the phenotype of BMSC derived chondrocytes is unstable, progressing to terminal hypertrophy and tissue mineralization¸ which ultimately leads to endochondral ossification [147-151]. Other mesenchymal stem cell (MSC) sources, such as adipose or synovial, also suffer hypertrophy or unstable phenotype [152, 153]. Recent work has identified chondroprogenitor cells within cartilage, which express lower levels of hypertrophy markers when cultured in hydrogels [154]. However, cell sourcing and expansion issues limit their applicability for cartilage engineering compared to BMSCs. In this light, a need exists for hydrogels that promote stable chondrogenic differentiation of BMSCs.

Moreover, hydrogels are needed that can control BMSC differentiation down multiple lineages to regenerate the cellular architecture of the growth plate cartilage. Multiple materials

and scaffold assembly approaches, including hydrogel bioinks and solid free form fabrication technologies, have been advanced to promote development of the natural layered cellular architecture of interfacial tissues, as well as osteochondral tissues, including discrete printing/encapsulation of different cell types or growth factors and multi-part scaffold assembly [68, 155-159]. Studies have attempted to guide BMSC differentiation *in situ* to recapitulate the cellular architecture [160, 161]. However, instability of the chondrocyte phenotype and uncontrolled differentiation down alternate lineages remain a difficulty.

To work towards regeneration of growth plate cartilage with BMSCs, this work sought to develop a photopolymerizable hydrogel to overcome these limitations, namely to drive BMSC chondrogenesis in situ without aberrant osteogenesis or mineralization.

The objective of this study was to characterize the PGH hydrogel and evaluate its effects on chondrogenesis and osteogenesis by BMSCs compared to the GEL-MA only hydrogel (GEL), which served as a control used for chondrogenic and osteogenic differentiation by BMSCs [154, 162]. We evaluated BMSC differentiation and growth in the hydrogels *in vitro* using cultures with chemically defined mediums, and *in vivo*, using implantation of scaffolds in subcutaneous pockets in immunocompromised mice.

4.2 Materials and Methods

4.2.1 Materials

PEGDA, GEL-MA, HEP-MA, and LAP were synthesized as described in section 2.2.2. Cell culture supplies were purchased from Atlanta Biologicals (Flowery Branch, GA) and Thermo

Fisher Scientific (Waltham, MA). Transforming growth factor beta-3 (TGFβ-3) was purchased from R&D Systems (Minneapolis, MN). The 16G Jorvet bone marrow needle was purchased from Henry Schein Animal Health (Melville, NY). Ficoll-Paque PLUS and other stem cell isolation supplies were purchased from Thermo Fisher Scientific. The Von Kossa Stain Kit was purchased from American MasterTech (Lodi, CA). Primers were synthesized by Integrated DNA Technologies (Coralville, IA). Immunocompromised mice, NOD.CB17-Prkdcscid/SzJ, were obtained from Jackson Laboratory (Bar Harbor, ME). Spanish goats were purchased from K-Bar Livestock, LLC (Sabinal, TX).

4.2.2 BMSCs Isolation and Culture

Human BMSCs (hBMSC) and expansion medium were purchased from RoosterBio, Inc (Frederick, MD). Goat BMSC were isolated from bone marrow aspirates drawn from the iliac crests of 3-month-old female Spanish goats using 16G bone marrow biopsy needles and 10mL syringes loaded with 3 mL α-MEM medium containing 180 U/mL heparin. Erythrocytes were removed via Ficoll-Paque PLUS following the manufacturer's protocol. The mononuclear cells were plated and goat BMSCs isolated as tissue culture adherent cells. Both human and goat BMSCs were expanded for three passages (1 week each) for experimental use. Cells were cultured until 80% confluence, trypsinized, and plated at 7.5×10^5 cells per 175 cm^2 cell culture flasks.

4.2.3 Hydrogel Fabrication

The hydrogel solutions were prepared by dissolving the modified polymers at 10% (w/v) in PBS and adding 0.01% (w/v) LAP. The PGH hydrogel was composed of PEGDA, GEL-MA, and HEP-MA at a 63:21:16 mass ratio. The GEL was composed of only GEL-MA. The prepared solutions were then mixed with human or goat BMSCs at 30 million/mL, cast in silicone molds as 2 mm thick sheets, and photocrosslinked with 2.5 J/cm^2/mm UV-A light (365 nm) for 3.5 minutes. Cylindrical hydrogel constructs were cut using 5 mm biopsy punches.

4.2.4 Material Effects on BMSCs *In Vitro*

To select BMSCs with potential to undergo chondrogenesis, cells from several goats were screened in a standard pellet culture over 6 weeks in chemically defined chondrogenic medium. Chondrogenic medium consisted of Gibco high glucose DMEM, ITS 1/100X, 100 μM L-ascorbic acid 2-phosphate, 100 nM dexamethasone, 40 μg/mL L-proline, 10 ng/mL TGFβ-3, and 0.1 mM non-essential amino acids. Three donors were selected with histological evidence of chondrogenesis (GAG staining) and used for replicates of the following experiments. To evaluate the hydrogel material effects under controlled conditions, scaffold cylinders were cultured in either osteogenic medium or chondrogenic medium for 6 weeks (n = 3 for each hydrogel type and culture medium). Osteogenic medium consisted of Gibco GLUTAMAX αMEM, 10% fetal bovine serum, 1% P/S, 10 nM dexamethasone, 5 mM β-glycerolphosphate, 50 μM L-ascorbic acid 2-phosphate. Following 6 weeks, the scaffolds were analyzed with histology for the presence of GAG and mineral.

4.2.5 Material Effects on BMSCs *In Vivo*

The PGH and GEL we loaded with pooled hBMSCs from two patients and with 50 ng/mL TGFβ-3 before crosslinking. The hydrogel cylinders were implanted in dorsal subcutaneous pockets in 5-week-old male mice under IACUC approval (n= 6 per scaffold type, 11 mice total). Briefly, two incisions were made cranial and caudal along the midline and pockets opened to the left and right using a blunt-tipped scissors. After placing the scaffold, incisions were closed with surgical clips. The animals were sacrificed at 8 weeks, and the constructs collected for analysis. The tissues were processed for cryosectioning, which entailed immersion in 30% (w/v) sucrose in PBS overnight followed by 40% (v/v) O.C.T. Compound (Thermo Fisher) in PBS for two days, followed by snap freezing and embedding in O.C.T. GAG deposition was detected by Safranin O staining (with Fast Green counterstain) and the percent of GAG positive cells was calculated (number of cells surrounded with GAG ÷ total number of cells). Minerals were detected by Von Kossa staining. Chondrogenic and osteogenic gene expression was analyzed by real-time polymerase chain reaction (PCR) for cartilage markers aggrecan (AG) and collagen type II (COL2), for the hypertrophic marker collagen type X1 (COL10), and the osteogenic marker bone sialoprotein-II (BSP) using our published primers [163]. RT-PCR results were calculated relative to the GEL, normalized to GAPDH expression, and plotted as "proportional fold change" to facilitate graphical interpretation, where increases are fold change minus 1.0 (i.e., $2^{-\Delta\Delta CT}$-1), decreases are the inverse of fold change minus 1.0 (i.e. -($2^{\Delta\Delta CT}$-1), and no change reads as 0.0.

4.2.6 Statistical Analysis

Results are expressed as mean ± standard deviation (SD). Significant differences in gene expression (PCR) were detected at anα=0.05 using t-tests on the $\Delta\Delta$CT values (normally distributed).

4.3 Results

4.3.1 Effect of PGH and GEL on Chondrogenesis and Osteogenesis *In Vitro*

Chondrogenesis was seen in both the PGH and the GEL in chondrogenic medium (Figure 4-1 A, B, respectively), with staining confined to the pericellular region and staining intensity stronger in the GEL (n=3 per scaffold). No evidence of GAG staining was found for scaffolds cultured in osteogenic medium (Figure 4-1 C, D). Signs of osteogenesis was only observed in the GEL in the osteogenic medium, as evidenced by mineralization staining (Figure 4-2 D). No Von Kossa staining was evident in the PGH (Figure 4-2 C). No sign of mineralization was observed in both hydrogels cultured in chondrogenic medium (Figure 4-2 A, B).

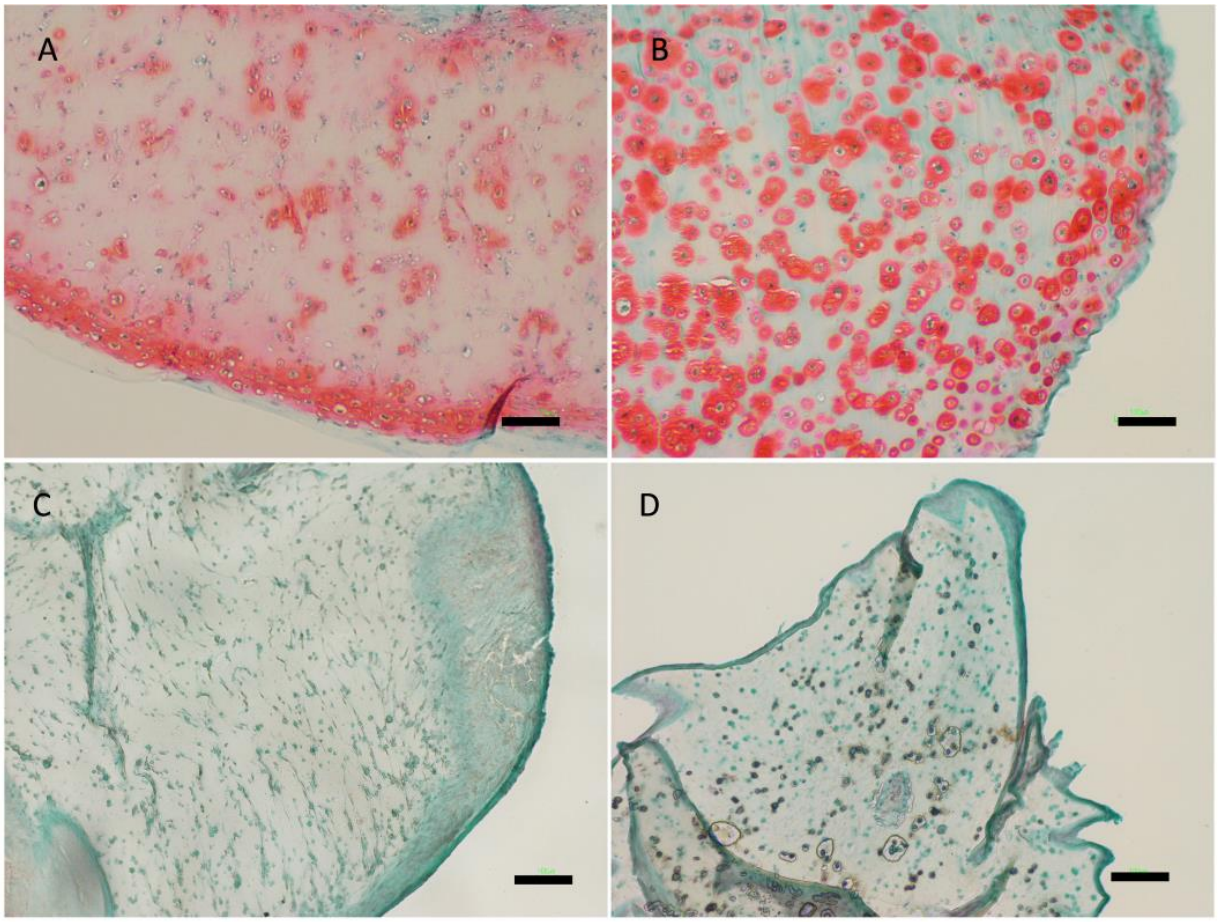

Figure 4-1 Safranin-O staining of PGH and GEL hydrogels containing goat BMSCs after *in vitro* culture. (A, B) Culture in chondrogenic medium. (C, D) Culture in osteogenic medium. Scale bar = 100 µm.

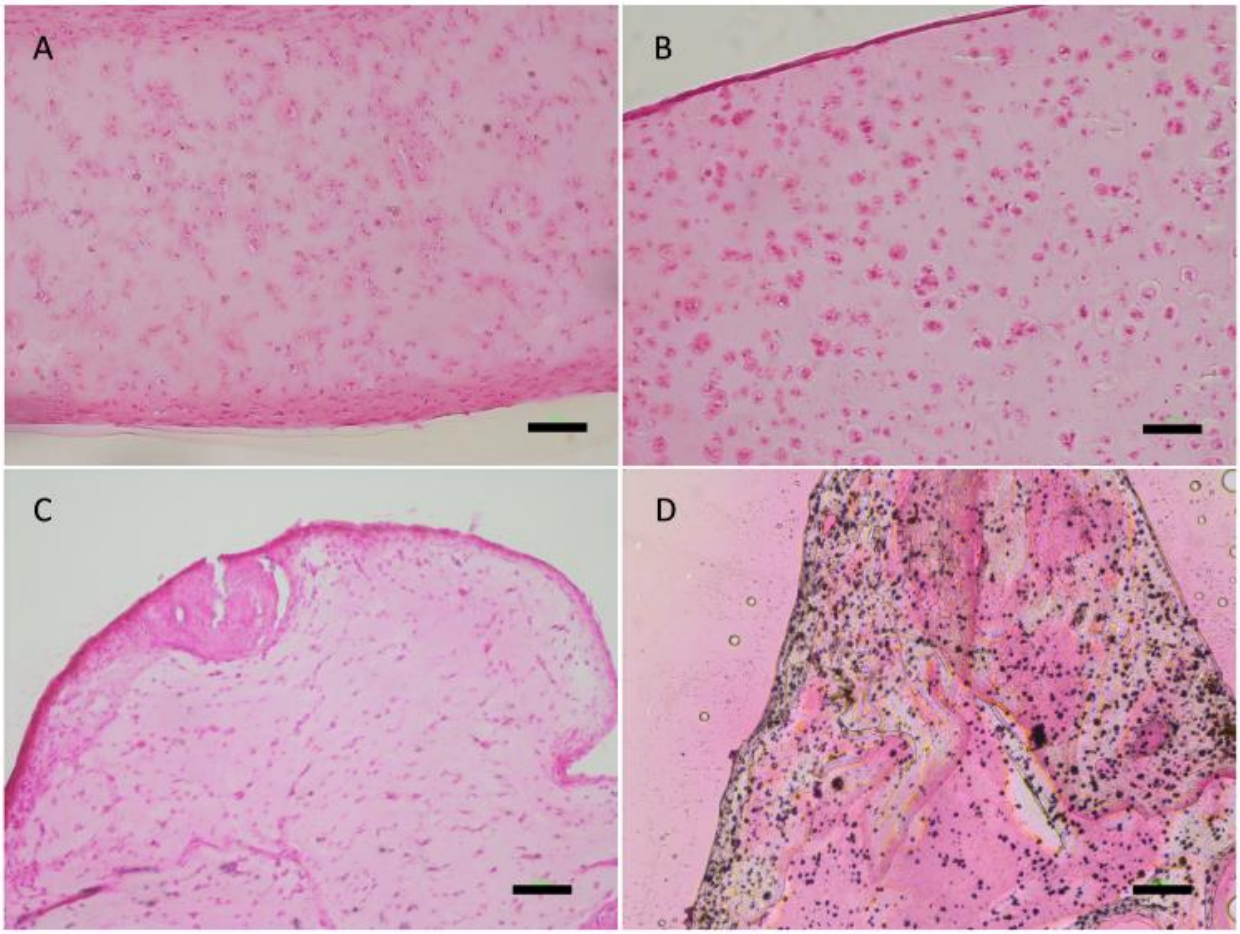

Figure 4-2 Von Kossa staining of PGH and GEL hydrogels containing goat BMSCs after in vitro culture. (A, B) Culture in chondrogenic medium. (C, D) Culture in osteogenic medium. Scale bar = 100 µm.

4.3.2 Effects of PGH and GEL on hBMSCs Differentiation *In Vivo*

Histology at 8 weeks revealed that with a single supplement of TGFβ-3 (supplemented into the hydrogel during fabrication), hBMSCs underwent chondrogenesis in both the PGH and the GEL (Figure 4-3 A, B). The cartilage formation was not robust, as indicated by the focal pericellular Safranin O staining. The GAG stain appeared more intense in the GEL than PGH. However, the PGH seemed to show a greater percent GAG positive cells (68 ± 4.3%) compared

to the GEL (48 ± 4.4%) as evidenced by Safranin O staining (Figure 4-4 B). hBMSCs in PGH expressed 9.4 fold higher type II collagen and 2.8-fold higher aggrecan after 8 weeks compared to in GEL as shown via PCR (Figure 4-4 A), confirming the percent of GAG positive cells. In addition, the PGH showed less fibrous tissue than the GEL, as indicated by Fast Green staining. Von Kossa staining showed the presence of phosphate and calcium only in GEL hydrogels (Figure 4-3 C, D). Consistent with histology, expression of type X collagen and bone sialoprotein in PGH were 8.4% and 1.7% of that in GEL (Figure 4-4 A).

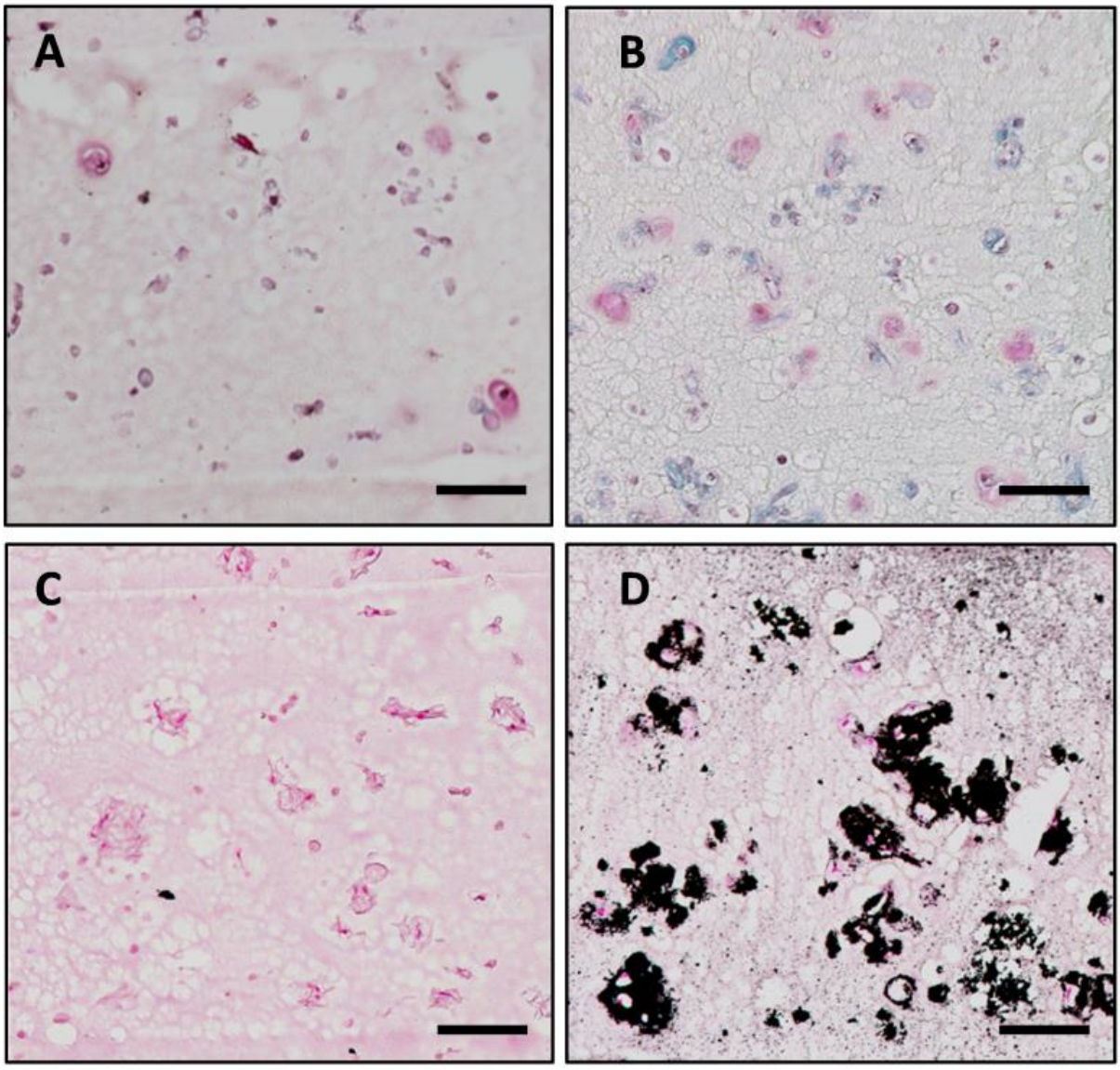

Figure 4-3 Histological staining of PGH and GEL hydrogels containing human BMSCs after 8 weeks of growth in subcutaneous pockets in immunocompromised mice. Safranin O staining of PGH (A) and GEL (B). Von Kossa staining of PGH (C) and GEL (D). Scale bar = 100 µm.

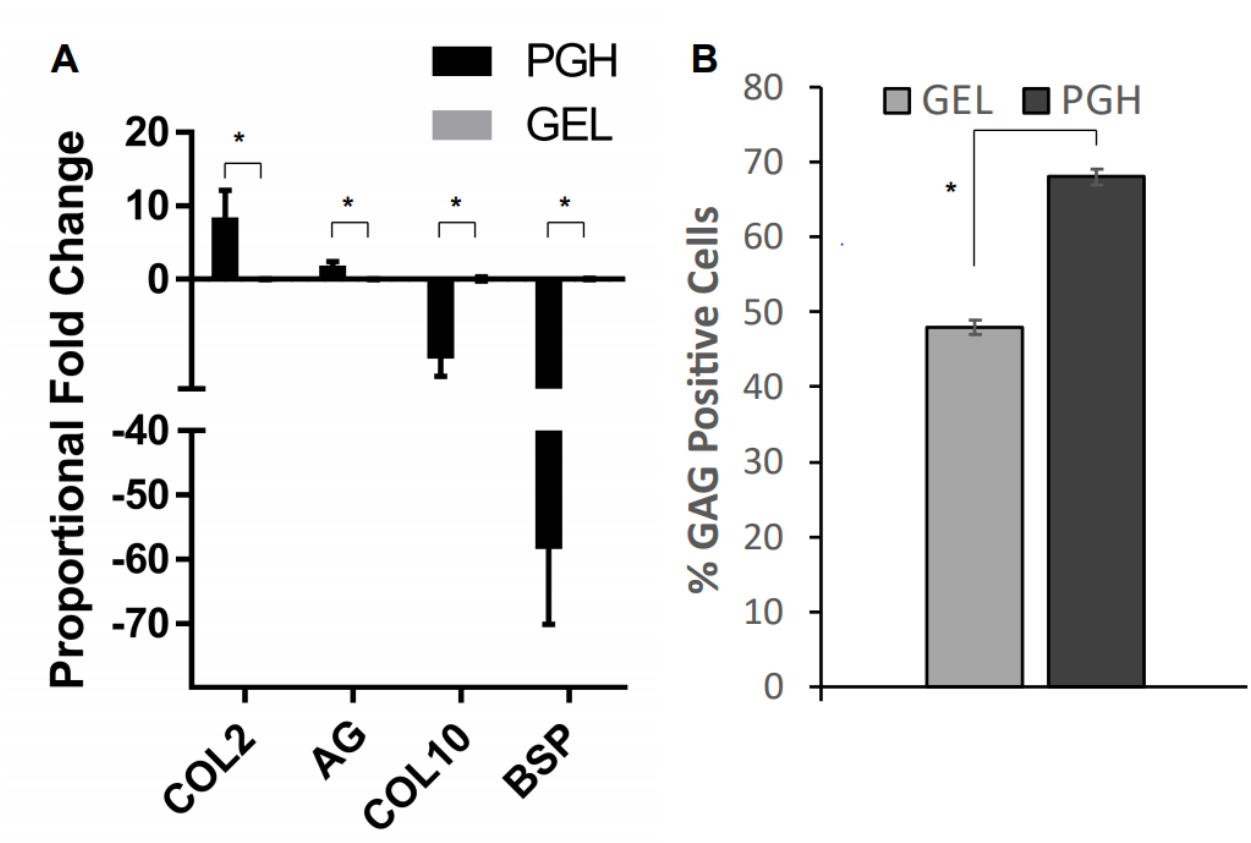

Figure 4-4 Quantification of human BMSC gene expression and GAG staining in PGH and GEL hydrogels grown for 8 weeks in mice. (A) Quantitative PCR analysis. PGH expressed 9.4 fold higher type II collagen and 2.8 fold higher aggrecan compared to in GEL. Expression of type X collagen and bone sialoprotein in PGH were 8.4% and 1.7% of that in GEL, respectively. (B) Fraction of cells staining for GAGs in their pericellular matrix. (* $p<0.01$).

4.4 Discussion

These results revealed that the PGH hydrogel appeared to promote chondrogenic differentiation of BMSCs while inhibiting osteogenic differentiation, while the conventional

gelatin hydrogel (GEL) is permissive to both chondrogenic and osteogenic differentiation. The *in vitro* assays with goat BMSCs showed that while permitting chondrogenesis the PGH did not support mineral deposition in an osteogenic environment, suggesting a lack of osteogenic differentiation. The results were supported by the *in vivo* study where the PGH had greater potential to induce chondrogenesis by human BMSCs than the GEL, evidenced by the elevated expression of aggrecan and type II collagen and a higher fraction of GAG positive cells after 8 weeks growth. However, the weak GAG deposition after 8 weeks growth *in vivo* showed that one-time dosing of TGFβ-3 in the hydrogels was ineffective in inducing rapid stem cell chondrogenesis, likely due to diffusion and loss of the growth factor. The *in vivo* study also suggested that PGH is anti-osteogenic, supported by the lack of mineral staining and biologically meaningful collagen type Xα1 and bone sialoprotein gene expression.

The PGH hydrogel is a potentially useful biomaterial for stable hyaline cartilage engineering and the regeneration of cartilaginous interfaces. The hydrogel itself supported hBMSC chondrogenesis *in vivo* while preventing chondrocyte hypertrophy (Collagen Type Xα1) and mineral deposition (Von Kossa). Hypertrophy is a well-known but often overlooked concern for cartilage regeneration using stem cells, especially for stable hyaline cartilage, where mineralization is undesirable [164]. Studies have investigated means to inhibit BMSC derived chondrocyte hypertrophy, such as modulating the scaffold stiffness [67], dynamic compressive loading of constructs [150, 165], incorporation of matrix molecules and soluble biofactors that modulate intracellular signaling pathways of hypertrophy [149, 151, 166], gene-level intervention, co-culturing with articular chondrocytes, lowering oxygen tension, and modification of culture substrates [167]. Among the approaches above, modulating the culture substrate or scaffold is most feasible for translation to clinical therapy. The mechanisms of the PGH effect on

chondrogenesis and mineralization are elusive. The heparin component is unique among the sulfated GAGs in its high binding of numerous growth factors [44-47]. Heparin is structurally similar to heparan sulfate (HS); HS-containing proteoglycans are co-receptors for over 200 proteins [168]. Heparin may preferentially sequester those that promote osteogenesis (e.g., BMP-2) [169] through binding and potentiation of endogenously secreted anti-osteogenic growth factors [41-47]. In addition, the highly anionic nature of heparin is similar to that of cartilage. At the concentrations in PGH, heparin may impact the transport of anionic species required for mineralization (as opposed to binding of calcium) [118, 119], namely phosphate *in vivo* and β-glycerophosphate *in vitro*, ergo in part why these are packaged within matrix vesicles of mineralizing cartilages [141]. Heparin has been shown to inhibit aggregation of hydroxyapatite crystals *in vitro* [170], and calcification of prosthetic heart valves [117]. Altered matrix mineralization may in turn impact progression of the hypertrophy in BMSC derived chondrocytes, and the ability of BMSCs to undergo osteogenesis, e.g., calcium and phosphate signaling. In this manner, incorporation of highly sulfated molecules such as heparin may be beneficial compared to incorporation nonsulfated polysaccharides such as hyaluronan [68]. Thus, the amount of heparin in the PGH hydrogel may be key for the observed anti-hypertrophic and anti-osteogenic effects of PGH.

By nature of their composition alone, the PGH and GEL hydrogels regulated BMSC differentiation down the different osteochondral lineages. To understand the effect of hydrogels on BMSC chondrogenesis, longer time course studies such as this are needed that investigate the phenotype stability of differentiated BMSCs [171]. As such, they can be applied to regenerate tissue for joint resurfacing *in situ*, without the need for predifferentiation of stem cells, discrete

encapsulation of different cell types or growth factors, multi-part scaffold assembly, and complex bioreactor systems [68, 155-158].

To control the spatial organization of tissue formation, many multilayer scaffold designs have been tested for the regeneration of the tendon/ligament enthesis (bone-cartilage-ligament interface) [172-177]. These works have focused on the high mechanical demands of these interfaces. Zhu et al. have developed gradients of mineral to anchor their trilayer designs [173]. Lee et al. instead have developed polymers, including nanofibers, of differing properties to withstand *in-situ* forces [175]. Since the growth plate cartilage does not experience tensile forces as do tendons and ligaments, a different approach is required for growth plate regeneration, with materials that perform well under compressive loads such as hydrogels. We believe that the PGH hydrogel can be used to regenerate the growth plate cartilage.

Future work will further investigate the mechanisms of phenotype stability of BMSC derived chondrocytes, including culture conditions that promote hypertrophy and mineralization.

4.5 Conclusion

Our *in vitro* experiment has suggested the inhibition of osteogenesis and maintenance of chondrocyte phenotype by BMSCs in a PGH hydrogel. This effect was confirmed with *in vivo* growth experiments over two months. Compared to GEL, the PGH hydrogel seemed to support stem cell chondrogenesis and cartilage matrix production while inhibiting direct osteogenesis, hypertrophy, and mineral deposition. The PGH hydrogel is a promising material to regenerate growth plate cartilage.

5.0 Specific Aim 4: Assess the Efficacy of the Stem Cell-laden PGH Hydrogel in Cartilage Regeneration and Bony Tether Prevention in a Growth Plate Injury Model in Goats

5.1 Introduction

Growth plate injury is a significant pediatric orthopedic problem; 15% of long bone fractures in children involve the growth plate, with a 35% prevalence in 10 to 15-year-old children. The overall incidence of growth plate injury in the juvenile population is 2.4 to 4.6 per 1,000 [178-183]. Up to 75% of these physeal injuries cause some growth disturbances, most often from the bony tethers bridging the epiphysis and metaphysis. In the lower limbs, tethers cause angulation deformity, length discrepancy, and substantial physical impairment. Surgical procedures are available to correct these deformities. However, they are associated with a number of disadvantages [9, 184]. For example, distraction osteogenesis is highly invasive, painful, and prolonged (3-6 months) [9]. Epiphysiodesis (hardware implantation and/or physeal bar rotation/excision to restrict growth) sacrifices patient height and is often followed with an osteotomy to reshape geometry or distraction to restore length [185]. The Langenskiold procedure (autologous transplant of fat as an interpositional material) has a high risk of bony tether recurrence [25].

Currently, there is no biological therapy available to regenerate the growth plate cartilage and prevent bony tether formation simultaneously [12]. Regenerative approaches have been under investigation for decades. By using a combination of stem cells, growth factors, and scaffolds as the interpositional material, some success has been reported in rabbits; nevertheless, such

treatment has not succeeded in large animals [9, 29, 30]. Large animals are better models for studying growth plate repair due to their relatively comparable size to humans. Besides, growth plates of smaller animals are very different from those of humans; rabbits have little cancellous bone in the metaphysis; cycle time of rat proliferative chondrocytes is twenty times faster than human [4, 12, 186].

In Aim 2, we have demonstrated that compared to GEL-MA only hydrogels, PGH hydrogel inhibits mineralization and osteogenesis while supports chondrogenesis by BMSCs.

In this portion of the work, we evaluated autologous BMSC-laden PGH hydrogels in a goat model for growth plate cartilage regeneration and bony tether prevention. We also tested tri-layered PGH hydrogels with the top layer supplemented with human parathyroid hormone (PTH) (1-34) and the bottom layer supplemented with triiodo-L-thyronine (T3), in an attempt to differentiate stem cells in these layers into proliferative and hypertrophic chondrocytes respectively. Our previous studies have shown that PTH (1-34) stimulates chondrocyte proliferation and inhibits hypertrophic differentiation; T3 induces hypertrophic phenotypes, up-regulating type X collagen, and alkaline phosphatase activity.

5.2 Materials and Methods

5.2.1 Materials

PEGDA, GEL-MA, HEP-MA, and LAPwere synthesized as described in Section 2.2.2. Cell culture supplies were purchased from Atlanta Biologicals (Flowery Branch, GA) and Thermo Fisher Scientific (Waltham, MA). Recombinant human transforming growth factor beta-1 (TGFβ-

1) was purchased from Peprotech (Rocky Hill, NJ). Human parathyroid hormone (PTH) (1-34) was purchased from Fisher Scientific. Triiodo-L-Thyronine (T3) was purchased from Sigma-Aldrich. Goat BMSCs were obtained as described in Aim 3. Ultra-clear PFA tubing, 4.5 mm drill bits, drill collars, and oil-resistant Buna-N rubber sheet were purchased from McMaster (Elmhurst, IL). Paraformaldehyde and chemicals to make phosphate buffered saline were obtained from Sigma-Aldrich. Immunocal® solution and disposable biopsy punches were purchased from Fisher Scientific. Spanish Boer goats were purchased from K-Bar Livestock, LLC (Sabinal, TX). Drill guide, Kirschner-wires, and other surgical tools were purchased from Synthes (Raynham, MA). Anti-RANK antibody [64C1385] (ab13918) and Methyl Green Pyronin Stain Kit (RNA DNA Stain) (ab150676) were purchased from Abcam (Cambridge, United Kingdom).

5.2.2 Hydrogel Fabrication

Goat BMSCs were plated the day before surgery to recover from cryo-storage overnight, then trypsinized and encapsulated in hydrogels on the day of surgery. Hydrogel solution was prepared by dissolving the modified polymers at 8% (w/v) in PBS and adding 0.01% (w/v) LAP (photoinitiator). The PGH hydrogel was composed of PEGDA, GEL-MA, and HEP-MA at a 63:21:16 mass ratio. The prepared solution was mixed with TGFβ-1 at 10 µg/mL and goat BMSCs at 30 million/mL. Two groups of hydrogels were fabricated. The homogenous group was cast in a 15 mm long Ultra-Clear PFA tube (4 mm inner diameter) and photocrosslinked with 2.5 J/cm^2/mm UV-A light. For the tri-layered group, the solution was divided into three separate tubes, one supplemented with PTH (1-34), one un-supplemented, and the third supplemented with T3. Three different molds were used for casting. A straight cut was made on a 15 mm PFA tube at 1/3 diameter, along the longitudinal plane, by using a razor blade. The shallow part was mold

A, and the deeper was mold B. A 2 mm high, 4 mm diameter rubber stopper was placed at one end of each mold to prevent leakage of the polymer solution. The bottom layer was cast first in mold A, using the T3 hydrogel solution. Crosslinking was performed as described above. The rubber stopper was then removed, and the hydrogel was pushed into mold B and placed at the bottom. TGFβ-1 only hydrogel solution was added on top of the bottom layer, filling mold B, then crosslinked. Following the crosslinking, the stopper was removed, and the bi-layered hydrogel was pushed into an uncut 15 mm tube and place at the bottom. The last mode was filled with PTH (1-34) hydrogel solution and exposed under the UV light to make the top layer. The hydrogel was then ready for implantation.

5.2.3 Surgical Procedures

In total, the growth plates in hind legs of 8 Spanish Boer goats (3-month-old females) were operated bilaterally (n=16 defects), under an IACUC approved protocol at the University of Pittsburgh. The defects were divided into the following experimental groups: homogenous hydrogel (n=4), tri-layered hydrogel (n=9), and untreated control (n=3). The animals fasted for 36 hours before surgery. A combination of ketamine (5 mg/kg) and xylazine (0.1 mg/kg) was used for anesthesia. Throughout the surgery, isoflurane was given by inhalation (2-3%). Ketoprofen was given intraoperatively via intravenous administration (1 mg/kg). A medial approach to the proximal tibial plateau was taken to locate the growth plate. The soft tissue was dissected, and a pin was inserted at the posterior aspect of the growth plate. The posterior placement was selected to avoid the undulation of the growth plate in the anterior region. A digital X-ray was taken by using a FIDEX Multi-Modality Veterinary scanner (Animage, Pleasanton, CA) to confirm that the pin was inserted at the growth plate margin. The angle of the drill was

calculated to follow the growth plate in a mediolateral direction. A 1 mm drill guide was inserted to a depth of 20 mm. Then, a 4.5 mm diameter hollow drill was used to create a defect with a depth of 15 mm. The defect was irrigated copiously with saline. Then, a solid metal rod of 4.5 mm was inserted to occupy the space and promote clotting. After 10 minutes, the hydrogel implant was inserted into the defects from the PFA tubes using a metal plunger. Kirschner wires were inserted in the epiphysis, metaphysis, and diaphysis of the proximal tibia to track bone growth throughout the study. The soft tissue was first sutured, followed by the fascia and then the overlying skin. An injection of antibiotics (ceftiofur, 5 mg/kg) was given. Following the surgery, the animals were allowed to bear weight. The animals were sacrificed at three months by administering Buthanasia intravenously (1 cc/10 kg). The proximal tibias were collected for analysis.

5.2.4 Histology Analysis

Computed tomography (CT) images of the tibia were taken by using the FIDEX scanner to assess the growth plate repair and bony tether formation. The samples were cut into approximately 3 × 3 × 3 cm blocks and fixed with 4% (w/v) formaldehyde solution for seven days. Samples were then decalcified in Immunocal® for seven days; decalcification was confirmed by X-ray. Following decalcification, the samples were cut in halves, along the plane of the defect. They were then immersed in 30% (w/v) sucrose solution overnight, 40% (v/v) optimal cutting temperature compound for two weeks, and cryosectioned at a thickness of 10 µm. Two sets of stains were performed, hematoxylin/eosin, and safranin O/Fast Green/hematoxylin. Anti-RANK antibody [64C1385] (ab13918) was used to immunostain the receptor activator of NF-κB (RANK). Methyl Green Pyronin Stain Kit (RNA DNA Stain) (ab150676) was used to

stain RNA and DNA. Slides stained with hematoxylin/eosin were analyzed by using NIS-Element AR. For this analysis, the growth plate defects were defined as the areas between borders of intact growth plates flanking the injury sites (Figure 5-1). Percentages of fat and bone within the defect sites were calculated as $\frac{\text{Area of bone or fat}}{\text{Area of defect}} \times 100\%$. Safranin O stained slides were used to analyze chondrogenesis. Percentage of the chondrogenic area was calculated as $\frac{\text{Area of the chondrogenic region}}{\text{Area of hydrogel}} \times 100\%$. Tissue composition within the drill holes was also analyzed. The regions of interest were defined as 15 mm × 2 mm rectangles within the drill holes. The drill holes were identified by landmarks such as clear boundaries of bone and fat, and residual hydrogel within cortical bones. Quantity and thickness of the bony tether were measured using NIS-Element AR.

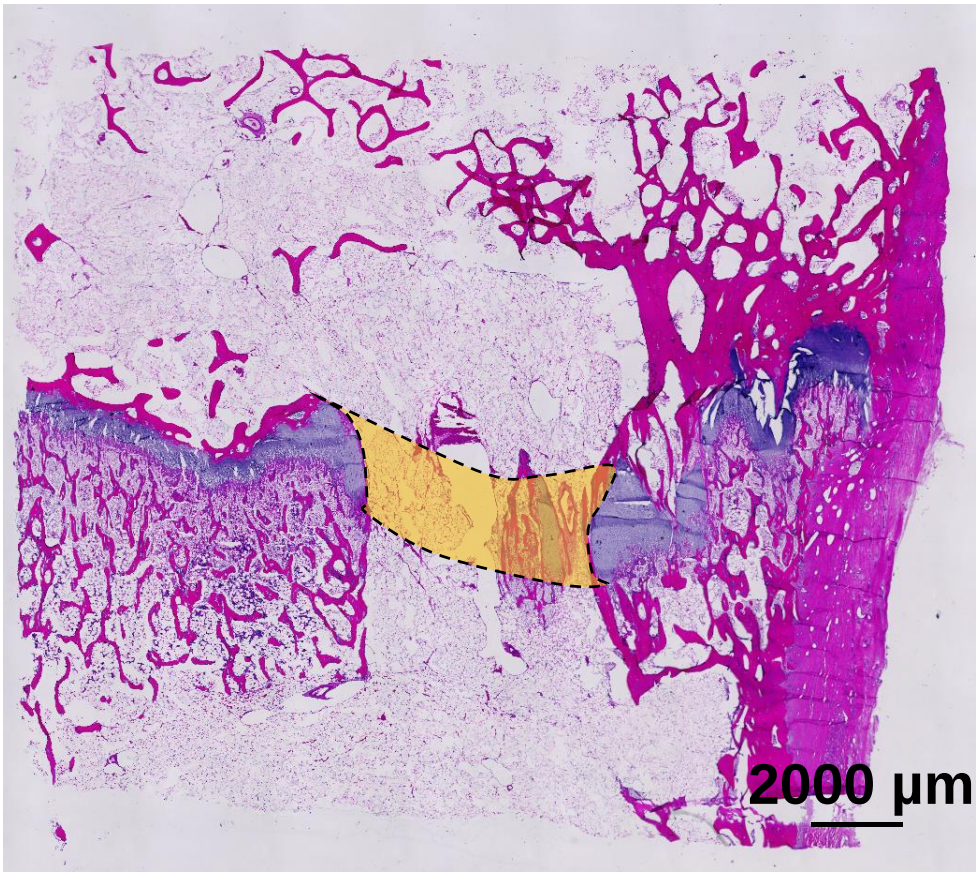

Figure 5-1 Area for growth plate defect analysis (yellow box).

5.2.5 Statistical Analysis

Statistical analysis was performed on histology measures using t-tests and one-way ANOVA with Tukey's HSD post-hoc tests. Data are presented as mean ± standard deviation.

5.3 Results

5.3.1 Growth Plate Defect Analysis

15 mm deep growth plate defects were created laterally on proximal tibias by using a 4.5 mm drill bit, mimicking the bony tether resection in pediatric patients. Two types of autologous BMSC-laden PGH hydrogels were used as the interpositional material in 13 legs, while the other three legs were left untreated. The groups were assigned randomly. One sample from the untreated group was lost during sectioning. Thus, 15 samples were analyzed.

After three months, the growth plate appeared severely damaged at the injury site, regardless of the groups. A radiolucent smear (Figure 5-2) was seen under the injured growth plate in all legs. Focal widening (Figure 5-3) of the growth plate occurred, with an average height of 2.83 ± 0.10 mm compared to normal 0.63 ± 0.07 mm. Fragments of growth plate cartilage were found deep in the metaphysis, with fainter Safranin O stain compared to the intact growth plate (Figure 5-4 A). In some cases, the hypertrophic cells in the trapped cartilage did not calcify. The appearance of the damaged growth plate varied. Some lost the columnar cellular organization while others were stretched by the growth of the adjacent columns (Figure 5-4 B).

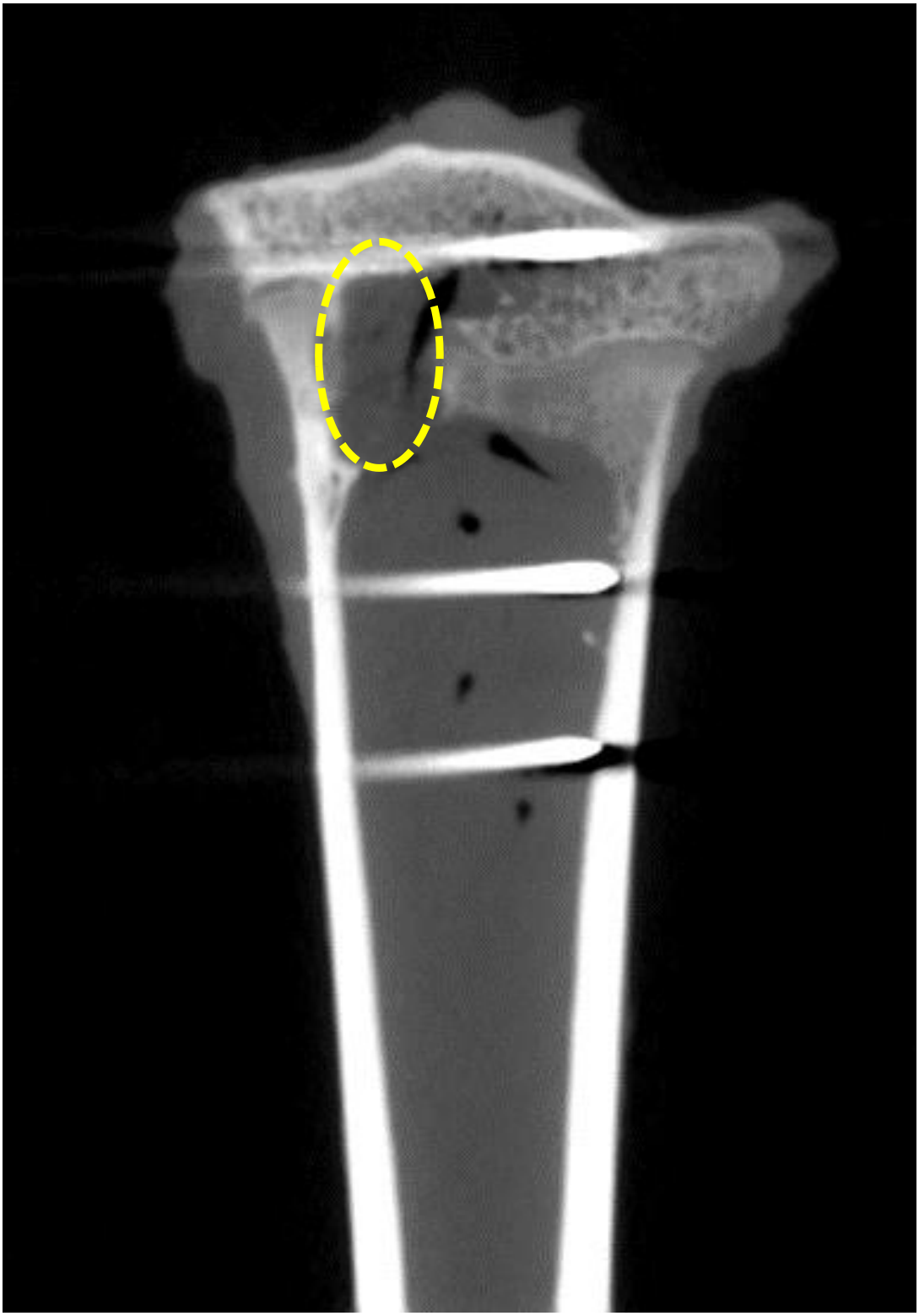

Figure 5-2 CT image. A radiolucent smear under the injured growth plate.

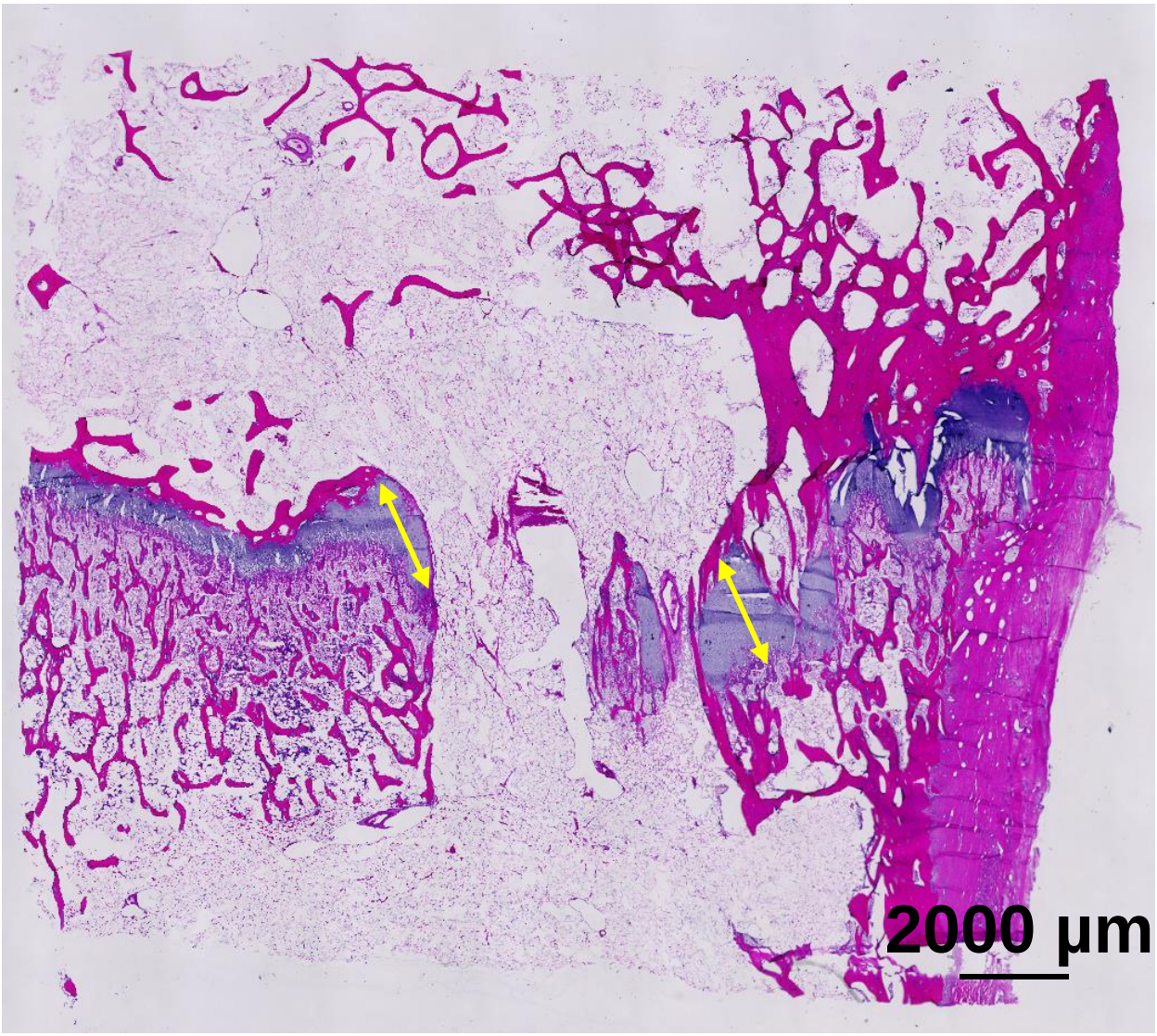

Figure 5-3 Widening of the injured growth plate. Hematoxylin and eosin staining of the growth plate.

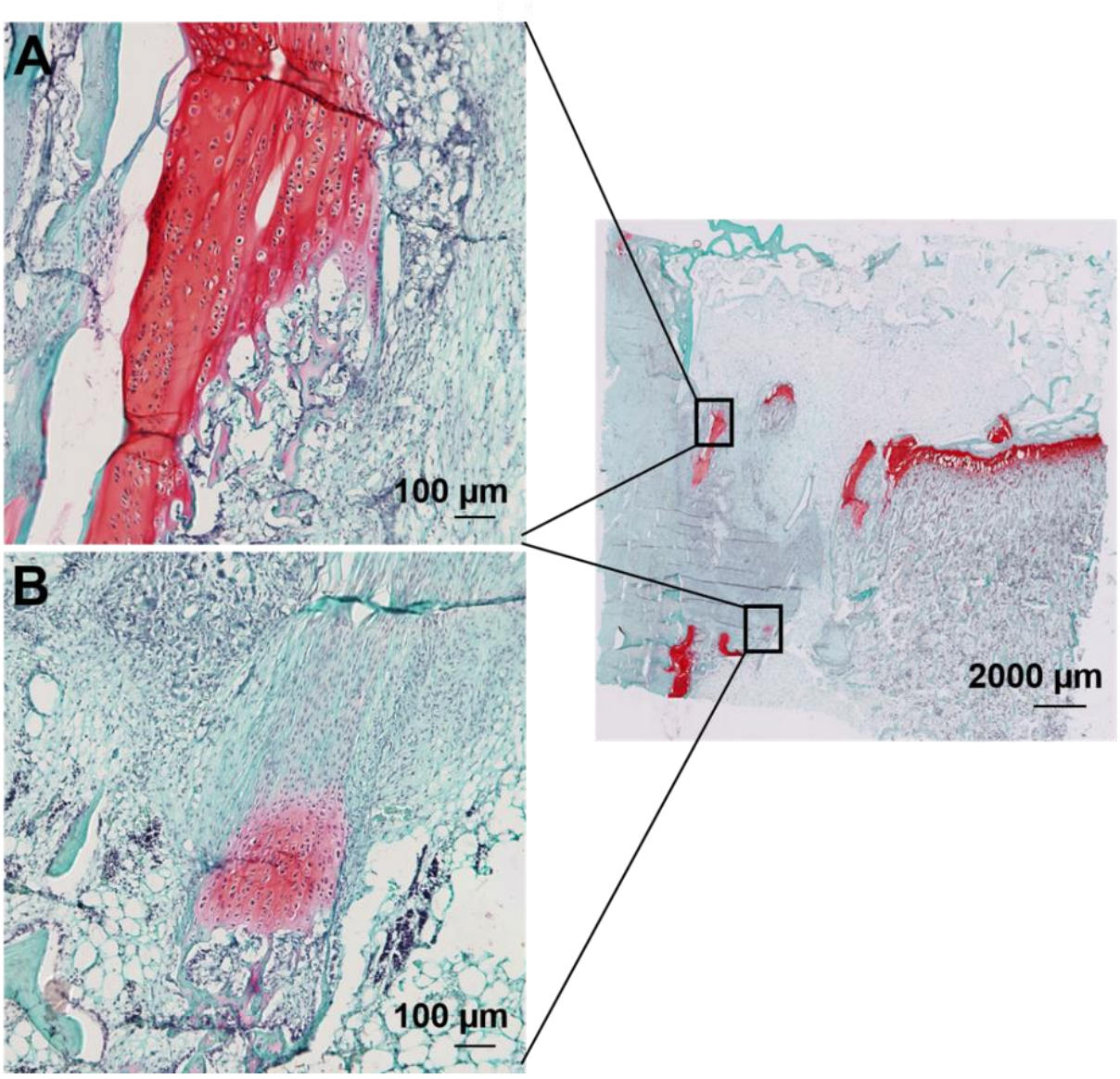

Figure 5-4 Fragments of growth plate cartilage. Safranin O staining of the growth plate. A) Cartilage in the metaphysis; B) stretched chondrocyte columns.

Trabecular bone, fat, growth plate fragments, and sometimes hydrogel fragments were found within the growth plate injury site. A small amount of fibrous tissue and blood vessels were also observed. The untreated defects contained higher bone content (53 ± 7.0%) compared to the

defects treated with tri-layered (18 ± 12%, p=0.0125) and homogeneous hydrogels (26 ± 12%, p=0.09). No significant difference was found between the two hydrogel groups. The tri-layered and homogenous hydrogel groups appeared to contain more fat compared to the untreated group (38 ± 25% and 35 ± 17% respectively versus 3.6 ± 3.62%).

The growth plate is an undulating disc in growing children rather than a flat and smooth plate seen in newborns [31]. Therefore, it is difficult to make a defect following the growth plate anatomy perfectly using a straight drill bit. Although all 15 defects analyzed involved the growth plate, only two were drilled right at the growth plate (Figure 5-5 A). In four samples, the majority of the drill hole was located in the epiphysis (Figure 5-5 B). Six were in the metaphysis (Figure 5-5Figure 5-5 C) and the other three intersecting the growth plate obliquely, with a part in the epiphysis and a part in the metaphysis (Figure 5-5 D). The epiphyseal drill holes had significantly more fat (68 ± 17%) compared to the ones made in the growth plate (39 ± 19%, p=0.0076) or the metaphysis (35 ± 26%, p=0.0241).

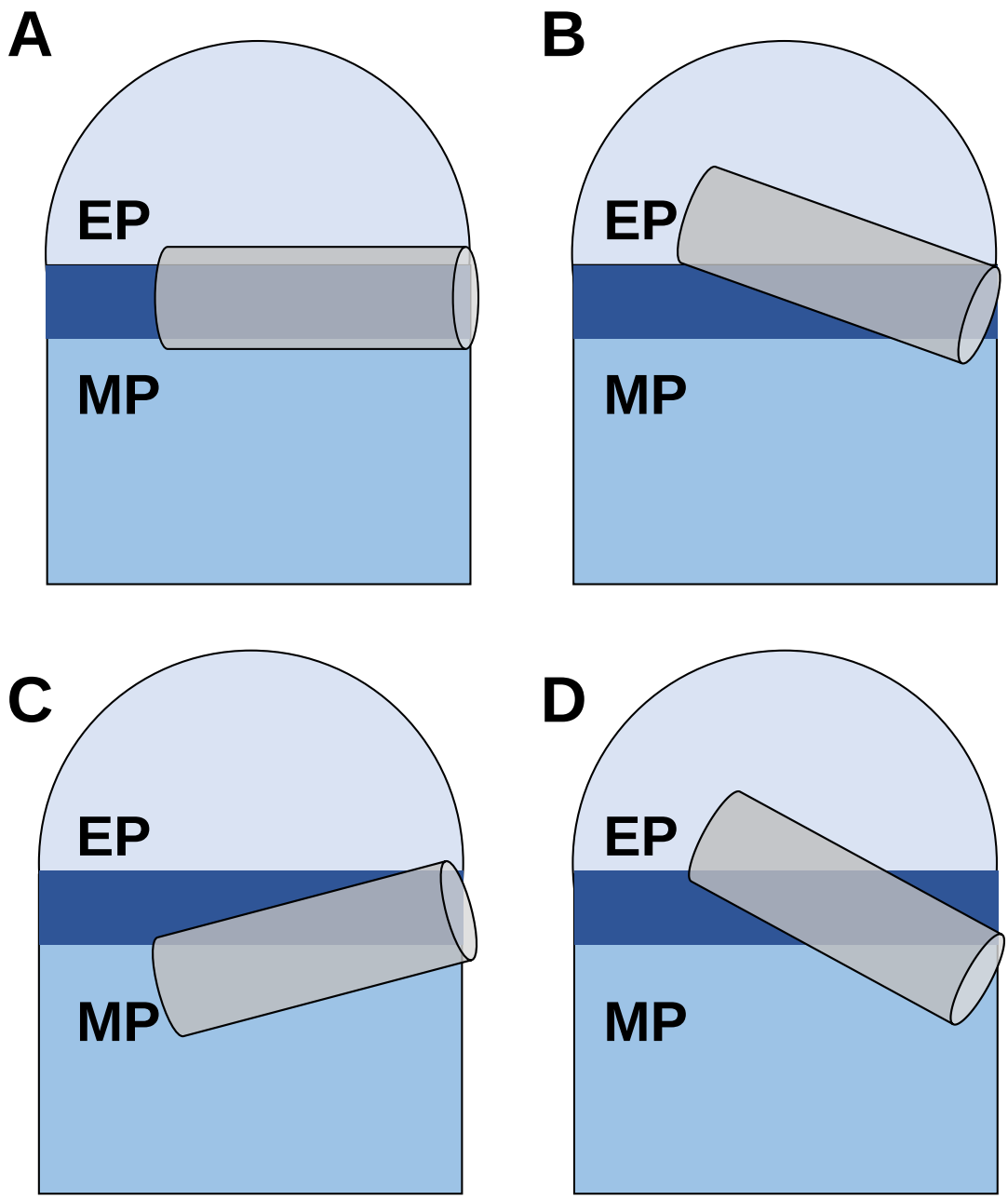

Figure 5-5 Schematic of hydrogel insertion. EP= epiphysis; MP= metaphysis. A) Right at the growth plate; B) majority in the epiphysis; C) majority in the metaphysis; D) part in the epiphysis and part in the metaphysis.

5.3.2 Bony Tethers

Bony tethers were seen in all legs, with widths ranging from 28 um to 1665 µm. A 100 µm tether was found between the inserted hydrogel and the neighboring growth plate (Figure 5-6). No significant difference was found in tether number or thickness between the groups.

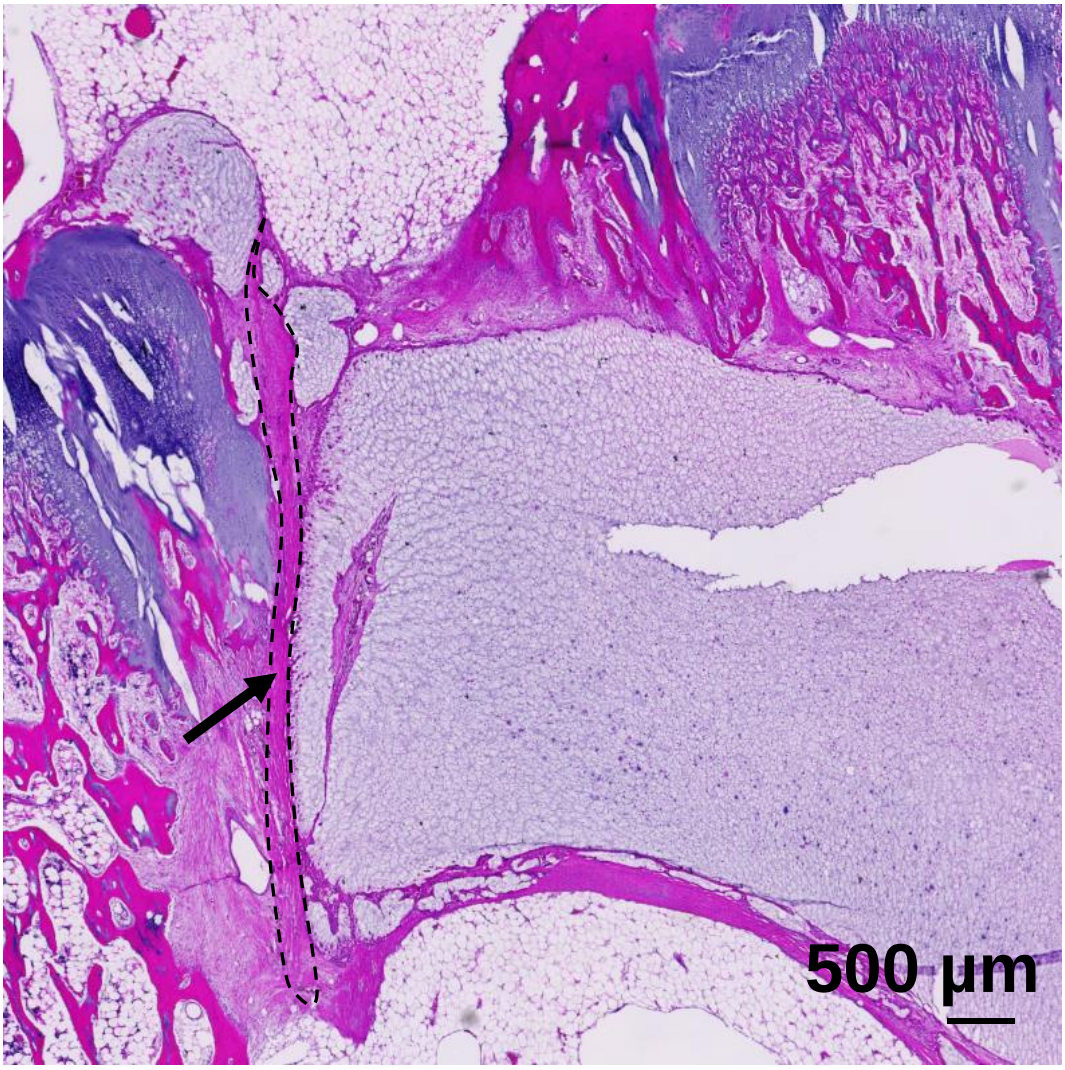

Figure 5-6 Bony tether between the hydrogel and the growth plate (indicated by the arrow). Hematoxylin and eosin staining of the growth plate.

5.3.3 The Fate of the Hydrogels and Stem cells

Histology revealed that the interpositional hydrogels had been resorbed in various degrees. The percent area occupied by hydrogel within the drill hole was significantly higher when in the metaphysis (27 ± 31 %) compared to in the epiphysis (0%, p=0.0001) and right at the growth plate (1.4 ± 3.8 %, p<0.0001). Small fragments (< 5 mm^2) were often trapped in the cortical bone, regardless of the location of insertion (Figure 5-7). Hydrogels initially inserted in the epiphysis were barely seen after three months. A large quantity of fat was present within the defect site, with some in shape and size resembling the cross section of the inserted hydrogel (Figure 5-8 A). In some cases, small fragments of hydrogels also appeared in the metaphysis (Figure 5-8 B. In contrast, the hydrogels placed in the metaphysis were more likely to remain (Figure 5-9). In three out of eight cases, the hydrogel area was greater than 21 mm^2, roughly 35% of the size at day 0. The hydrogels below the growth plate did not travel up as the bone grew. The hydrogels inserted into the growth plate cartilage were mostly resorbed.

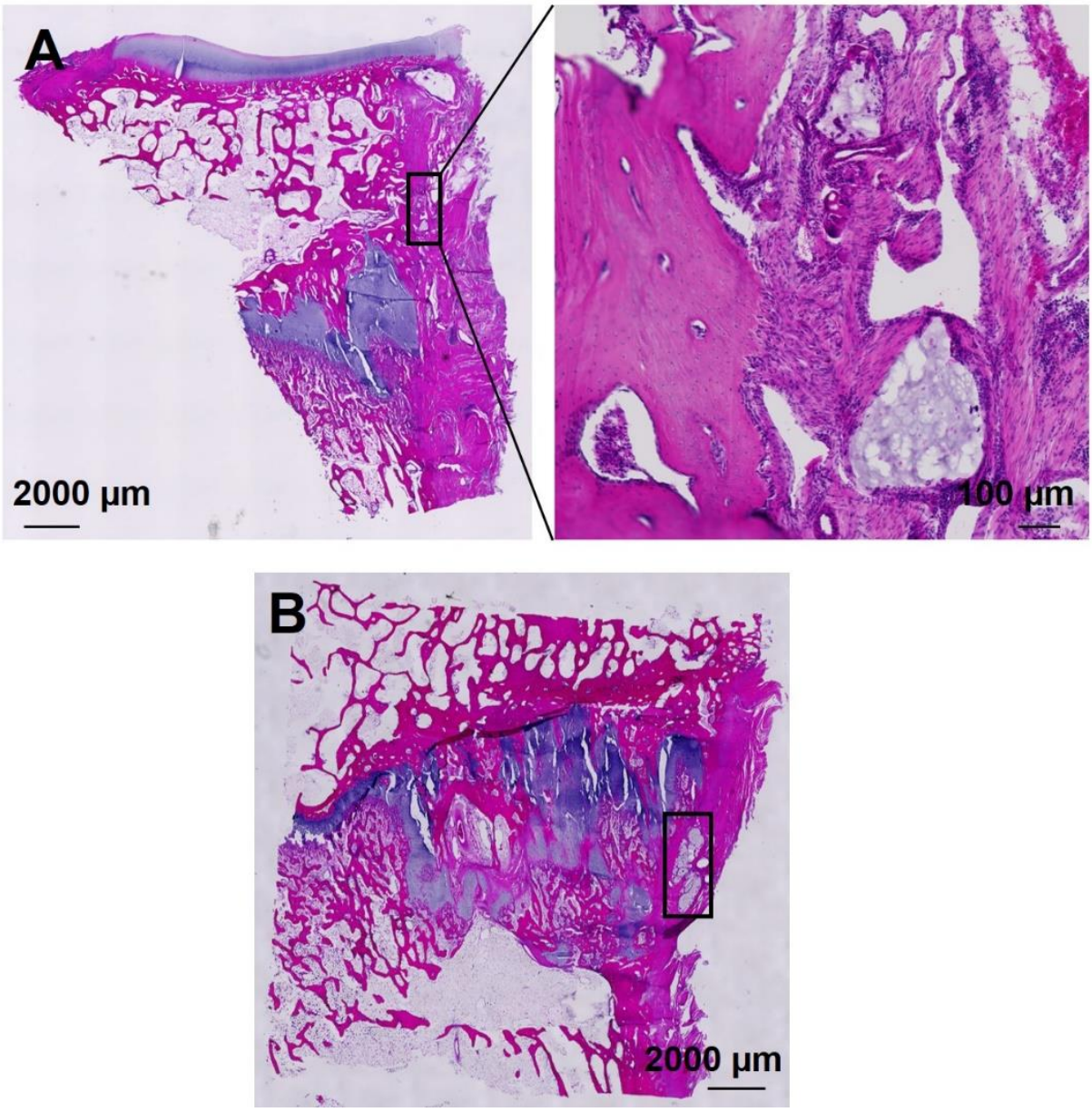

Figure 5-7 Hydrogel fragments in cortical bone. Hematoxylin and eosin staining of the growth plate. A) Epiphyseal; B) metaphyseal.

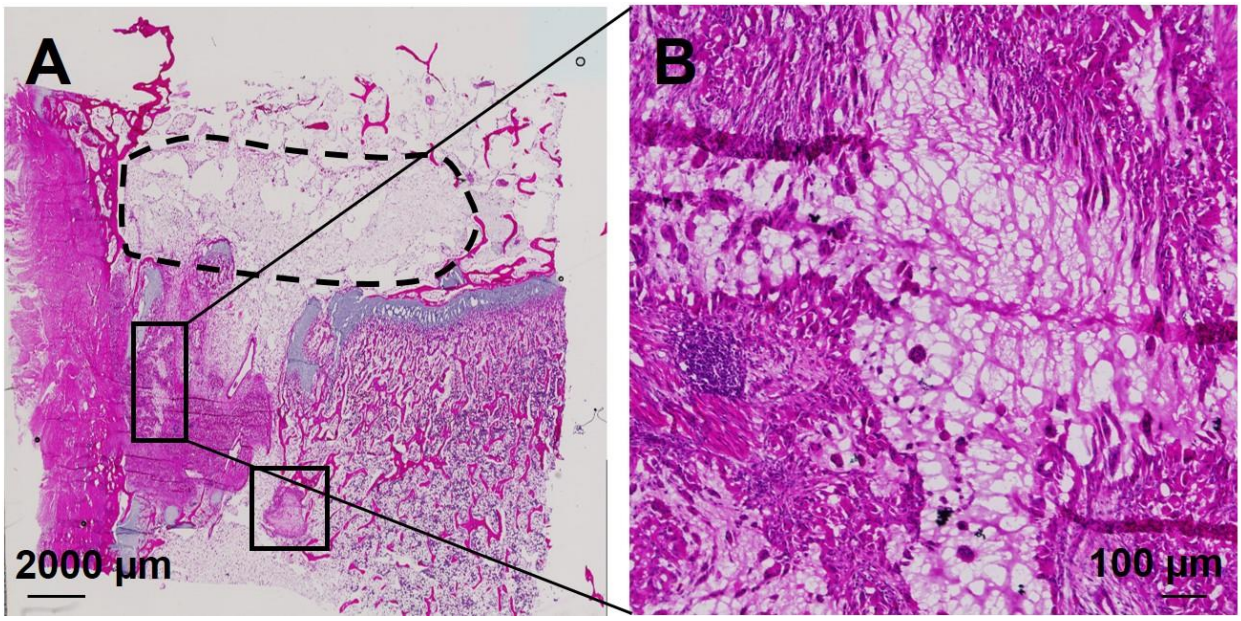

Figure 5-8 Hematoxylin and eosin staining of the growth plate. A) Fat in the epiphysis (dashed line); B) hydrogel fragments in the metaphysis.

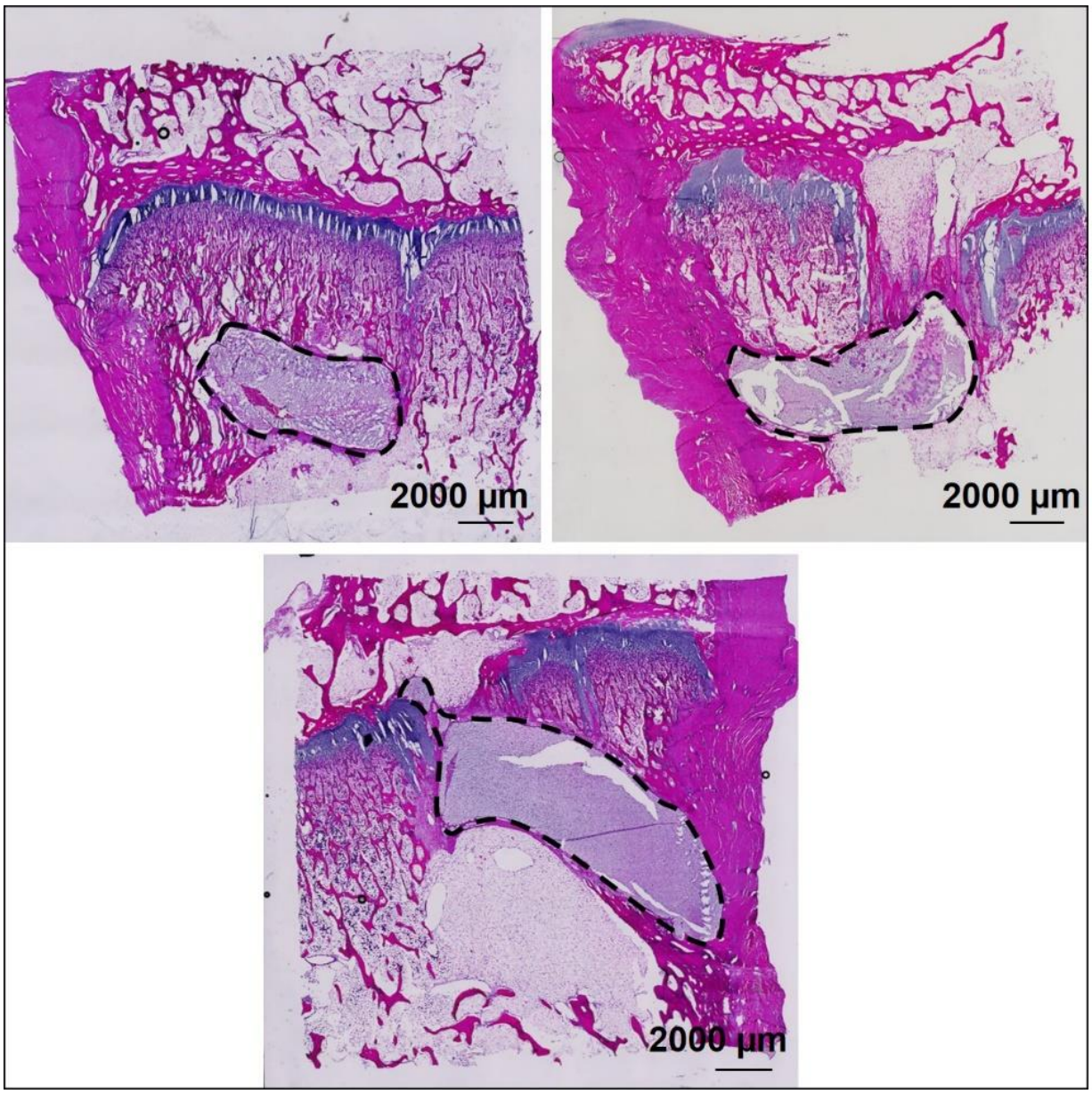

Figure 5-9 Hematoxylin and eosin staining of the growth plate. The hydrogels placed in the metaphysis were more likely to remain.

The remnant hydrogels were surrounded by fibrous capsules (Figure 5-10 A, B). Multinucleated giant cells were seen within the capsules as well as on the periphery of the

hydrogels (Figure 5-10 B). These cells were crescent-shaped, with nuclei aggregated on one end of the cells, and appeared to have ruffle border (Figure 5-10 C). These cells also stained positive for RANK (Figure 5-10 D).

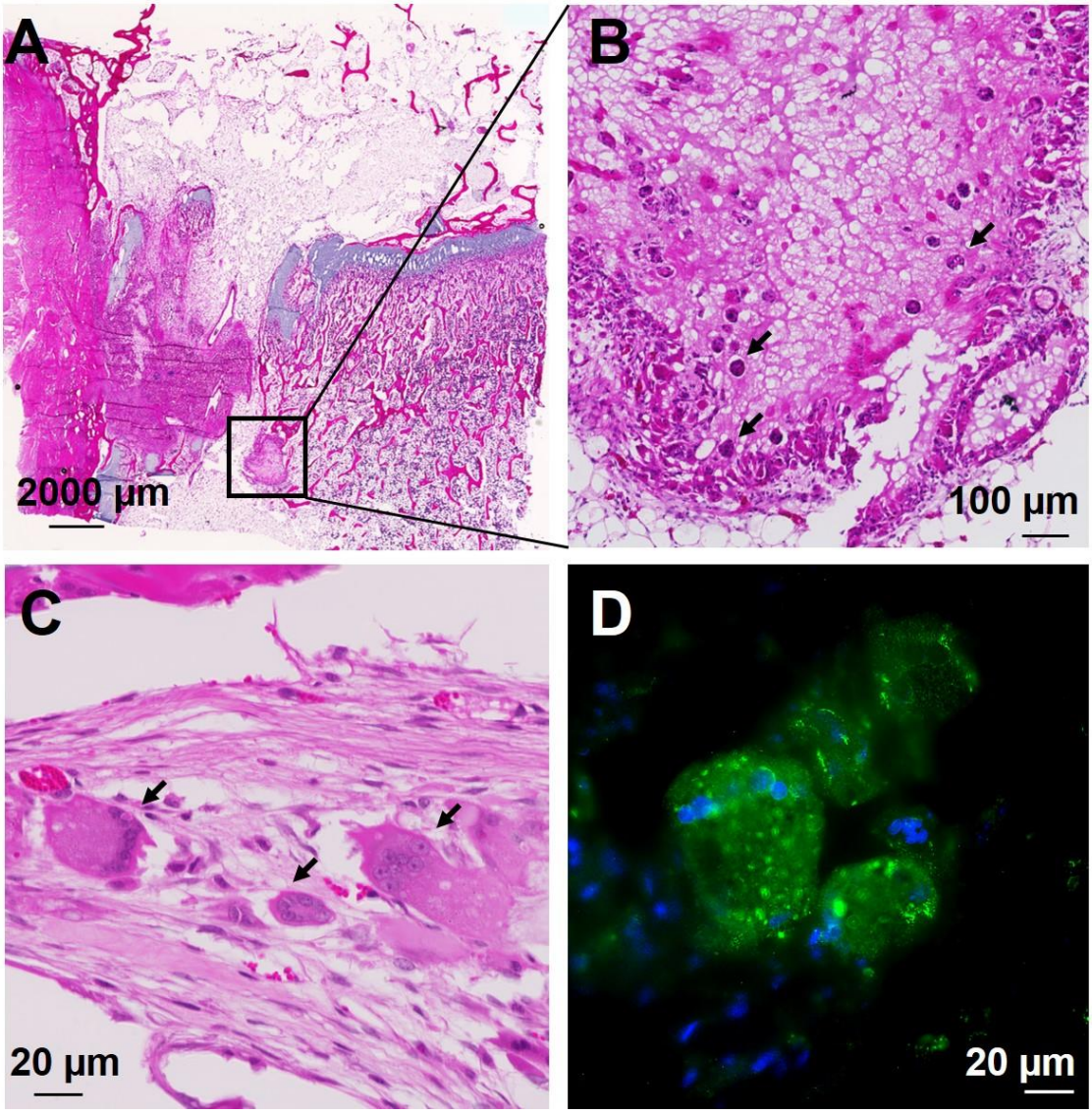

Figure 5-10 Hematoxylin and eosin staining of the growth plate(A-C). A) Hydrogel surrounded by a fibrous capsule; B) multinucleated giant cells within the capsules and on the periphery of the hydrogels; C) morphology of the multinucleated giant cells; D) RANK immunostain (green).

Chondrogenesis was observed in the three largest metaphyseal hydrogel implants (Figure 5-11). The most proteoglycan matrix was seen in a homogenous hydrogel (Figure 5-11 A), having 4.6% Safranin O stained area. The other two hydrogels, one tri-layered (Figure 5-11 B) and one homogenous (Figure 5-11 C), showed a few cells with faint Safranin O stain. Interestingly, the non-chondrogenic cells in these hydrogels can be categorized into two types: one had nucleus stained dark purple by hematoxylin, often found near proteoglycan producing chondrocytes; the other was not stained by hematoxylin, but Fast Green or eosin only. These "ghost cells" were seen in all remanent hydrogels, distributed throughout the scaffold, regardless of whether chondrogenesis occurred or not. DAPI stain showed that the "ghost cells" had nuclei, though the stain was much fainter compared to the hematoxylin positive cells (Figure 5-12 A). To further investigate the identity of the "ghost cells," they were stained by Methyl Green Pyronin. The results showed that these cells had DNA, but RNA was undetectable (Figure 5-12 B).

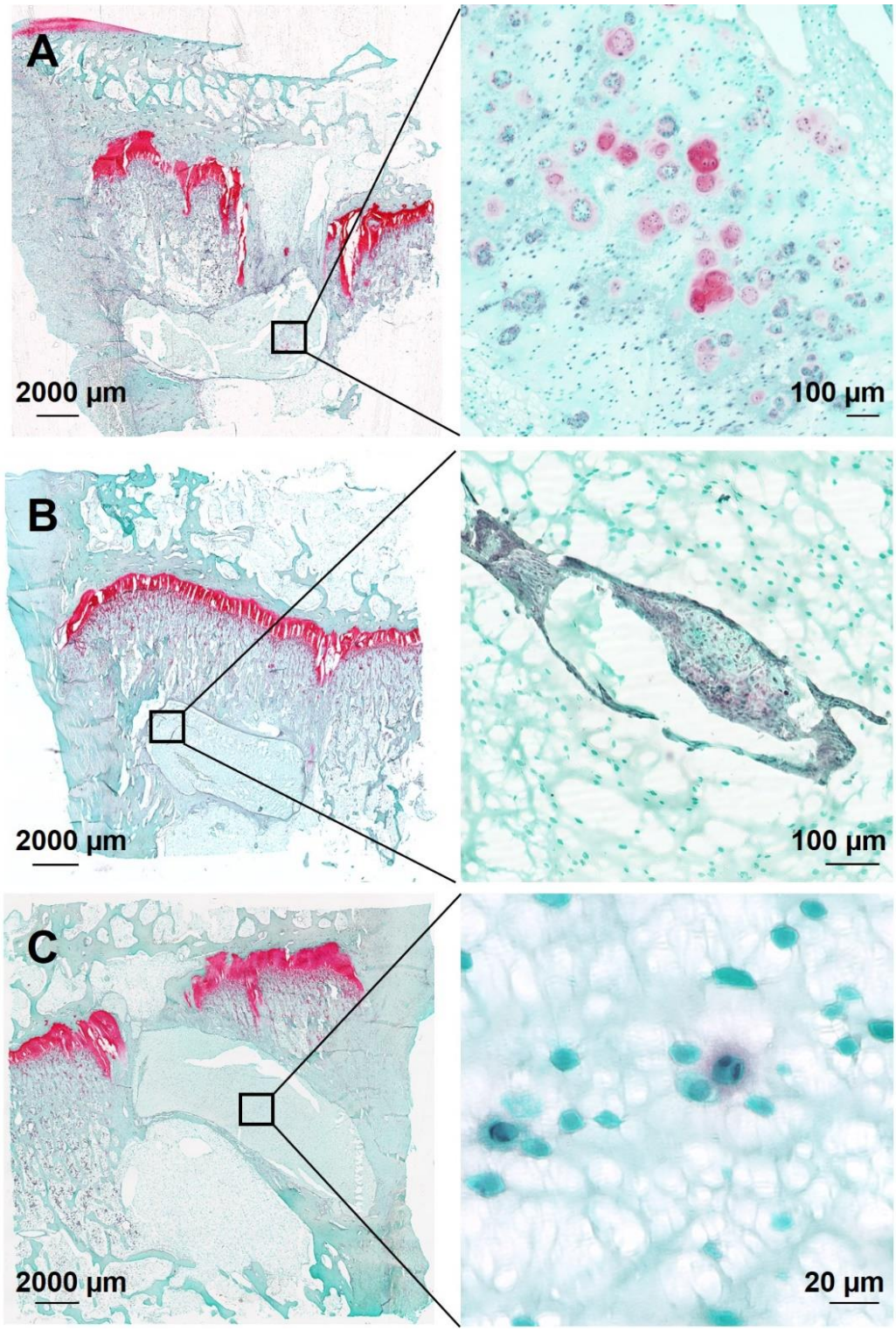

Figure 5-11 Chondrogenesis in the hydrogels. Safranin O staining of the growth plate (GAG = red and pink).

A) Homogeneous hydrogel (most GAG); B) Tri-layered hydrogel; C) homogenous hydrogel.

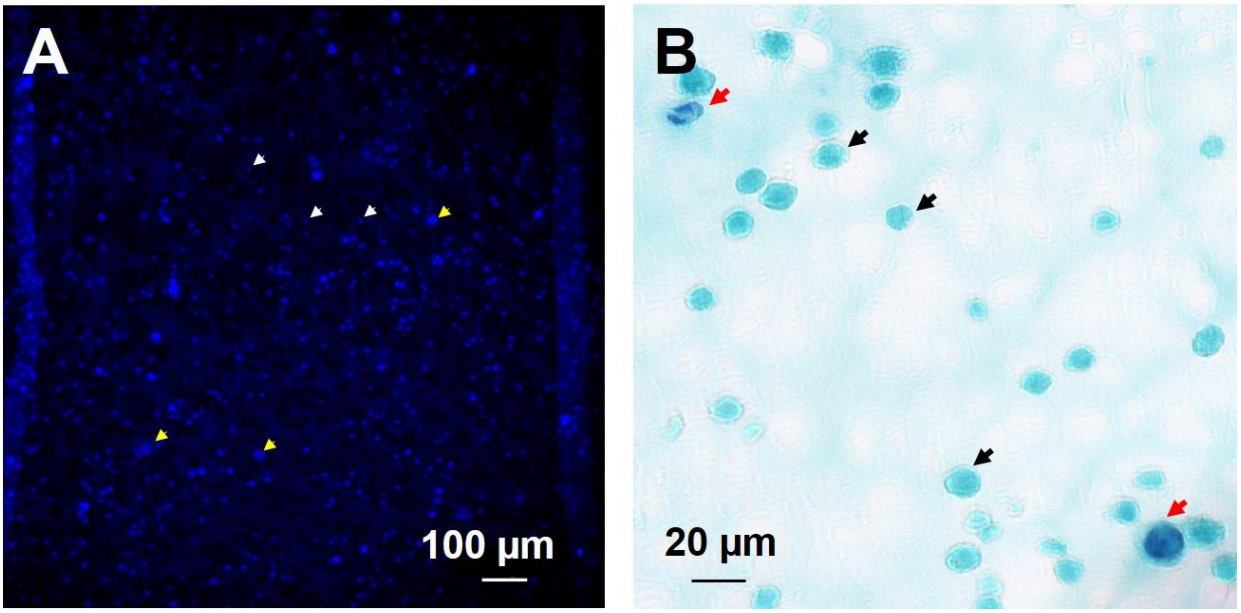

Figure 5-12 A) DAPI staining (blue). "Ghost cells" are indicated by white arrows; hematoxylin positive cells are indicated by yellow arrows. B) Methyl Green Pyronin staining. Methyl Green = bluish green (DNA); Pyronin Y = pink (RNA). Purple = presence of both DNA and RNA. "Ghost cells" are indicated by black arrows; hematoxylin positive cells are indicated by red arrows.

No bone formation was observed within the hydrogels. The PGH hydrogels did not mineralize even when encapsulated in a bony environment (e.g., cortical bone), confirmed by CT images. Nevertheless, the hydrogel was susceptible to host tissue intrusion. Fibrous tissue and bone were frequently seen penetrating the hydrogels (Figure 5-13), cutting them into smaller fragments.

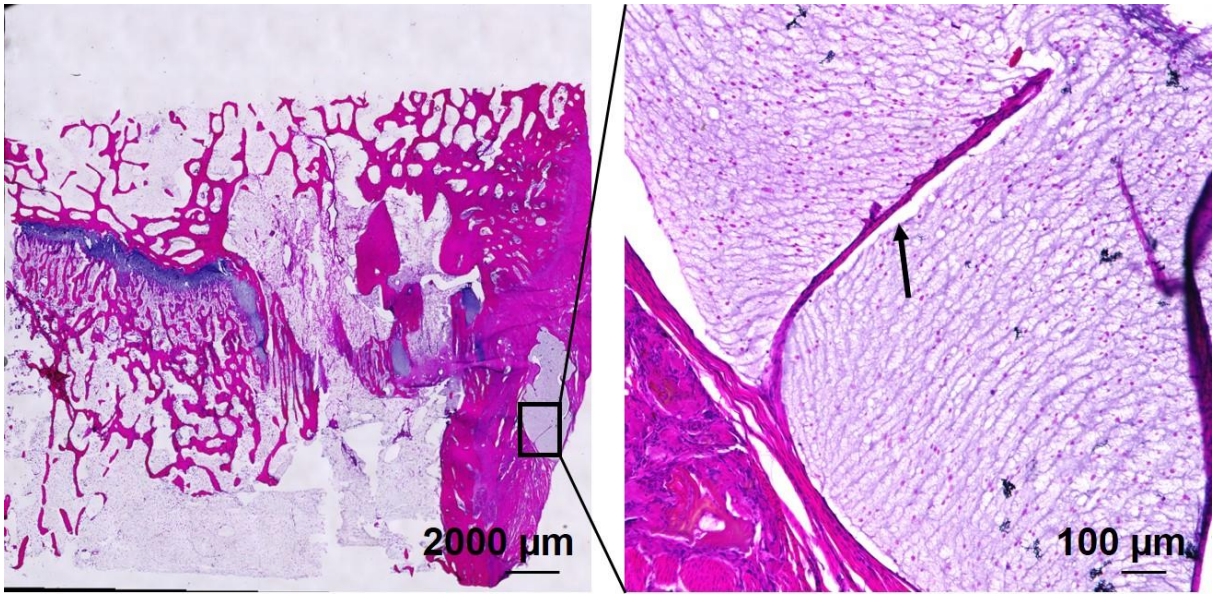

Figure 5-13 Bone penetrating hydrogel. Hematoxylin and eosin staining.

5.4 Discussion

This study demonstrated that goat could be used as a large animal model for studying growth plate injury. The PGH hydrogel was biodegradable and able to support stem cell chondrogenesis in situ. However, the use of a chondrogenic, mineralization resistant hydrogel alone as the interpositional material was not sufficient to prevent bony tether formation.

A radiolucent cavity under the injured growth plate was seen three months post-implantation. Similar cavities had been observed in children and minipig after fat implantation [186], as well as in sheep after allogenic growth plate chondrocyte implantation [27]. Such cavities had been shown to contain fat and elongate as the bone grew [186].

Widening of the growth plate was likely caused by damage to the metaphyseal blood vessels during the surgery. Increase in growth plate height after interrupting the metaphyseal

blood supply was reported by Trueta et al. and Nguyen et al. Insult to these blood vessels stopped alkaline phosphatase activity, arrested hypertrophic chondrocyte calcification and apoptosis, and eventually resulted in abnormally high cell numbers in the physeal column and persistent cartilage within the metaphysis [5, 187]. When the blood supply was restored, calcification resumed quickly [187].

Similar to many previous attempts to repair the damaged growth plate through regenerative approaches, PGH hydrogels failed to prevent bony tether formation in this study. We found thin tethers, less than 100 μm in width, fitting tightly between the injured growth plate and the hydrogel. This observation suggested that the use of an interpositional material alone was unable to prevent cell infiltration between the epiphysis and metaphysis and the subsequent bony tether formation, regardless of how precisely it was implanted. Bony tether formation begins with infiltration of inflammatory cells into the injured site, followed by MSC-like progenitor cells. Then, the progenitor cells undergo chondrogenesis, osteogenesis, and angiogenesis. Ultimately, the cartilaginous tissue diminishes, and bone matrix matures [9]. In the present study, some tethers seemed stretched and elongated, probably due to tension generated by the growth of the surrounding healthy growth plate. The process of the architectural growth of bony tethers is unknown. Blood vessels were frequently observed within growth plate defects, as well as in the fibrous capsules surrounding the remanent hydrogel. Trueta et al. noted that the bony bridge formation always occurred following vascular invasion into the injured growth plate cartilage [187]. Chung et al. showed that systemic administration of an anti-VEGF antibody decreased bony tether formation in the damaged growth plate [188]. Therefore, using an interpositional material that releases anti-angiogenic or anti-osteogenic factors might be a more practical approach to prevent bony tethers.

Although unable to prevent tether formation, the PGH hydrogels appeared to decrease bone and increase fat within the growth plate injury sites compared to the untreated group. Most of the tethers seemed to have originated from the epiphysis, extending into the metaphysis. The epiphyseal hydrogel insertion site was often seen filled with adipose tissue. From these observations, it can be inferred that during the bony tether treatment procedure, accessing the tether and inserting the hydrogel from the epiphysis might favor fat formation rather than bone, refraining tether reformation. In the future, 3D analysis of tether size via CT is necessary to make a more precise comparison between the treated and the untreated groups. Also, it would be beneficial to determine the minimum size of a tether that would result in growth disturbance to design the success criteria for future interpostional materials.

As expected, the PGH hydrogels were biodegradable in-situ. The degree of resorption appeared to be location-dependent rather than group-dependent. Hydrogels initially placed in the epiphysis were hardly seen after three months, whereas those in the metaphysis were more likely to remain. The metaphyseal hydrogels did not travel upwards with the growth plate as the bone grew; instead, they were buried deep into the metaphyseal bone. Maintaining proximity to the damaged growth plate is essential for local delivery of bioactive factors to prevent bony tether. This result further supported the inference that the interpositional hydrogel should be placed closer to the epiphysis rather than the metaphysis. Although 8% (w/v) hydrogels were mostly degraded after three months, 10% (w/v) hydrogel were seen to remain in the epiphysis in a previous study, suggesting the speed of gel degradation can be controlled by altering polymer concentration.

The remanent hydrogels were found surrounded by fibrous capsules, suggesting the occurrence of foreign body reaction, a wound healing response after implantation of a biomaterial,

medical device, or prosthesis [189]. Multinucleated giant cells were observed within the fibrous capsules as well as on the periphery of the hydrogels, appearing to resorb the material. These cells seemed to be polarized, with nuclei aggregated on one side of the cell. Ruffle border was also seen under 60x magnification. This observation suggested that these cells were osteoclasts, which has morphology well described in the literature [190-192]. Enishi et al. and Kadoya et al. have reported osteoclast-like cells near implants in bone [193, 194]. To confirm the identity of these cells, staining for osteoclast markers is necessary. Tartrate-resistant acid phosphatase (TRAP) is one of the most commonly used markers for osteoclasts. However, in the present study, this marker was unsuitable due to the decalcification agent used. RANK is another osteoclast marker. Interaction between RANK and its receptor RANKL plays a vital role in osteoclast development [195, 196]. Immunostain showed that these crescent-shaped cells were indeed RANK positive. Nevertheless, RANK alone cannot confirm the identity of the cells. A panel of markers for osteoclasts is needed, such as vitronectin receptor, calcitonin receptor, cathepsin K protein, carbonic anhydrase II, vacuolar H^+-ATPase, and integrin β3 [197-199].

Sparse Safranin O stain in the hydrogel was observed in three samples, indicating the PGH was able to support BMSC chondrogenesis in-situ. No bone was formed within the hydrogel, confirmed by the CT results (not shown), consistent with our previous finding that the PGH hydrogel supported chondrogenesis and inhibited osteogenesis. However, to use PGH hydrogel as an interpostional material to regenerate physeal cartilage, further modification is needed to enhance chondrogenesis, for example, by incorporating a drug delivery system.

The implanted stem cells and the host cells were distinguished by morphology and cell distribution, with the host cells having a fibroblast-like appearance and being more concentrated at the periphery of the hydrogel implant. Besides chondrocytes, two other types of cells were seen

within the hydrogel. One was often found adjacent to committed chondrocytes, round, with nuclei visible under hematoxylin, DAPI, and methyl green stains, and positive for Pyronin Y, an RNA stain. We speculate that these cells were at a very early stage of chondrogenesis, as a spectrum of chondrocyte-like cells were seen, from small round cells with faint GAG on the periphery, to large chondrocyte clusters rich in matrix molecules.

The other was the majority of the cells, also round, unstained with hematoxylin or Pyronin Y, but DAPI and methyl green positive (DNA stains). They were uniformly distributed within the implanted hydrogel, suggesting the cells we encapsulated stayed alive throughout the experiment. Interestingly, the hematoxylin positive cells stained more strongly with DAPI than the hematoxylin negative cells, suggesting the chromatins might be packed differently between the two cell types, resulting in different dye-binding affinities. The hematoxylin-mordant complex is positively charged and binds strongly to both DNA and RNA [200, 201]. The lack of hematoxylin and Pyronin Y stains indicated that these cells contained an extremely low level of RNA, a characteristic of quiescent stem cells [202, 203]. To further investigate the identity of these cells, staining for stem cell markers are needed, as well as techniques to detect quiescent cells, which lack proliferation makers, such as Ki-67 and PCNA, and retain cell labels, such as 5' bromo-2'-deoxyuridine (BrdU) and tritiated thymidine. Being in the quiescent state is believed to prolong the survival of stem cells under metabolic stress and maintain their long-term genomic integrity [202, 204]. Therefore, a hydrogel inducing quiescence might enable lasting preservation of stem cells at the target site for regeneration.

It is worth noting that the present study was primarily based on histological analysis, which revealed limited information due to its 2-dimensional nature and the plane of sectioning.

Bone volume quantification of using computed tomography will be performed in the future to further access the bony tethers and efficacy of the implanted hydrogels.

5.5 Conclusion

We have successfully created a goat model to study growth plate injuries. The PGH hydrogels were biodegradable and supported stem cell chondrogenesis *in situ* without showing mineral deposition. Although unable to prevent bony tether formation, implantation of the PGH hydrogels reduced bone and increased fat content within the damaged growth plate. Incorporating anti-angiogenic or anti-osteogenic factors into the interpositional hydrogel, and inserting the hydrogel from the epiphyseal end might be keys to prevent bony tether formation.

6.0 Overall conclusion and future work

6.1 Conclusion

Recapitulating the zonal architecture is deemed the key to regenerate functional growth plate cartilage [12]. The five success criteria of growth plate cartilage regeneration are 1) support cartilage formation; 2) prevent bony tether; 3) restore the zonal cell organization; 4) reestablish the appropriate signaling; 5) restore normal growth. This dissertation has focused on developing an interpositional device that meets the first two criteria. Based on the findings of the present study, the device will be optimized in the future, aiming to meet all five criteria.

We have presented the development and evaluation of a stem cell-laden PEGDA-(GEL-MA)-(HEP-MA) (PGH) hydrogel for growth plate injury repair. The PGH hydrogel was fabricated in-house and characterized for physiochemical properties including mechanical stiffness, swelling properties, and cytocompatibility. To evaluate the potential of the hydrogel to recreate the growth plate structure, its effects on chondrocyte phenotype progression were analyzed *in vivo* and compared to a conventional methacrylated gelatin hydrogel (GEL-MA only, often used in bioprinting applications and cartilage engineering). To evaluate its ability to drive differentiation of stem cells to growth plate chondrocytes, its effects on stem cell chondrogenic and osteogenic differentiation were evaluated both *in vitro* and *in vivo*. Finally, the efficacy of the stem cell-laden PGH hydrogel in regenerating cartilage and preventing bony tethers was accessed in a growth plate defect model in goats.

The results showed that the PGH hydrogel was cytocompatible and able to maintain chondrocyte phenotypes. Compared to the GEL-MA only hydrogel, the PGH hydrogel

maintained glycosaminoglycan production by hypertrophic chondrocytes, arrested terminal differentiation, and successfully inhibited mineralization. While supporting chondrogenesis, it did not permit osteogenesis or mineral deposition by stem cells. When implanted into a growth plate defect, the PGH hydrogel was biodegradable and supported stem cell chondrogenesis. Although unable to completely prevent bony tether formation, implantation of the PGH hydrogel reduced bone and increased fat content at the defect site. To better evaluate the efficacy of the PGH hydrogel, the critical tether size needs to be determined.

Overall, the PGH hydrogel has shown some degree of success in supporting cartilage formation and preventing bony tether formation. However, it failed to restore the zonal cell organization and normal growth. The reasons for the failure can be concluded as the following: 1) The growth plate is a dynamic tissue. By the time BMSCs differentiate into chondrocytes, the growth plate has already traveled away from the implanted hydrogel; 2) The current PGH hydrogel degraded too fast when placed in the epiphysis; 3) Even when the hydrogel was placed properly into the growth plate defect, tethers were able to form around it.

From this study, we have learned that using an interpositional material that releases anti-angiogenic or anti-osteogenic factors might be a more practical approach to prevent bony tethers. Also, during the bony tether treatment procedure, accessing the tether and inserting the hydrogel from the epiphysis might favor fat formation rather than bone, hampering tether reformation. The composition of the hydrogel needs to be optimized for slower degradation.

This work demonstrated that the PGH hydrogel has the potential to regenerate growth plate cartilage while preventing bony tether formation. It may also be suitable to regenerate other stratified cartilaginous interfacial tissues that contain zones of different cellular phenotypes, such as the temporal mandibular condyle.

6.2 Future Work

The mechanisms of the PGH hydrogel's effects on chondrocyte phenotypes and stem cells chondrogenesis and mineralization may be better defined through continued investigations.

We hypothesize that heparin plays a significant role in driving the material effects by binding to consensus sequences, modulating and prolonging signaling of endogenous growth factors that promote GAG production and inhibit terminal differentiation [74, 132, 133]. For example, heparin prolongs TGFβ activity by protecting them from enzymatic degradation [46, 133]. As a result, more TGFβ-2 might be available to upregulate PTHrp expression, thereby enhancing its downstream activities, such as chondrocyte proliferation, matrix production, and hypertrophy prevention [128-131]. Heparin also promotes FGF signaling by facilitating its interaction with the FGFR (FGF receptor) [134, 135]. FGF has been reported to obstruct chondrocyte hypertrophy and terminal differentiation [2, 126, 127]. In addition, heparin strengthens the interaction of hedgehog (Hh) with interference hedgehog, a component of the Hh signaling pathway parallel or upstream of Patched (Ptc) [132, 136]. IHH has been shown to delay chondrocyte hypertrophy by stimulating the production of PTHrp [2]. Heparin may also interfere with the Wnt signaling pathways, which are critical in chondrocyte differentiation. Heparin binds to metalloproteinases MMP-13, ADAMTS-4, ADAMTS-5 as well as a tissue inhibitor of metalloproteinases, TIMP3. Such binding prevents the interaction of these factors with LRP1 [205], an endocytic receptor that facilitates coendocytoses of MMP-13, ADAMTS-5, and TIMP-3 [206]. LRP1 has also been shown to inhibit the canonical Wnt signaling pathway by disrupting the formation of the Wnt receptor HFz1-LRP6 complex [207] and the subsequent chondrocyte terminal differentiation [208, 209]. Binding of heparin with LRP1 ligands might increase the availability of LRP1 to block the canonical Wnt signaling, leading to inhibition of hypertrophy.

The non-canonical Wnt signaling pathway is speculated to be unaffected by LRP1 because it does not involve LRP6 [167, 210]. The hypothesized signaling mechanisms discussed above are summarized in Figure 6-5. It would also be interesting to study mineralization in the PGH hydrogels without cells, matrix vesicle secretion by chondrocytes, the composition and crystal structure of mineral deposited, and the effect of substrate stiffness on the cytoskeletal structure and focal adhesion complex.

Future work may also be conducted to improve the current PGH hydrogel by a) incorporating anti-angiogenic or anti-osteogenic factors to prevent bony tether formation entirely, and b) incorporating a drug delivery system to enhance stem cell chondrogenesis. Furthermore, it may be beneficial to characterize and optimize physiochemical properties of the PGH hydrogel so that it can be of potential use in other applications, such as monolithic casting, injectable, and bioprinting.

Appendix A Supplementary Figures for Specific Aim 2

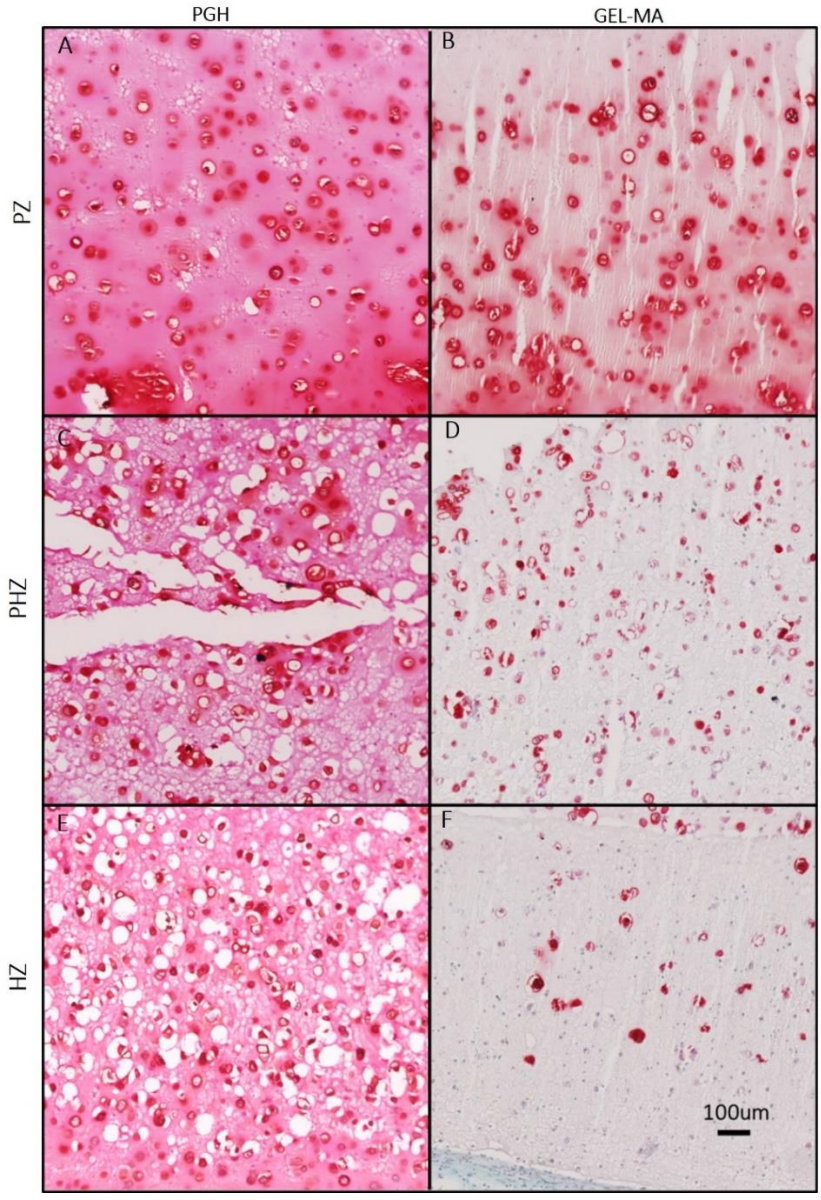

Figure 6-1 Subcutaneous growth for 8 weeks, Safranin O and Fast Green. PGH augmented GAG secretion in all three zones compared to GEL and maintained PHZ and HZ cells in a GAG producing state.

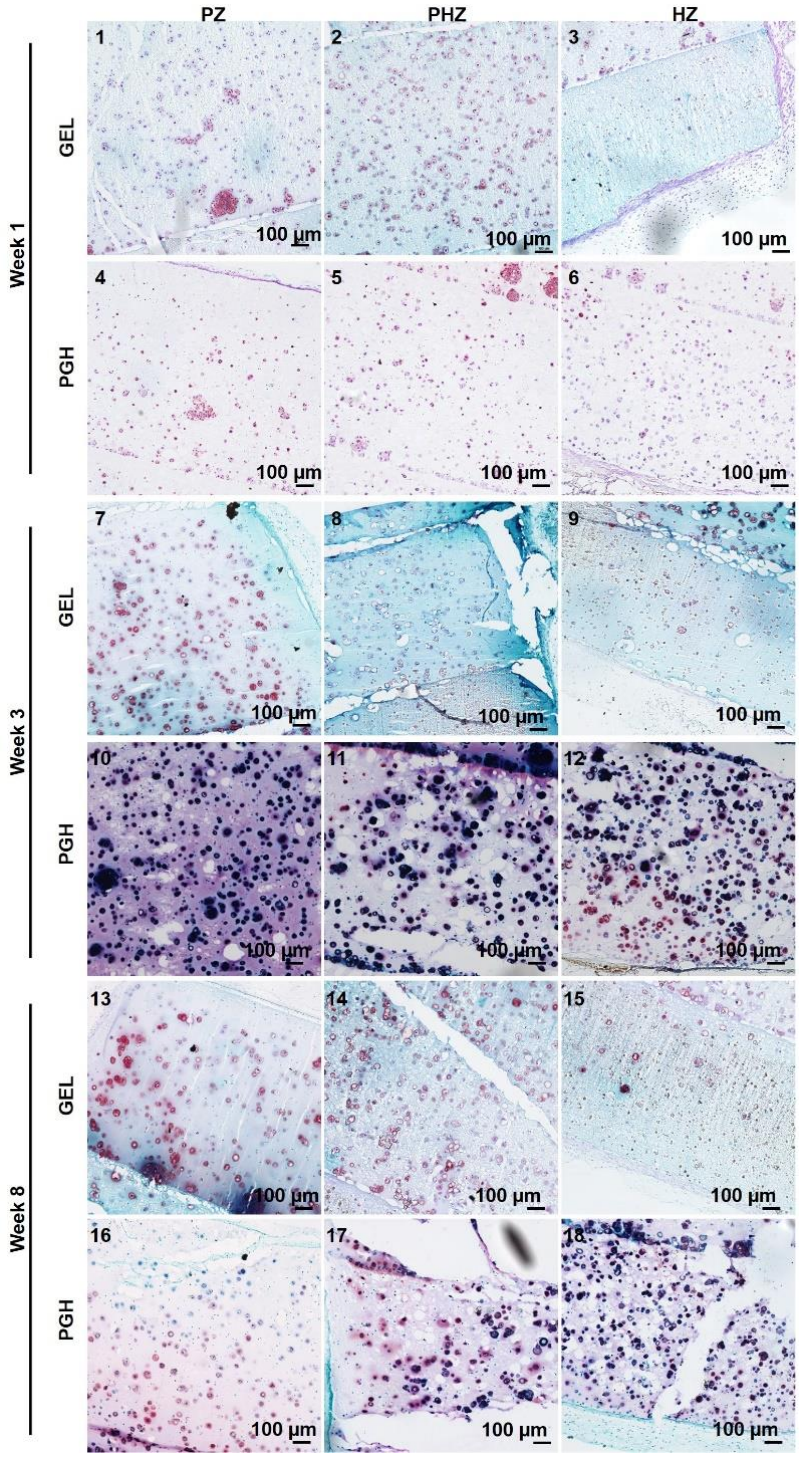

Figure 6-2 Methyl Green Pyronin Y Staining revealed that compared to GEL (1-3, 7-9, 13-15), PGH (4-6, 10-12, 16-18) maintained RNA level (indicating protein synthesis) in hypertrophic chondrocytes over 8 weeks of growth. Blue = Methyl green (DNA); red = Pyronin Y (RNA); purple = both DNA and RNA.

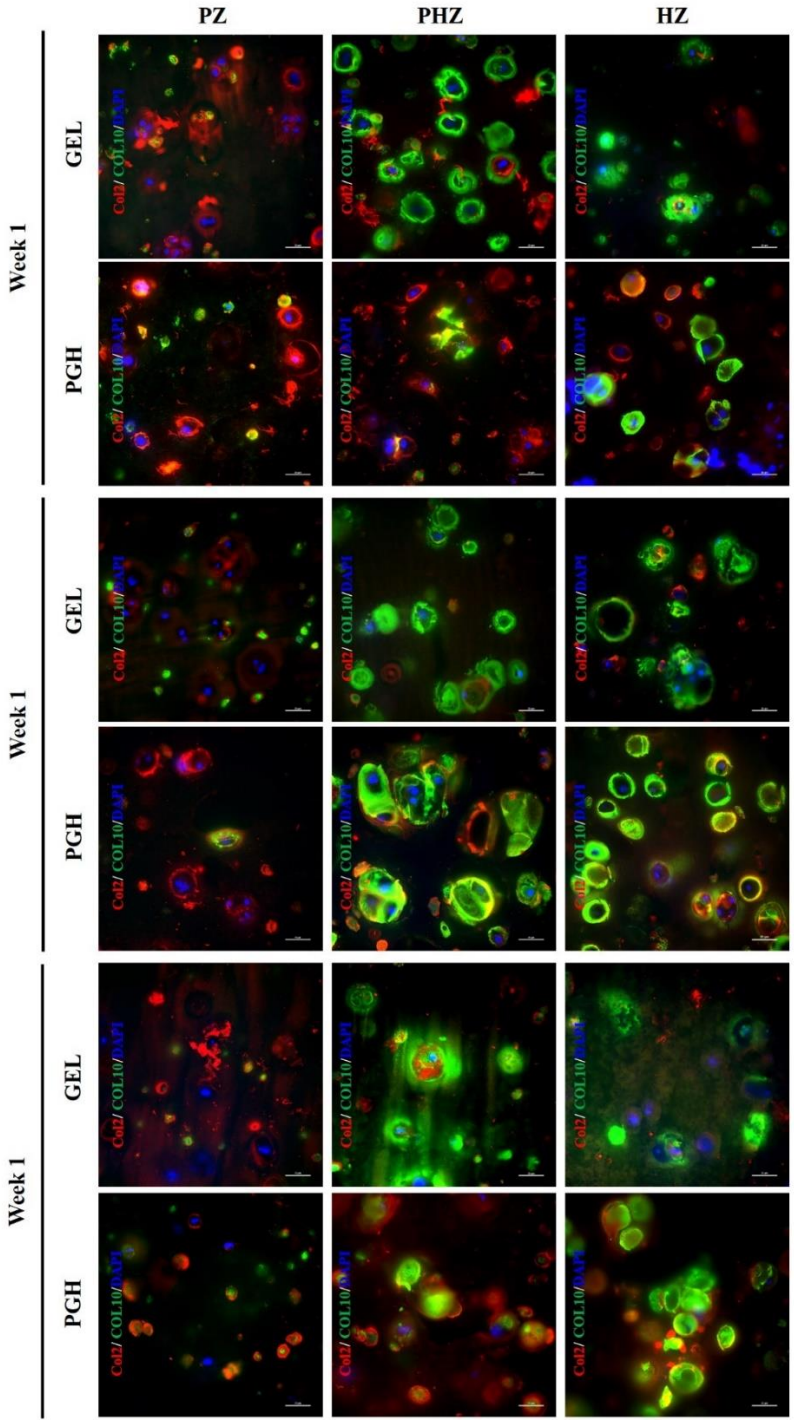

Figure 6-3 Col2 and Col10 deposition by the different chondrocyte populations over 1, 3, and 8 weeks of growth in vivo in GEL and PGH hydrogel constructs. Immunostain red = Col2, green = Col10, blue = nuclei. Scale bar = 20 µm.

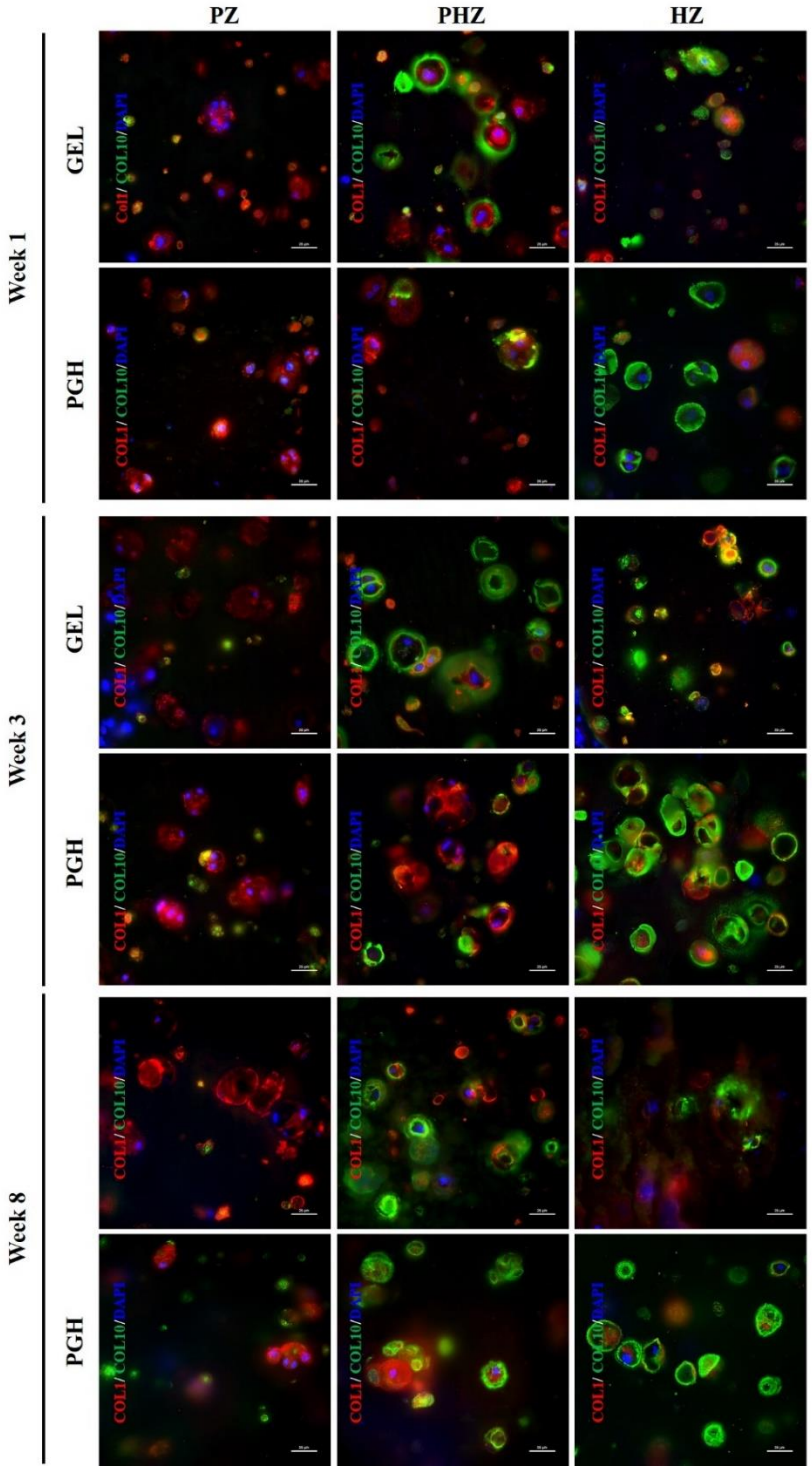

Figure 6-4 Col1 and Col10 deposition by the different chondrocyte populations over 1, 3, and 8 weeks of growth in vivo in GEL and PGH hydrogel constructs. Immunostain red = Col1, green = Col10, blue = nuclei. Scale bar = 20 µm.

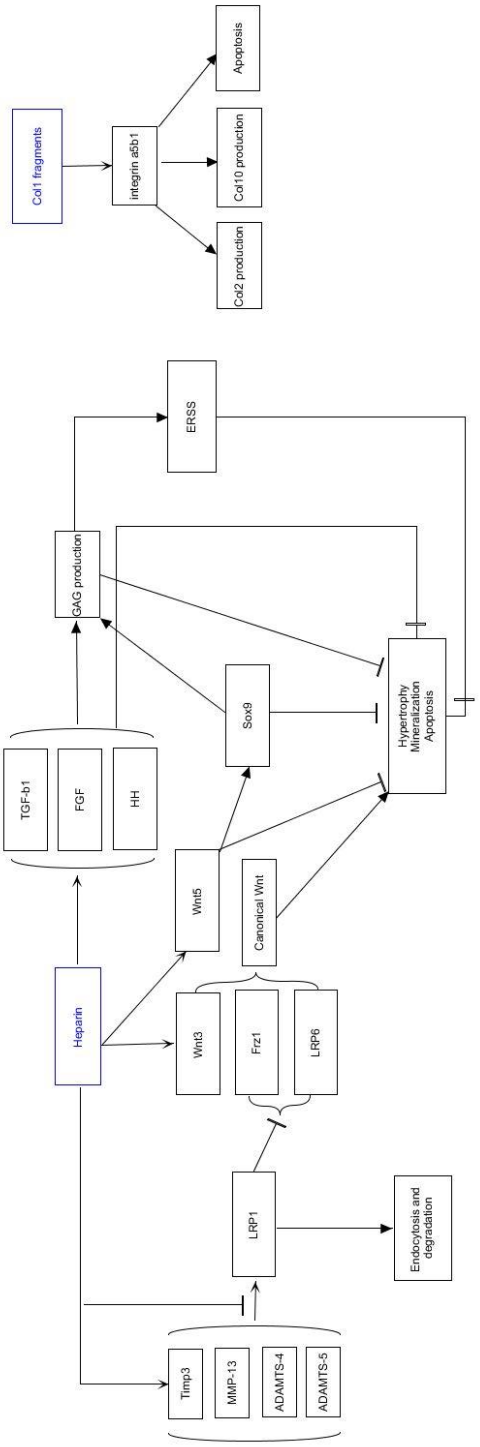

Figure 6-5 Hypothesized signaling pathway underlying the effects of PGH on chondrocyte GAG production and terminal differentiation.

Appendix B Investigation of the Potential Mechanisms that Drive Hydrogel Effects

B.1 Effects of metalloproteinases inhibitor on chondrocyte phenotype

To determine the mechanism that drives hydrogel effects, we further investigated differentiation state progression using *in vitro* cultures where we added inhibitors of matrix metalloproteinases (MMP, inhibitor =GM6001) to the constructs with chick chondrocytes (n=3). Samples were collected after one week for histological and PCR analysis.

We hypothesized that the greater collagen content in GEL-MA compared to PGH hydrogels caused the faster progression to hypertrophy and mineralization in GEL-MA, because endogenous MMP activity would produce collagen fragments that promote hypertrophy [211] However, the MMP inhibition did not significantly alter COL10 secretion in GEL-MA *in vitro*, but it did increase GAG and COL2 matrix secretion. This is likely not due to increased retention of these secreted molecules because PCR results also show up-regulation of GAG and COL2 gene expression. We propose that the PGH hydrogel composition promotes retention and activation of biomolecules that promote cartilage matrix production and phenotype state maintenance.

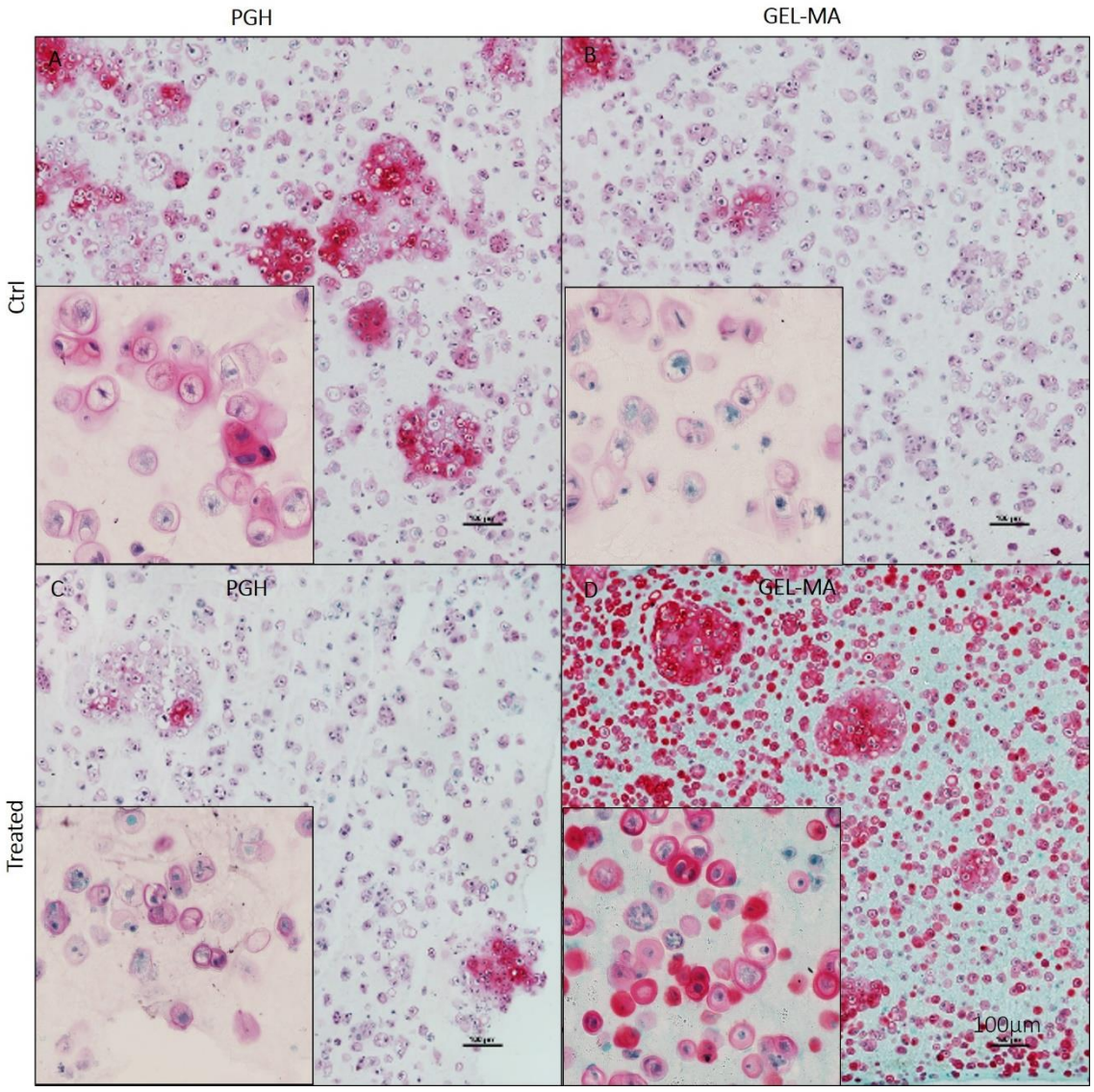

Figure 6-6 In vitro cultures of hypertrophic chondrocytes at 1 week. S.O & Fast Green. Control= untreated and treated= GM6001 supplemented.

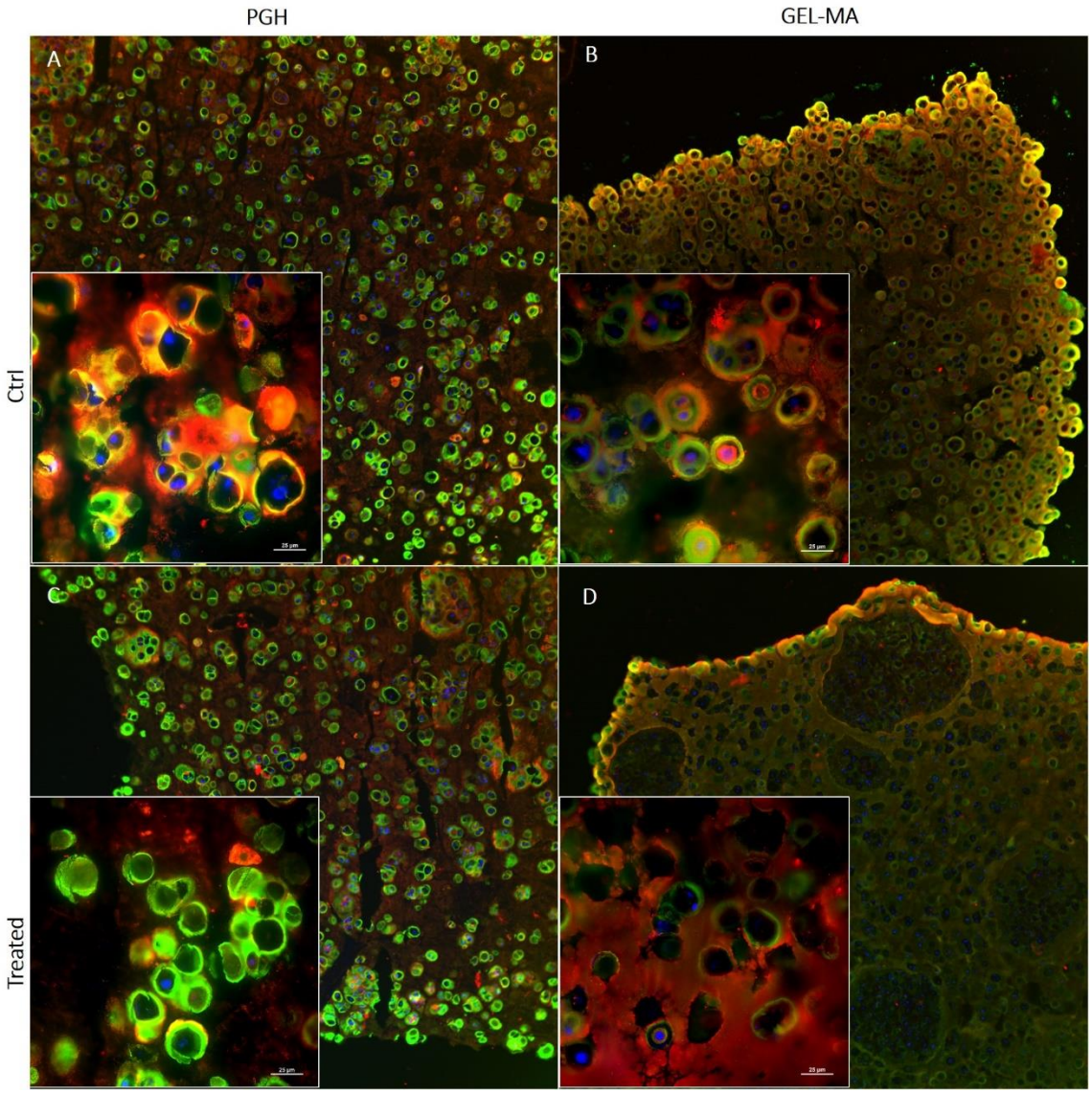

Figure 6-7 In vitro cultures of hypertrophic chondrocytes at 1 week. Green=COL10; Red=COL2; blue=nuclei; yellow=co-localization of COL2 and COL10. Control= untreated and treated= GM6001 supplemented.

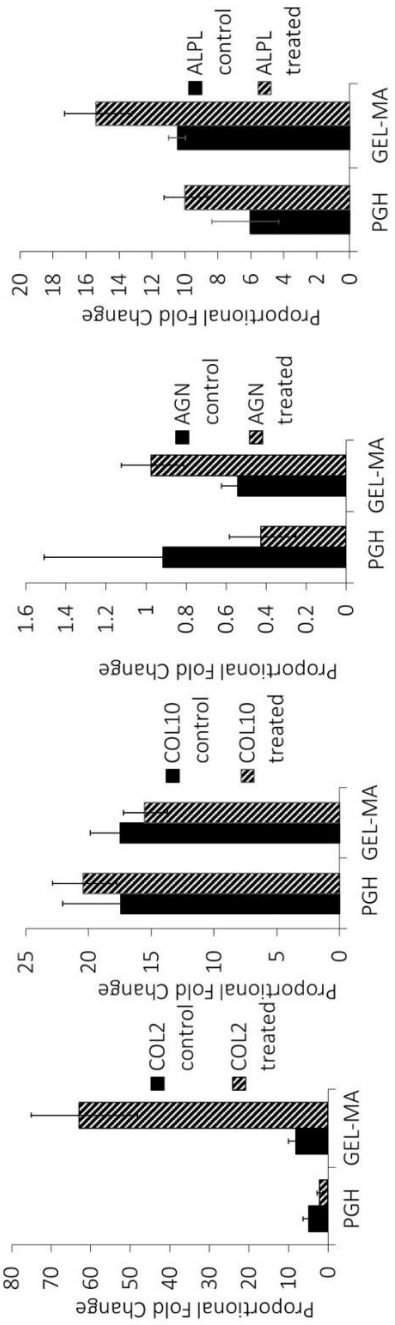

Figure 6-8 Gene expression analysis of untreated (Control) and GM6001 supplemented (Treated) hydrogel cultures at 1 week (normalized to GAPDH). COL2=collagen type 2α1, COL10=collagen type 10, AGN=aggrecan, ALPL= tissue non-specific alkaline phosphatase.

Appendix C Effects of PGH Alone on Mineral Deposition

Cell-free GEL and PGH were cast in transwells (12 well dish, 1cm^2 culture area, 3µm pore size). 10x PBS (pH 7.4, 67 mM PO4) was added to one side of the well, and 100 mM $CaCl_2$ solution was added to the other (n=3, bottom well=2 mL, top well = 500 µL solution). Photographs were taken at 0, 0.5, 1, and 3 hours to monitor mineral deposition. Compared to GEL hydrogels, PGH hydrogels appeared to be less permissive for mineral deposition. Further analysis is needed.

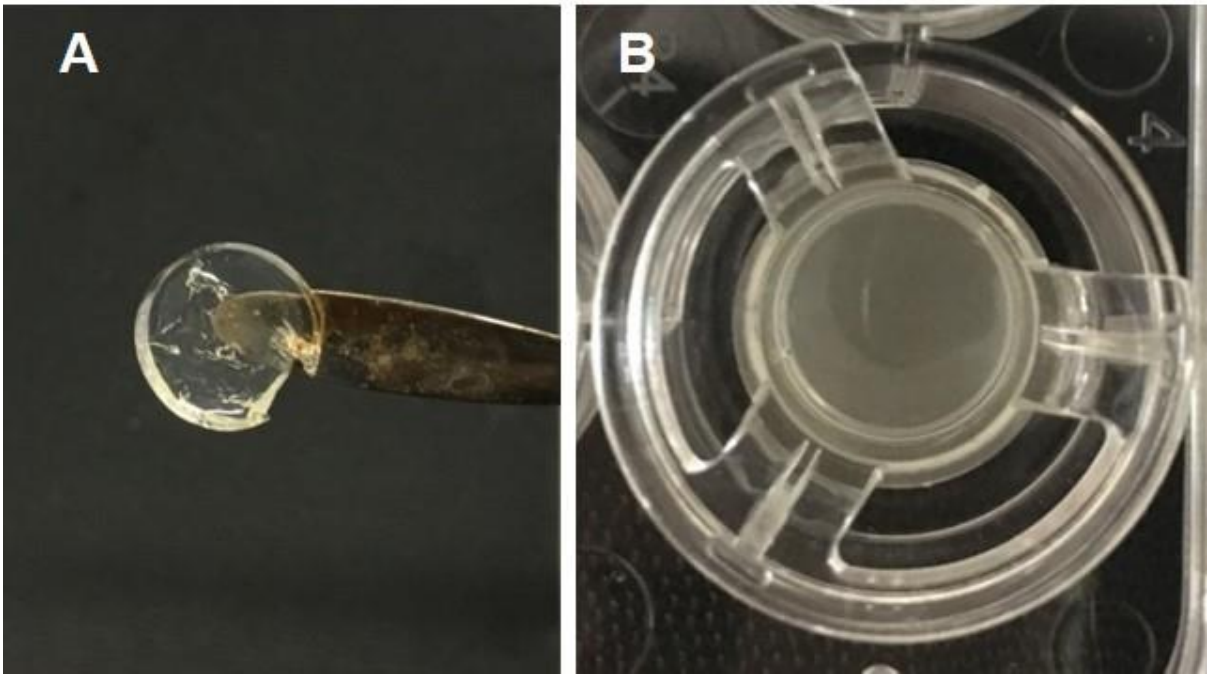

Figure 6-9 A) GEL hydrogel at time 0. B) GEL hydrogel in transwell at time 0.

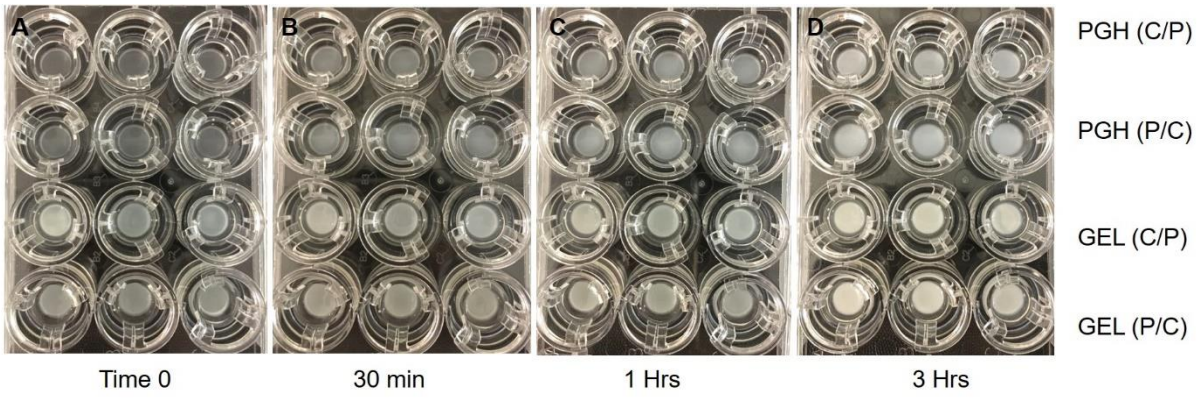

Figure 6-10 Photographs of the hydrogels at 0 (A), 0.5 (B), 1 (C), and 3 hours (D). Both PGH and GEL hydrogels appeared to be more opaque after 3 hours. C/P= CaCl2 in the top insert and PBS in the bottom well. P/C = PBS in the top insert and CaCl2 in the bottom well.

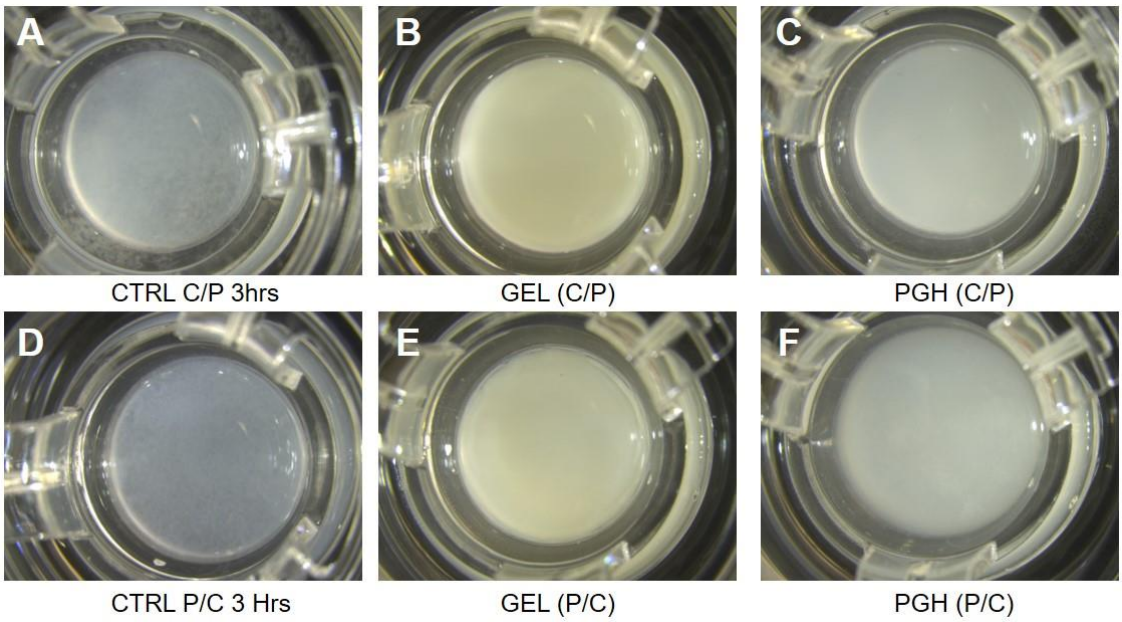

Figure 6-11 Photographs of the hydrogels at 3 hours. A and D are no hydrogel controls. B and E are GEL hydrogels. C and F are PGH hydrogels. C/P= CaCl2 in the top insert and PBS in the bottom well. P/C = PBS in the top insert and CaCl2 in the bottom well.

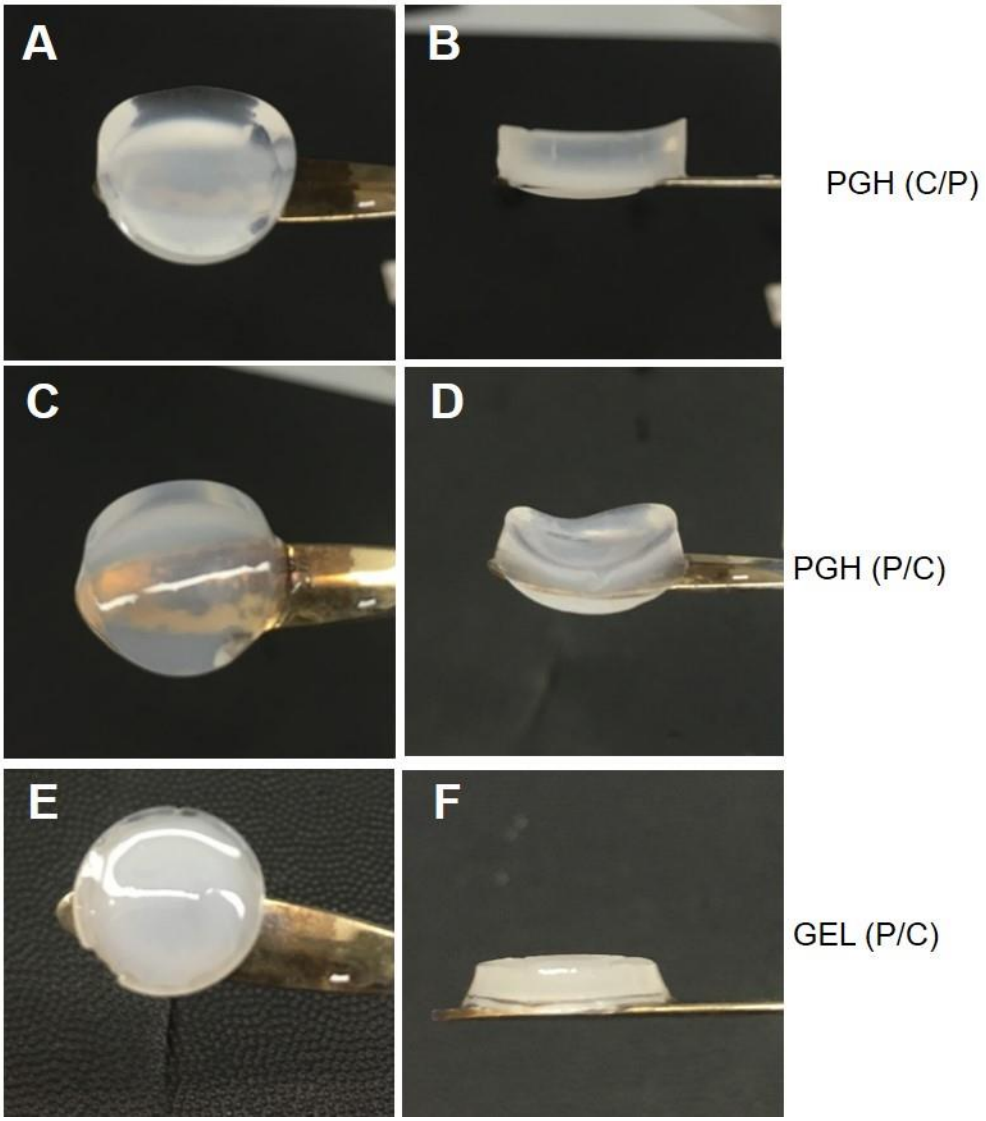

Figure 6-12 Photographs of the hydrogels at 3 hours. A - D are PGH hydrogels. E and F are GEL hydrogels. GEL C/P hydrogels adhered tightly to transwell membranes and could not be removed without damaging the hydrogels. C/P= CaCl2 in the top insert and PBS in the bottom well. P/C = PBS in the top insert and CaCl2 in the bottom well.

Bibliography

1. Olsen, B.R., A.M. Reginato, and W. Wang, *Bone development.* Annu Rev Cell Dev Biol, 2000. **16**: p. 191-220.

2. Kronenberg, H.M., *Developmental regulation of the growth plate.* Nature, 2003. **423**(6937): p. 332-6.

3. Grigoriou, E., A. Trocle, and J.P. Dormans, *140 - The Growth Plate: Embryologic Origin, Structure, and Function*, in *Fetal and Neonatal Physiology (Fifth Edition)*, R.A. Polin, et al., Editors. 2017, Elsevier. p. 1421-1429.e2.

4. Kember, N.F. and H.A. Sissons, *Quantitative histology of the human growth plate.* J Bone Joint Surg Br, 1976. **58-b**(4): p. 426-35.

5. Nguyen, J.C., et al., *Imaging of Pediatric Growth Plate Disturbances.* Radiographics, 2017. **37**(6): p. 1791-1812.

6. Hunziker, E.B., *Mechanism of longitudinal bone growth and its regulation by growth plate chondrocytes.* Microsc Res Tech, 1994. **28**(6): p. 505-19.

7. Alman, B.A., *The role of hedgehog signalling in skeletal health and disease.* Nat Rev Rheumatol, 2015. **11**(9): p. 552-60.

8. Tsang, K.Y., D. Chan, and K.S. Cheah, *Fate of growth plate hypertrophic chondrocytes: death or lineage extension?* Dev Growth Differ, 2015. **57**(2): p. 179-92.

9. Chung, R. and C.J. Xian, *Recent research on the growth plate: Mechanisms for growth plate injury repair and potential cell-based therapies for regeneration.* J Mol Endocrinol, 2014. **53**(1): p. T45-61.

10. Hunziker, E.B., R.K. Schenk, and L.M. Cruz-Orive, *Quantitation of chondrocyte performance in growth-plate cartilage during longitudinal bone growth.* J Bone Joint Surg Am, 1987. **69**(2): p. 162-73.

11. Kirsch, T. and R.E. Wuthier, *Stimulation of calcification of growth plate cartilage matrix vesicles by binding to type II and X collagens.* J Biol Chem, 1994. **269**(15): p. 11462-9.

12. Shaw, N., et al., *Regenerative Medicine Approaches for the Treatment of Pediatric Physeal Injuries.* Tissue Eng Part B Rev, 2018. **24**(2): p. 85-97.

13. Villemure, I. and I.A. Stokes, *Growth plate mechanics and mechanobiology. A survey of present understanding.* J Biomech, 2009. **42**(12): p. 1793-803.

14. Breur, G.J., et al., *Linear relationship between the volume of hypertrophic chondrocytes and the rate of longitudinal bone growth in growth plates.* J Orthop Res, 1991. **9**(3): p. 348-59.

15. Randall, R.M., et al., *Activation of Wnt Planar Cell Polarity (PCP) signaling promotes growth plate column formation in vitro.* J Orthop Res, 2012. **30**(12): p. 1906-14.

16. Frances, J.M., et al., *What is quality of life in children with bone sarcoma?* Clin Orthop Relat Res, 2007. **459**: p. 34-9.

17. Ecklund, K. and D. Jaramillo, *Patterns of premature physeal arrest: MR imaging of 111 children.* AJR Am J Roentgenol, 2002. **178**(4): p. 967-72.

18. Cepela, D.J., et al., *Classifications In Brief: Salter-Harris Classification of Pediatric Physeal Fractures.* Clin Orthop Relat Res, 2016. **474**(11): p. 2531-2537.

19. Arasapam, G., et al., *Roles of COX-2 and iNOS in the bony repair of the injured growth plate cartilage.* J Cell Biochem, 2006. **99**(2): p. 450-61.

20. Chung, R., et al., *Roles of neutrophil-mediated inflammatory response in the bony repair of injured growth plate cartilage in young rats.* J Leukoc Biol, 2006. **80**(6): p. 1272-80.

21. Shapiro, F., *Epiphyseal Disorders.* New England Journal of Medicine, 1987. **317**(27): p. 1702-1710.

22. Langenskiold, A., *An operation for partial closure of an epiphysial plate in children, and its experimental basis.* J Bone Joint Surg Br, 1975. **57**(3): p. 325-30.

23. Osterman, K., *Operative elimination of partial premature epiphyseal closure. An experimental study.* Acta Orthop Scand Suppl, 1972: p. 3-79.

24. Tobita, M., et al., *Treatment of growth plate injury with autogenous chondrocytes: a study in rabbits.* Acta Orthop Scand, 2002. **73**(3): p. 352-8.

25. Hasler, C.C. and B.K. Foster, *Secondary tethers after physeal bar resection: a common source of failure?* Clin Orthop Relat Res, 2002(405): p. 242-9.

26. Chung, R., B. Foster, and C. Xian, *Preclinical Studies on Mesenchymal Stem Cell-Based Therapy for Growth Plate Cartilage Injury Repair*. Vol. 2011. 2011. 570125.

27. Foster, B.K., et al., *Reimplantation of growth plate chondrocytes into growth plate defects in sheep.* J Orthop Res, 1990. **8**(4): p. 555-64.

28. Lee, E.H., et al., *Treatment of growth arrest by transfer of cultured chondrocytes into physeal defects.* J Pediatr Orthop, 1998. **18**(2): p. 155-60.

29. Park, J., et al., *Transgene-activated mesenchymal cells for articular cartilage repair: a comparison of primary bone marrow-, perichondrium/periosteum- and fat-derived cells.* J Gene Med, 2006. **8**(1): p. 112-25.

30. Schmitt, J.F., et al., *Sequential differentiation of mesenchymal stem cells in an agarose scaffold promotes a physis-like zonal alignment of chondrocytes.* J Orthop Res, 2012. **30**(11): p. 1753-9.

31. Liu, M., et al., *Injectable hydrogels for cartilage and bone tissue engineering.* Bone research, 2017. **5**: p. 17014-17014.

32. Nguyen, K.T. and J.L. West, *Photopolymerizable hydrogels for tissue engineering applications.* Biomaterials, 2002. **23**(22): p. 4307-4314.

33. Steinmetz, N.J., et al., *Mechanical loading regulates human MSC differentiation in a multi-layer hydrogel for osteochondral tissue engineering.* Acta Biomater, 2015. **21**: p. 142-53.

34. Yang, J., et al., *Cell-laden hydrogels for osteochondral and cartilage tissue engineering.* Acta Biomater, 2017. **57**: p. 1-25.

35. Degoricija, L., et al., *Hydrogels for osteochondral repair based on photocrosslinkable carbamate dendrimers.* Biomacromolecules, 2008. **9**(10): p. 2863-72.

36. Zhu, J., *Bioactive modification of poly(ethylene glycol) hydrogels for tissue engineering.* Biomaterials, 2010. **31**(17): p. 4639-56.

37. Morgan, A.W., et al., *Detection of growth factor binding to gelatin and heparin using a photonic crystal optical biosensor.* Materials Science and Engineering: C, 2010. **30**(5): p. 686-690.

38. Ikada, Y. and Y. Tabata, *Protein release from gelatin matrices.* Adv Drug Deliv Rev, 1998. **31**(3): p. 287-301.

39. Aszodi, A., et al., *Beta1 integrins regulate chondrocyte rotation, G1 progression, and cytokinesis.* Genes Dev, 2003. **17**(19): p. 2465-79.

40. Gao, G., et al., *Improved properties of bone and cartilage tissue from 3D inkjet-bioprinted human mesenchymal stem cells by simultaneous deposition and photocrosslinking in PEG-GelMA.* Biotechnol Lett, 2015. **37**(11): p. 2349-55.

41. Ashikari-Hada, S., et al., *Characterization of growth factor-binding structures in heparin/heparan sulfate using an octasaccharide library.* J Biol Chem, 2004. **279**(13): p. 12346-54.

42. Tae, G., et al., *PEG-cross-linked heparin is an affinity hydrogel for sustained release of vascular endothelial growth factor.* J Biomater Sci Polym Ed, 2006. **17**(1-2): p. 187-97.

43. Choi, D., et al., *Preparation of poly(ethylene glycol) hydrogels with different network structures for the application of enzyme immobilization.* Biomed Mater Eng, 2008. **18**(6): p. 345-56.

44. Murugesan, S., J. Xie, and R.J. Linhardt, *Immobilization of heparin: approaches and applications.* Curr Top Med Chem, 2008. **8**(2): p. 80-100.

45. Kamerzell, T.J., et al., *Parathyroid hormone is a heparin/polyanion binding protein: binding energetics and structure modification.* Protein Sci, 2007. **16**(6): p. 1193-203.

46. Lyon, M., G. Rushton, and J.T. Gallagher, *The interaction of the transforming growth factor-betas with heparin/heparan sulfate is isoform-specific.* J Biol Chem, 1997. **272**(29): p. 18000-6.

47. Rider, C.C. and B. Mulloy, *Heparin, Heparan Sulphate and the TGF-beta Cytokine Superfamily*. Molecules, 2017. **22**(5).

48. Veraldi, N., et al., *Structural Features of Heparan Sulfate from Multiple Osteochondromas and Chondrosarcomas*. Vol. 23. 2018. 3277.

49. Pacifici, M., et al., *Retinoic acid treatment induces type X collagen gene expression in cultured chick chondrocytes.* Exp Cell Res, 1991. **195**(1): p. 38-46.

50. Hansen, N.M., et al., *Aggregation of hydroxyapatite crystals.* Biochim Biophys Acta, 1976. **451**(2): p. 549-59.

51. Termine, J.D. and A.S. Posner, *Calcium phosphate formation in vitro. I. Factors affecting initial phase separation.* Arch Biochem Biophys, 1970. **140**(2): p. 307-17.

52. Chen, C.C., A.L. Boskey, and L.C. Rosenberg, *The inhibitory effect of cartilage proteoglycans on hydroxyapatite growth.* Calcif Tissue Int, 1984. **36**(3): p. 285-90.

53. Rees, S.G., et al., *Effect of serum albumin on glycosaminoglycan inhibition of hydroxyapatite formation.* Biomaterials, 2004. **25**(6): p. 971-7.

54. Bhandari, M., et al., *The effects of standard and low molecular weight heparin on bone nodule formation in vitro.* Thromb Haemost, 1998. **80**(3): p. 413-7.

55. Hausser, H.J. and R.E. Brenner, *Low doses and high doses of heparin have different effects on osteoblast-like Saos-2 cells in vitro.* J Cell Biochem, 2004. **91**(5): p. 1062-73.

56. Silverman, L. and A.L. Boskey, *Diffusion systems for evaluation of biomineralization.* Calcified tissue international, 2004. **75**(6): p. 494-501.

57. Zhang, T., et al., *Softening Substrates Promote Chondrocytes Phenotype via RhoA/ROCK Pathway.* ACS Appl Mater Interfaces, 2016. **8**(35): p. 22884-91.

58. Liu, Q., et al., *Effects of mechanical stress on chondrocyte phenotype and chondrocyte extracellular matrix expression.* Vol. 6. 2016. 37268.

59. Nichol, J.W., et al., *Cell-laden microengineered gelatin methacrylate hydrogels.* Biomaterials, 2010. **31**(21): p. 5536-5544.

60. Lin-Gibson, S., et al., *Synthesis and characterization of PEG dimethacrylates and their hydrogels.* Biomacromolecules, 2004. **5**(4): p. 1280-7.

61. Schuurman, W., et al., *Gelatin-methacrylamide hydrogels as potential biomaterials for fabrication of tissue-engineered cartilage constructs.* Macromol Biosci, 2013. **13**(5): p. 551-61.

62. Benoit, D.S., A.R. Durney, and K.S. Anseth, *The effect of heparin-functionalized PEG hydrogels on three-dimensional human mesenchymal stem cell osteogenic differentiation.* Biomaterials, 2007. **28**(1): p. 66-77.

63. Majima, T., W. Schnabel, and W. Weber, *Phenyl‐2,4,6‐trimethylbenzoylphosphinates as water‐soluble photoinitiators. Generation and reactivity of O□Ṗ(C6H5)(O−) radical anions*. Vol. 192. 2003. 2307-2315.

64. Son, K.H. and J.W. Lee, *Synthesis and Characterization of Poly(Ethylene Glycol) Based Thermo-Responsive Hydrogels for Cell Sheet Engineering.* Materials (Basel), 2016. **9**(10).

65. Wang, Z., et al., *Comparative study of gelatin methacrylate hydrogels from different sources for biofabrication applications.* Biofabrication, 2017. **9**(4): p. 044101.

66. Nilasaroya, A., et al., *Structural and functional characterisation of poly(vinyl alcohol) and heparin hydrogels.* Biomaterials, 2008. **29**(35): p. 4658-64.

67. Costantini, M., et al., *3D bioprinting of BM-MSCs-loaded ECM biomimetic hydrogels for in vitro neocartilage formation.* Biofabrication, 2016. **8**(3): p. 035002.

68. Shim, J.H., et al., *Three-dimensional bioprinting of multilayered constructs containing human mesenchymal stromal cells for osteochondral tissue regeneration in the rabbit knee joint.* Biofabrication, 2016. **8**(1): p. 014102.

69. Damron, T.A., et al., *Histomorphometric evidence of growth plate recovery potential after fractionated radiotherapy: an in vivo model.* Radiat Res, 2008. **170**(3): p. 284-91.

70. Gerber, H.P., et al., *VEGF couples hypertrophic cartilage remodeling, ossification and angiogenesis during endochondral bone formation.* Nat Med, 1999. **5**(6): p. 623-8.

71. Abad, V., et al., *The role of the resting zone in growth plate chondrogenesis.* Endocrinology, 2002. **143**(5): p. 1851-7.

72. Morales, T.I., *Chondrocyte moves: clever strategies?* Osteoarthritis Cartilage, 2007. **15**(8): p. 861-71.

73. Beier, F., *Cell-cycle control and the cartilage growth plate.* J Cell Physiol, 2005. **202**(1): p. 1-8.

74. D'Angelo, M. and M. Pacifici, *Articular chondrocytes produce factors that inhibit maturation of sternal chondrocytes in serum-free agarose cultures: a TGF-beta independent process.* J Bone Miner Res, 1997. **12**(9): p. 1368-77.

75. Hunter, G., et al., *Inhibition of hydroxyapatite formation in collagen gels by chondroitin sulfate*. Vol. 228. 1985. 463-9.

76. Studer, D., et al., *Molecular and biophysical mechanisms regulating hypertrophic differentiation in chondrocytes and mesenchymal stem cells.* Eur Cell Mater, 2012. **24**: p. 118-35; discussion 135.

77. Ravindran, S., et al., *Assessment of epiphyseal plate allograft viability and function after ex vivo storage in University of Wisconsin Solution.* J Pediatr Orthop, 2011. **31**(7): p. 803-10.

78. Boyer, M.I., P.W. Bray, and C.V. Bowen, *Epiphyseal plate transplantation: an historical review.* Br J Plast Surg, 1994. **47**(8): p. 563-9.

79. Hirsch, M.S., et al., *Chondrocyte survival and differentiation in situ are integrin mediated.* Dev Dyn, 1997. **210**(3): p. 249-63.

80. Harrington, E.K., L.E. Lunsford, and K.K. Svoboda, *Chondrocyte terminal differentiation, apoptosis, and type X collagen expression are downregulated by parathyroid hormone.* Anat Rec A Discov Mol Cell Evol Biol, 2004. **281**(2): p. 1286-95.

81. Harrington, E.K., et al., *Parathyroid hormone/parathyroid hormone-related peptide modulates growth of avian sternal cartilage via chondrocytic proliferation.* Anat Rec (Hoboken), 2007. **290**(2): p. 155-67.

82. Alini, M., et al., *The extracellular matrix of cartilage in the growth plate before and during calcification: changes in composition and degradation of type II collagen.* Calcif Tissue Int, 1992. **50**(4): p. 327-35.

83. von der Mark, K. and H. von der Mark, *The role of three genetically distinct collagen types in endochondral ossification and calcification of cartilage.* J Bone Joint Surg Br, 1977. **59-b**(4): p. 458-64.

84. Yasui, N., et al., *Transitions in collagen types during endochondral ossification in human growth cartilage.* Clin Orthop Relat Res, 1984(183): p. 215-8.

85. Siffert, R.S., *The role of alkaline phosphatase in osteogenesis.* The Journal of experimental medicine, 1951. **93**(5): p. 415-426.

86. Kirsch, T. and K. von der Mark, *Remodelling of collagen types I, II and X and calcification of human fetal cartilage.* Bone Miner, 1992. **18**(2): p. 107-17.

87. Adams, C.S. and I.M. Shapiro, *The fate of the terminally differentiated chondrocyte: evidence for microenvironmental regulation of chondrocyte apoptosis.* Crit Rev Oral Biol Med, 2002. **13**(6): p. 465-73.

88. Eyre, D.R. and J.J. Wu, *Collagen of fibrocartilage: a distinctive molecular phenotype in bovine meniscus.* FEBS Lett, 1983. **158**(2): p. 265-70.

89. Kiani, C., et al., *Structure and function of aggrecan.* Cell Res, 2002. **12**(1): p. 19-32.

90. Nguyen, L.H., et al., *Engineering articular cartilage with spatially-varying matrix composition and mechanical properties from a single stem cell population using a multi-layered hydrogel.* Biomaterials, 2011. **32**(29): p. 6946-52.

91. Lammi, P.E., et al., *Site-specific immunostaining for type X collagen in noncalcified articular cartilage of canine stifle knee joint.* Bone, 2002. **31**(6): p. 690-6.

92. Eerola, I., et al., *Type X collagen, a natural component of mouse articular cartilage: association with growth, aging, and osteoarthritis.* Arthritis Rheum, 1998. **41**(7): p. 1287-95.

93. Miao, D. and A. Scutt, *Histochemical Localization of Alkaline Phosphatase Activity in Decalcified Bone and Cartilage.* Journal of Histochemistry & Cytochemistry, 2002. **50**(3): p. 333-340.

94. Sharma, B., et al., *Designing zonal organization into tissue-engineered cartilage.* Tissue Eng, 2007. **13**(2): p. 405-14.

95. Ng, K.W., G.A. Ateshian, and C.T. Hung, *Zonal chondrocytes seeded in a layered agarose hydrogel create engineered cartilage with depth-dependent cellular and mechanical inhomogeneity.* Tissue Eng Part A, 2009. **15**(9): p. 2315-24.

96. Bellairs, R., M. Osmond, and I. ebrary, *The atlas of chick development*. Third ed. 2014, Waltham, MA;Oxford, UK;: Academic Press.

97. Boere, K.W., et al., *Covalent attachment of a three-dimensionally printed thermoplast to a gelatin hydrogel for mechanically enhanced cartilage constructs.* Acta Biomater, 2014. **10**(6): p. 2602-11.

98. Schuurman, W., et al., *Gelatin-Methacrylamide Hydrogels as Potential Biomaterials for Fabrication of Tissue-Engineered Cartilage Constructs.* Macromolecular Bioscience, 2013. **13**(5): p. 551-561.

99. Klotz, B.J., et al., *Gelatin-Methacryloyl Hydrogels: Towards Biofabrication-Based Tissue Repair.* Trends Biotechnol, 2016. **34**(5): p. 394-407.

100. Levett, P.A., et al., *A biomimetic extracellular matrix for cartilage tissue engineering centered on photocurable gelatin, hyaluronic acid and chondroitin sulfate.* Acta Biomater, 2014. **10**(1): p. 214-23.

101. Guo, Y., et al., *Hydrogels of collagen/chondroitin sulfate/hyaluronan interpenetrating polymer network for cartilage tissue engineering.* Journal of Materials Science: Materials in Medicine, 2012. **23**(9): p. 2267-2279.

102. Onofrillo, C., et al., *Biofabrication of human articular cartilage: a path towards the development of a clinical treatment.* Biofabrication, 2018. **10**(4): p. 045006.

103. Brown, G.C.J., et al., *Covalent Incorporation of Heparin Improves Chondrogenesis in Photocurable Gelatin-Methacryloyl Hydrogels.* Macromol Biosci, 2017. **17**(12).

104. Ylärinne, J.H., C. Qu, and M.J. Lammi, *HyStem™ and HydroMatrix™ scaffolds for articular cartilage tissue engineering.* Osteoarthritis and Cartilage, 2016. **24**: p. S466.

105. Hayami, J.W.S., S.D. Waldman, and B.G. Amsden, *Photo-cross-linked methacrylated polysaccharide solution blends with high chondrocyte viability, minimal swelling, and moduli similar to load bearing soft tissues.* European Polymer Journal, 2015. **72**: p. 687-697.

106. Bian, L., et al., *The influence of hyaluronic acid hydrogel crosslinking density and macromolecular diffusivity on human MSC chondrogenesis and hypertrophy.* Biomaterials, 2013. **34**(2): p. 413-21.

107. Pomin, V.H. and B. Mulloy, *Glycosaminoglycans and Proteoglycans.* Pharmaceuticals (Basel, Switzerland), 2018. **11**(1): p. 27.

108. Mizumoto, S., D. Fongmoon, and K. Sugahara, *Interaction of chondroitin sulfate and dermatan sulfate from various biological sources with heparin-binding growth factors and cytokines.* Glycoconj J, 2013. **30**(6): p. 619-32.

109. Ayerst, B.I., C.L.R. Merry, and A.J. Day, *The Good the Bad and the Ugly of Glycosaminoglycans in Tissue Engineering Applications.* Pharmaceuticals (Basel, Switzerland), 2017. **10**(2): p. 54.

110. Liu, G., et al., *Multi-Layered Hydrogels for Biomedical Applications.* Frontiers in chemistry, 2018. **6**: p. 439-439.

111. Horton, W.A., et al., *Immunohistochemistry of types I and II collagen in undecalcified skeletal tissues.* J Histochem Cytochem, 1983. **31**(3): p. 417-25.

112. Sandberg, M. and E. Vuorio, *Localization of types I, II, and III collagen mRNAs in developing human skeletal tissues by in situ hybridization.* J Cell Biol, 1987. **104**(4): p. 1077-84.

113. Ryu, J.H., et al., *Regulation of the chondrocyte phenotype by beta-catenin.* Development, 2002. **129**(23): p. 5541-50.

114. Cheng, T., et al., *Comparison of gene expression patterns in articular cartilage and dedifferentiated articular chondrocytes.* Journal of Orthopaedic Research, 2012. **30**(2): p. 234-245.

115. Treilleux, I., et al., *Localization of the expression of type I, II, III collagen, and aggrecan core protein genes in developing human articular cartilage.* Matrix, 1992. **12**(3): p. 221-32.

116. Roach, H.I. and J.R. Shearer, *Cartilage resorption and endochondral bone formation during the development of long bones in chick embryos.* Bone Miner, 1989. **6**(3): p. 289-309.

117. Badria, A., et al., *The effect of heparin hydrogel embedding on glutaraldehyde fixed bovine pericardial tissues: Mechanical behavior and anticalcification potential.* J Mater Sci Mater Med, 2018. **29**(11): p. 175.

118. Bajpayee, A.G., et al., *Electrostatic interactions enable rapid penetration, enhanced uptake and retention of intra-articular injected avidin in rat knee joints.* J Orthop Res, 2014. **32**(8): p. 1044-51.

119. Cuervo, L.A., J.C. Pita, and D.S. Howell, *Inhibition of calcium phosphate mineral growth by proteoglycan aggregate fractions in a synthetic lymph.* Calcified Tissue Research, 1973. **13**(1): p. 1-10.

120. Kudo, T., et al., *Supplemented Chondroitin Sulfate and Hyaluronic Acid Suppress Mineralization of the Chondrogenic Cell Line, ATDC5, via Direct Inhibition of Alkaline Phosphatase.* Biol Pharm Bull, 2017. **40**(12): p. 2075-2080.

121. Boskey, A.L., et al., *Treatment of proteoglycan aggregates with physeal enzymes reduces their ability to inhibit hydroxyapatite proliferation in a gelatin gel.* J Orthop Res, 1992. **10**(3): p. 313-9.

122. Jubeck, B., et al., *Type II collagen levels correlate with mineralization by articular cartilage vesicles.* Arthritis Rheum, 2009. **60**(9): p. 2741-6.

123. Kim, H.J. and T. Kirsch, *Collagen/annexin V interactions regulate chondrocyte mineralization.* J Biol Chem, 2008. **283**(16): p. 10310-7.

124. Inoue, T., et al., *In vivo analysis of Arg-Gly-Asp sequence/integrin alpha5beta1-mediated signal involvement in embryonic enchondral ossification by exo utero development system.* J Bone Miner Res, 2014. **29**(7): p. 1554-63.

125. Garciadiego-Cazares, D., et al., *Coordination of chondrocyte differentiation and joint formation by alpha5beta1 integrin in the developing appendicular skeleton.* Development, 2004. **131**(19): p. 4735-42.

126. Ornitz, D.M. and P.J. Marie, *Fibroblast growth factor signaling in skeletal development and disease.* Genes Dev, 2015. **29**(14): p. 1463-86.

127. Bohme, K., et al., *Induction of proliferation or hypertrophy of chondrocytes in serum-free culture: the role of insulin-like growth factor-I, insulin, or thyroxine.* J Cell Biol, 1992. **116**(4): p. 1035-42.

128. Kakonen, S.M., et al., *Transforming growth factor-beta stimulates parathyroid hormone-related protein and osteolytic metastases via Smad and mitogen-activated protein kinase signaling pathways.* J Biol Chem, 2002. **277**(27): p. 24571-8.

129. Li, T.F., R.J. O'Keefe, and D. Chen, *TGF-beta signaling in chondrocytes.* Front Biosci, 2005. **10**: p. 681-8.

130. Sridhar, B.V., et al., *Covalently tethered TGF-beta1 with encapsulated chondrocytes in a PEG hydrogel system enhances extracellular matrix production.* J Biomed Mater Res A, 2014. **102**(12): p. 4464-72.

131. Ornitz, D.M. and P.J. Marie, *FGF signaling pathways in endochondral and intramembranous bone development and human genetic disease.* Genes Dev, 2002. **16**(12): p. 1446-65.

132. Zhang, F., et al., *Kinetic and structural studies on interactions between heparin or heparan sulfate and proteins of the hedgehog signaling pathway.* Biochemistry, 2007. **46**(13): p. 3933-41.

133. Capila, I. and R.J. Linhardt, *Heparin-protein interactions.* Angew Chem Int Ed Engl, 2002. **41**(3): p. 391-412.

134. Whitelock, J.M. and R.V. Iozzo, *Heparan sulfate: a complex polymer charged with biological activity.* Chem Rev, 2005. **105**(7): p. 2745-64.

135. Lin, X., *Functions of heparan sulfate proteoglycans in cell signaling during development.* Development, 2004. **131**(24): p. 6009-21.

136. McLellan, J.S., et al., *Structure of a heparin-dependent complex of Hedgehog and Ihog.* Proc Natl Acad Sci U S A, 2006. **103**(46): p. 17208-13.

137. Brown, C.C. and G. Balian, *Effect of heparin on synthesis of short chain collagen by chondrocytes and smooth muscle cells.* J Cell Biol, 1987. **105**(2): p. 1007-12.

138. Lu, C., et al., *Wnt-mediated reciprocal regulation between cartilage and bone development during endochondral ossification.* Bone, 2013. **53**(2): p. 566-74.

139. Tamamura, Y., et al., *Developmental regulation of Wnt/beta-catenin signals is required for growth plate assembly, cartilage integrity, and endochondral ossification.* J Biol Chem, 2005. **280**(19): p. 19185-95.

140. Kirkeby, S. and C.E. Thomsen, *Quantitative immunohistochemistry of fluorescence labelled probes using low-cost software.* J Immunol Methods, 2005. **301**(1-2): p. 102-13.

141. Solomon, D.H., et al., *Characterisation of inorganic phosphate transport in bovine articular chondrocytes.* Cell Physiol Biochem, 2007. **20**(1-4): p. 99-108.

142. Hirsch, M.S. and K.H. Svoboda, *Establishment of a whole-chick sternum model that recapitulates normal cartilage development.* Biotechniques, 1998. **24**(4): p. 632-6.

143. Vega, S.L., M.Y. Kwon, and J.A. Burdick, *Recent advances in hydrogels for cartilage tissue engineering.* Eur Cell Mater, 2017. **33**: p. 59-75.

144. Jin, G.Z. and H.W. Kim, *Efficacy of collagen and alginate hydrogels for the prevention of rat chondrocyte dedifferentiation.* J Tissue Eng, 2018. **9**: p. 2041731418802438.

145. Bian, L., et al., *Coculture of human mesenchymal stem cells and articular chondrocytes reduces hypertrophy and enhances functional properties of engineered cartilage.* Tissue Eng Part A, 2011. **17**(7-8): p. 1137-45.

146. Gabay, O., C. Sanchez, and J.M. Taboas, *Update in cartilage bio-engineering.* Joint Bone Spine, 2010. **77**(4): p. 283-6.

147. Roseti, L., et al., *Three-Dimensional Bioprinting of Cartilage by the Use of Stem Cells: A Strategy to Improve Regeneration.* Materials (Basel), 2018. **11**(9).

148. Sekiya, I., et al., *In vitro cartilage formation by human adult stem cells from bone marrow stroma defines the sequence of cellular and molecular events during chondrogenesis.* Proc Natl Acad Sci U S A, 2002. **99**(7): p. 4397-402.

149. Chen, Y., et al., *Exosomes derived from mature chondrocytes facilitate subcutaneous stable ectopic chondrogenesis of cartilage progenitor cells.* Stem Cell Res Ther, 2018. **9**(1): p. 318.

150. Aisenbrey, E.A. and S.J. Bryant, *The role of chondroitin sulfate in regulating hypertrophy during MSC chondrogenesis in a cartilage mimetic hydrogel under dynamic loading.* Biomaterials, 2019. **190-191**: p. 51-62.

151. Liu, Q., et al., *Suppressing mesenchymal stem cell hypertrophy and endochondral ossification in 3D cartilage regeneration with nanofibrous poly(l-lactic acid) scaffold and matrilin-3.* Acta Biomater, 2018. **76**: p. 29-38.

152. Dickhut, A., et al., *Calcification or dedifferentiation: Requirement to lock mesenchymal stem cells in a desired differentiation stage.* Journal of Cellular Physiology, 2009. **219**(1): p. 219-226.

153. De Bari, C., F. Dell'Accio, and F.P. Luyten, *Failure of in vitro-differentiated mesenchymal stem cells from the synovial membrane to form ectopic stable cartilage in vivo.* Arthritis Rheum, 2004. **50**(1): p. 142-50.

154. Levato, R., et al., *The bio in the ink: cartilage regeneration with bioprintable hydrogels and articular cartilage-derived progenitor cells.* Acta Biomater, 2017. **61**: p. 41-53.

155. Sheehy, E.J., et al., *Engineering osteochondral constructs through spatial regulation of endochondral ossification.* Acta Biomaterialia, 2013. **9**(3): p. 5484-5492.

156. Lee, W.D., et al., *Engineering of hyaline cartilage with a calcified zone using bone marrow stromal cells.* Osteoarthritis and Cartilage, 2015. **23**(8): p. 1307-1315.

157. Zhang, T., et al., *Biomimetic design and fabrication of multilayered osteochondral scaffolds by low-temperature deposition manufacturing and thermal-induced phase-separation techniques.* Biofabrication, 2017. **9**(2): p. 025021.

158. Schek, R.M., et al., *Engineered osteochondral grafts using biphasic composite solid free-form fabricated scaffolds.* Tissue Eng, 2004. **10**(9-10): p. 1376-85.

159. Schek, R.M., et al., *Tissue engineering osteochondral implants for temporomandibular joint repair.* Orthod Craniofac Res, 2005. **8**(4): p. 313-9.

160. Mazaki, T., et al., *A novel, visible light-induced, rapidly cross-linkable gelatin scaffold for osteochondral tissue engineering.* Sci Rep, 2014. **4**: p. 4457.

161. Guo, X., et al., *Repair of osteochondral defects with biodegradable hydrogel composites encapsulating marrow mesenchymal stem cells in a rabbit model.* Acta Biomater, 2010. **6**(1): p. 39-47.

162. Celikkin, N., et al., *Gelatin methacrylate scaffold for bone tissue engineering: The influence of polymer concentration.* J Biomed Mater Res A, 2018. **106**(1): p. 201-209.

163. Wang, D., J.M. Taboas, and R.S. Tuan, *PTHrP overexpression partially inhibits a mechanical strain-induced arthritic phenotype in chondrocytes.* Osteoarthritis Cartilage, 2011. **19**(2): p. 213-21.

164. Mueller, M.B., et al., *Hypertrophy in mesenchymal stem cell chondrogenesis: effect of TGF-beta isoforms and chondrogenic conditioning.* Cells Tissues Organs, 2010. **192**(3): p. 158-66.

165. Bian, L., et al., *Dynamic compressive loading enhances cartilage matrix synthesis and distribution and suppresses hypertrophy in hMSC-laden hyaluronic acid hydrogels.* Tissue Eng Part A, 2012. **18**(7-8): p. 715-24.

166. Deng, Y., et al., *Engineering hyaline cartilage from mesenchymal stem cells with low hypertrophy potential via modulation of culture conditions and Wnt/beta-catenin pathway.* Biomaterials, 2019. **192**: p. 569-578.

167. Chen, S., et al., *Strategies to minimize hypertrophy in cartilage engineering and regeneration.* Genes Dis, 2015. **2**(1): p. 76-95.

168. Nie, T., et al., *Production of heparin-functionalized hydrogels for the development of responsive and controlled growth factor delivery systems.* J Control Release, 2007. **122**(3): p. 287-96.

169. Kanzaki, S., et al., *Heparin inhibits BMP-2 osteogenic bioactivity by binding to both BMP-2 and BMP receptor.* Journal of Cellular Physiology, 2008. **216**(3): p. 844-850.

170. Hansen, N.M., et al., *Aggregation of hydroxyapatite crystals.* Biochimica et Biophysica Acta (BBA) - General Subjects, 1976. **451**(2): p. 549-559.

171. Daly, A.C., et al., *A comparison of different bioinks for 3D bioprinting of fibrocartilage and hyaline cartilage.* Biofabrication, 2016. **8**(4): p. 045002.

172. Zhu, C., et al., *Inverse Opal Scaffolds with Gradations in Mineral Content for Spatial Control of Osteogenesis.* Adv Mater, 2018: p. e1706706.

173. Zhu, C., et al., *Design and Fabrication of a Hierarchically Structured Scaffold for Tendon-to-Bone Repair.* Adv Mater, 2018. **30**(16): p. e1707306.

174. Lipner, J., et al., *Toughening of fibrous scaffolds by mobile mineral deposits.* Acta Biomater, 2017. **58**: p. 492-501.

175. Lee, N.M., et al., *Polymer fiber-based models of connective tissue repair and healing.* Biomaterials, 2017. **112**: p. 303-312.

176. Mosher, C.Z., J.P. Spalazzi, and H.H. Lu, *Stratified scaffold design for engineering composite tissues.* Methods, 2015. **84**: p. 99-102.

177. Khanarian, N.T., et al., *A functional agarose-hydroxyapatite scaffold for osteochondral interface regeneration.* Biomaterials, 2012. **33**(21): p. 5247-58.

178. SALTER, R.B. and W.R. HARRIS, *Injuries Involving the Epiphyseal Plate*. Vol. 45. 1963. 587-622.

179. Mizuta, T., et al., *Statistical analysis of the incidence of physeal injuries.* J Pediatr Orthop, 1987. **7**(5): p. 518-23.

180. Rennie, L., et al., *The epidemiology of fractures in children.* Injury, 2007. **38**(8): p. 913-22.

181. Eilert, R.E., *Pediatric Orthopedic Deformities: Basic Science, Diagnosis, and Treatment*. Vol. 85. 2003. 2067-2067.

182. Caine, D., J. DiFiori, and N. Maffulli, *Physeal injuries in children's and youth sports: reasons for concern?* Br J Sports Med, 2006. **40**(9): p. 749-60.

183. Riseborough, E.J., I.R. Barrett, and F. Shapiro, *Growth disturbances following distal femoral physeal fracture-separations.* J Bone Joint Surg Am, 1983. **65**(7): p. 885-93.

184. Babu, L.V., et al., *Epiphysiodesis for limb length discrepancy: a comparison of two methods.* Strategies in trauma and limb reconstruction (Online), 2014. **9**(1): p. 1-3.

185. Ruzbarsky, J.J., C. Goodbody, and E. Dodwell, *Closing the growth plate: a review of indications and surgical options.* Curr Opin Pediatr, 2017. **29**(1): p. 80-86.

186. Langenskiold, A., T. Videman, and T. Nevalainen, *The fate of fat transplants in operations for partial closure of the growth plate. Clinical examples and an experimental study.* J Bone Joint Surg Br, 1986. **68**(2): p. 234-8.

187. Trueta, J. and V.P. Amato, *The vascular contribution to osteogenesis. III. Changes in the growth cartilage caused by experimentally induced ischaemia.* J Bone Joint Surg Br, 1960. **42-b**: p. 571-87.

188. Chung, R., B.K. Foster, and C.J. Xian, *The potential role of VEGF-induced vascularisation in the bony repair of injured growth plate cartilage.* J Endocrinol, 2014. **221**(1): p. 63-75.

189. Anderson, J.M., A. Rodriguez, and D.T. Chang, *Foreign body reaction to biomaterials.* Semin Immunol, 2008. **20**(2): p. 86-100.

190. Nordahl, J., G. Andersson, and F.P. Reinholt, *Chondroclasts and osteoclasts in bones of young rats: comparison of ultrastructural and functional features.* Calcif Tissue Int, 1998. **63**(5): p. 401-8.

191. Florencio-Silva, R., et al., *Biology of Bone Tissue: Structure, Function, and Factors That Influence Bone Cells.* Biomed Res Int, 2015. **2015**: p. 421746.

192. Nakamura, H., *Morphology, Function, and Differentiation of Bone Cells.* Journal of Hard Tissue Biology, 2007. **16**(1): p. 15-22.

193. Enishi, T., et al., *Hypertrophic chondrocytes in the rabbit growth plate can proliferate and differentiate into osteogenic cells when capillary invasion is interposed by a membrane filter.* PLoS One, 2014. **9**(8): p. e104638.

194. Kadoya, Y., et al., *The expression of osteoclast markers on foreign body giant cells.* Bone Miner, 1994. **27**(2): p. 85-96.

195. Leibbrandt, A. and J.M. Penninger, *RANK/RANKL: regulators of immune responses and bone physiology.* Ann N Y Acad Sci, 2008. **1143**: p. 123-50.

196. Kido, S., et al., *Expression of RANK is dependent upon differentiation into the macrophage/osteoclast lineage: induction by 1alpha,25-dihydroxyvitamin D3 and TPA in a human myelomonocytic cell line, HL60.* Bone, 2003. **32**(6): p. 621-9.

197. Jiang, J., et al., *Quantitative analysis of osteoclast-specific gene markers stimulated by lipopolysaccharide.* J Endod, 2006. **32**(8): p. 742-6.

198. Castillo, L.M., C.A. Guerrero, and O. Acosta, *Expression of typical osteoclast markers by PBMCs after PEG-induced fusion as a model for studying osteoclast differentiation.* J Mol Histol, 2017. **48**(3): p. 169-185.

199. Miron, R.J., et al., *Giant cells around bone biomaterials: Osteoclasts or multi-nucleated giant cells?* Acta Biomater, 2016. **46**: p. 15-28.

200. Renshaw, S., *Chapter 4.2 - Immunohistochemistry and Immunocytochemistry*, in *The Immunoassay Handbook (Fourth Edition)*, D. Wild, Editor. 2013, Elsevier: Oxford. p. 357-377.

201. *4 - The Basics of In Situ Hybridization*, in *In Situ Molecular Pathology and Co-Expression Analyses*, G.J. Nuovo, Editor. 2013, Academic Press: San Diego. p. 81-131.

202. Cheung, T.H. and T.A. Rando, *Molecular regulation of stem cell quiescence.* Nat Rev Mol Cell Biol, 2013. **14**(6): p. 329-40.

203. Kim, K.H. and J.M. Sederstrom, *Assaying Cell Cycle Status Using Flow Cytometry.* Curr Protoc Mol Biol, 2015. **111**: p. 28.6.1-11.

204. Rodgers, J.T., et al., *mTORC1 controls the adaptive transition of quiescent stem cells from G0 to G(Alert).* Nature, 2014. **510**(7505): p. 393-6.

205. Yu, W.H. and J.F. Woessner, Jr., *Heparan sulfate proteoglycans as extracellular docking molecules for matrilysin (matrix metalloproteinase 7).* J Biol Chem, 2000. **275**(6): p. 4183-91.

206. Flannery, C.R., et al., *Autocatalytic cleavage of ADAMTS-4 (Aggrecanase-1) reveals multiple glycosaminoglycan-binding sites.* J Biol Chem, 2002. **277**(45): p. 42775-80.

207. Zilberberg, A., A. Yaniv, and A. Gazit, *The low density lipoprotein receptor-1, LRP1, interacts with the human frizzled-1 (HFz1) and down-regulates the canonical Wnt signaling pathway.* J Biol Chem, 2004. **279**(17): p. 17535-42.

208. Ellman, M.B., et al., *Fibroblast growth factor control of cartilage homeostasis.* J Cell Biochem, 2013. **114**(4): p. 735-42.

209. Kim, Y.J., H.J. Kim, and G.I. Im, *PTHrP promotes chondrogenesis and suppresses hypertrophy from both bone marrow-derived and adipose tissue-derived MSCs.* Biochem Biophys Res Commun, 2008. **373**(1): p. 104-8.

210. Fuerer, C., S.J. Habib, and R. Nusse, *A study on the interactions between heparan sulfate proteoglycans and Wnt proteins.* Dev Dyn, 2010. **239**(1): p. 184-90.

211. J. Gauci, S., et al., *Proteoglycan and Collagen Degradation in Osteoarthritis*. 2017. 41-61.